Universidade do Minho
Escola de Medicina

Daniela Raquel Cunha Garcia

Impact of astrocytic calcium suppression in the pathogenesis of Machado-Joseph disease

janeiro de 2021

Impact of astrocytic calcium suppression in the pathogenesis of Machado-Joseph disease
Daniela Raquel Cunha Garcia
UMinho | 2021

Universidade do Minho
Escola de Medicina

Daniela Raquel Cunha Garcia

Impact of astrocytic calcium suppression in the pathogenesis of Machado-Joseph disease

Dissertação de Mestrado
Mestrado em Ciências da Saúde

Trabalho efetuado sob a orientação da
Doutora Sara Duarte Silva
e da
Professora Doutora Patrícia Maciel

janeiro de 2021

AGRADECIMENTOS

Primeiramente, eu gostaria de agradecer à professora Patrícia Maciel pela oportunidade de integrar o seu grupo de investigação e pela sua orientação durante este projeto de dissertação. Sou grata por ter sido acolhida por um grupo tão diversificado e de excelência: Sara Silva, Stéphanie Oliveira, Daniela Monteiro, Andreia Carvalho, Joana Correia, Marta Costa, Andreia Castro, Jorge Silva, Joana Sousa, Catarina Ferreira, Ana Bela Campos, Daniela Campos, Liliana Costa, Jorge Fernandes, Bruno Almeida, Beatriz Ferreira e Margarida Sousa. Um reconhecimento especial à Sara Silva, Stéphanie Oliveira, Daniela Monteiro, Andreia Carvalho, Joana Correia, Marta Costa e Andreia Castro, que contribuíram diretamente na minha evolução pessoal e científica. Aprendi muitas coisas convosco e sou grata pela vossa boa vontade.

Obrigada também à toda a comunidade da Escola de Medicina, a todos os NeRD e a todos os meus colegas de mestrado, que de alguma forma contribuíram para o sucesso do meu percurso escolar e a pessoa que eu hoje sou.

À Sara Silva, minha "mãe científica", muito obrigada! Sou muito grata por ser tua aluna! Sem dúvida, tiveste um papel muito ativo na minha aprendizagem e aquisição de conhecimentos. Obrigada por me teres dado sempre liberdade para poder errar e confiança para enfrentar as adversidades. Para além de uma profissional formidável, és uma pessoa extremamente honesta, humilde e com bom coração. Admiro-te muito!

Termino agradecendo à minha família e amigos, que me apoiam incondicionalmente. Gratidão!

FUNDING

The work presented in this thesis was performed in the Life and Health Sciences Research Institute (ICVS), Minho University. Financial support was provided by grants from the ICVS Scientific Microscopy Platform, member of the national infrastructure PPBI - Portuguese Platform of Bioimaging (PPBI-POCI-01-0145-FEDER-022122; by National funds, through the Foundation for Science and Technology (FCT) - project UIDB/50026/2020 and UIDP/50026/2020; and by the projects NORTE-01-0145-FEDER-000013 and NORTE-01-0145-FEDER-000023, supported by Norte Portugal Regional Operational Programme (NORTE 2020), under the PORTUGAL 2020 Partnership Agreement, through the European Regional Development Fund (ERDF).

STATEMENT OF INTEGRITY

I hereby declare having conducted this academic work with integrity. I confirm that I have not used plagiarism or any form of undue use of information or falsification of results along the process leading to its elaboration.

I further declare that I have fully acknowledged the Code of Ethical Conduct of the University of Minho.

RESUMO

A supressão da sinalização do cálcio nos astrócitos e o seu impacto na patogénese da doença de Machado-Joseph

A doença de Machado-Joseph (DMJ) é uma doença neurodegenerativa hereditária rara, causada por uma expansão anormal de glutaminas na proteína Ataxina-3 (ATXN3), levando a uma degeneração lenta de células neuronais em regiões específicas do cérebro e da espinhal medula, conduzindo ao aparecimento de sintomas diversificados, maioritariamente motores. Embora a DMJ se caracterize por morte neuronal, outras células não-neuronais encontram-se envolvidas na patogénese da doença, incluindo os astrócitos. A astrogliose é um achado patológico comum em pacientes com DMJ e em modelos animais da doença, incluindo o modelo transgénico da DMJ gerado no nosso laboratório – o ratinho CMVMJD135. Neste modelo, foi encontrado um aumento da reatividade astrocítica na espinhal medula e na *substância nigra*, mas não nos núcleos pônticos, sugerindo uma especificidade regional. Também, neste modelo de ratinho, os animais apresentam um perfil inflamatório alterado nos estágios finais da doença. Para além disto, em estudos *in vitro* foi descrito que a proteína mutante ATXN3 interage com o recetor IP_3R1 e afeta a sua função. Com base nestas observações, nós levantamos a hipótese que o mesmo acontecesse com o recetor IP_3R2 que apresenta grande homologia com o primeiro. No cérebro de roedores, o recetor IP_3R2 é predominantemente expresso nos astrócitos, onde desempenha um papel crucial na via de sinalização do Cálcio (Ca^{2+}) e modula as ondas de Ca^{2+} características destas células. Neste trabalho questionámos se alterações na sinalização do Ca^{2+} nos astrócitos contribuiriam para a progressão da DMJ. Para averiguar esta questão, usámos um ratinho mutante cuja sinalização de Ca^{2+} intracelular nos astrócitos se encontra alterada - os ratinhos IP_3R2 KO - que cruzámos com o modelo de ratinho CMVMJD135. Em seguida, fizemos uma caracterização longitudinal extensa do comportamento deste duplo mutante. Em suma, os resultados de um painel de testes comportamentais demonstram que, em geral, o duplo mutante não apresenta um comportamento diferente do modelo da DMJ; no entanto, foram encontradas alterações pontuais ligeiras na marcha destes animais. Os resultados sugerem que a ablação do IP_3R2 no contexto da DMJ não tem uma função neuroprotetora nem, por outro lado, neurotóxica, visto que funcionalmente não foram encontradas alterações significativas.

Palavras-Chave: astrócitos, comportamento motor, doença de Machado-Joseph, ratinhos CMVMJD135, ratinhos IP_3R2 KO.

ABSTRACT

Impact of astrocytic calcium suppression in the pathogenesis of Machado-Joseph disease

Machado-joseph disease (MJD) is a rare inherited neurodegenerative disease, caused by an abnormal glutamine expansion within the protein Ataxin-3 (ATXN3), leading to a slow neuronal degeneration of specific brain regions and spinal cord, resulting in a wide variety of symptoms, mainly motor-related. Despite the well-known neuronal death, other non-neuronal cells are involved in MJD pathogenesis, including astrocytes. Astrogliosis is a common pathological finding in MJD and has been found both in humans and in animal models of the disorder, including the MJD mouse model generated in the lab – the CMVMJD135 mouse model. In the CMVMJD135 mice, astrocytic reactivity was found in the spinal cord and *substancia nigra* but not in the pontine nuclei, suggesting a region-specific astrocytic involvement. Also, in this mouse model, an altered inflammatory profile was observed in late stages of the disease. Besides that, in *in vitro* studies it was described that the mutant ATXN3 physically interacts with the IP_3R1 receptor and affects its function. Based on these observations, we hypothesized that the same would happen with the IP_3R2 receptor, which has great homology with the first. In the rodent brain, the IP_3R2 receptor is predominantly expressed in astrocytes, in which it plays a crucial role in calcium (Ca^{2+}) signalling and modulates the "Ca^{2+} waves" characteristic of these cells. In this study, we asked whether abnormal Ca^{2+} signalling in astrocytes could contribute to MJD disease process. To answer this question, we took advantage of a mutant mouse model with disturbed global intracellular Ca^{2+} signalling in astrocytes - the IP_3R2 KO mice - that we crossed with the CMVMJD135 mouse model. Then, we performed an extensive longitudinal behavioural characterization of the double mutant mice. Globally, the results of a panel of behavioural tests demonstrate that the double mutants do not present a different behaviour from the transgenic mice of MJD; nevertheless, mild detrimental effects on the gait of the double mutant mice were found. Together, these results suggest that the ablation of IP_3R2 receptor in the context of MJD do not have a neuroprotective nor a neurotoxic function, since functionally no significant alterations were found.

Keywords: astrocytes, behaviour, CMVMJD135 mice, IP_3R2 KO mice, Machado-Joseph disease, motor behaviour.

INDEX

ABBREVIATION LIST

ALS – Amyotrophic Lateral Sclerosis

ATXN3 – Ataxin-3

Ca^{2+} – Calcium Ion

CAG – Cytosine-Adenine-Guanidine

CNS – Central Nervous System

DUB – Deubiquitinating (Enzyme)

GFAP – Glial Fibrillary Acidic Protein

Het – Heterozygous

IP_3 – Inositol-1,4,5-trisphosphate

IP_3R1 – Inositol-1,4,5-trisphosphate receptor type 1

IP_3R2 – Inositol-1,4,5-trisphosphate receptor type 2

IP_3R2 KO – Inositol 1,4,5-trisphosphate receptor type 2 knock-out

IP_3R2 (-/-) – Inositol 1,4,5-trisphosphate receptor type 2 knock-out

IP_3R2 HET – Inositol 1,4,5-trisphosphate receptor type 2 heterozygous

IP_3R2 (+/-) – Inositol 1,4,5-trisphosphate receptor type 2 heterozygous

KO – Knockout

mGluRs – Metabotropic Glutamate Receptors

MJD – Machado-Joseph Disease

PolyQ – Polyglutamine

qRT-PCR – Quantitative Real-Time Polymerase Chain Reaction

RT – Room Temperature

SCAs – Spinocerebellar Ataxias

SCA3 – Spinocerebellar Ataxia Type 3

SEM – Standard Error of the Mean

WT – Wild-type

LIST OF FIGURES

LIST OF TABLES

1. INTRODUCTION

1.1. Machado-Joseph disease: a historical perspective

Machado-Joseph disease (MJD) was first reported in the 1970s. Three Portuguese families that emigrated from Azorean islands to the United States were found to be affected by a "new" hereditary neurological condition.

In 1972, members of William Machado's family were diagnosed with progressive cerebellar degeneration transmitted in an autosomal dominant manner. The ataxia appeared late in life, around 40 years of age, and patients presented a considerable variation in the severity and expressivity of the symptoms. This "new" condition was originally called Machado disease (1). In the same year, another family was described to suffer from an autosomal dominant illness. Affected members of the Thomas family were diagnosed with ataxia (limb and gait), degeneration of the spinal cord and cerebellar regions – spinocerebellar degeneration – as well as progressive ophthalmoplegia (weakness of the eye muscles). Besides that, the symptoms appeared early in life, between 17 and 46 years old. Since different phenotypes as well as different ages of onset of the symptoms were observed, it was thought that the Machado and the Thomas family suffered from different genetic diseases. Therefore, the Thomas family illness was termed "Nigro-spino-dentatal degeneration with nuclear ophthalmoplegia" (2). Some years later, in 1976, another family with Portuguese ancestry was described to have a "genetic neurologic disorder associated with striatonigral degeneration". The Joseph family members had gait imbalance, rigidity, progressive spasticity (stiffenning or tightening of muscles), difficulty with speech and swallowing, limited eye movements as well as facial and lingual fasciculations (muscle twitch) that appeared early in life (around 25 years of age). Like, in the other families, the disease was transmitted in an autosomal dominant fashion (3).

In 1977, Paula Coutinho and Jorge Sequeiros were pioneers in proposing the unification of the disease, suggesting that the illness that affected the Machado, the Thomas, and the Joseph families had the same genetic origin with variable phenotypic expression (4). The research performed by Corino Andrade and Paula Coutinho in the Azorean islands and in the Portuguese mainland made a key contribution to the definition of the disease (5). Along with the existing literature, they could define for the first-time a classification of the disease subtype's (6) and clinical criteria to diagnose the patients with MJD.

In the 1980s, the disease was officially called Machado-Joseph disease (7). Machado, for being the first family to be described and Joseph for being the largest and most well-studied family with MJD (5). A later proposed designation for MJD is Spinocerebellar Ataxia type 3 (SCA3) (8–10). From this moment on, the disease will be referred by the designation MJD.

1.1.1 Epidemiology, prevalence and world distribution

The first descriptions of MJD came from families with Portuguese ancestry, but quickly, the disease was found in families from other geographic locations and ethnic backgrounds.

Although the Spinocerebellar Ataxias (SCAs) are a group of rare disorders, MJD is now known to be a common dominant form of SCA worldwide (11,12). Epidemiologic data published early this year (Orphadata, 2020) estimates that the prevalence of MJD is 1.5 per 100 000 inhabitants around the globe (13).

At the same time, the disease geographic distribution pattern is not the same within each country. The relative frequency of autosomal dominant ataxias is higher in certain regions of Portugal (58–74%) (14,15), Brazil (69–92%) (16–19), China (48-73%) (20–22), the Netherlands (44%) (23), Germany (42%)(24), and Japan (28-63%) (25,26), while in Canada (24%) (27), USA (21%) (28), México (12%) (29) and Australia (12%) (30), the prevalence is relative lower. In countries such as India (3-14%) (31,32), South Africa (4%) (33) and Italy (1%)(34), MJD is considered a very rare disorder. Also, within Portugal, the disease is rare in the mainland but highly prevalent in the Azorean islands (5).

Furthermore, studies suggested that two different mutational events may have arisen in the Asian and Portuguese population; the spreading of these two independent mutations is thought to be due to population migrations (35–37).

1.1.2. Clinical spectrum and subtype classification

As previously noted, physicians had troubles to interconnect the existing cases reports and classify them into a unique disease due to the fact that MJD displays a remarkably broad range of phenotypes (38).

The most common clinical hallmark is progressive ataxia, which is a motor coordination dysfunction that affects gait and balance. As the disease progresses, the motor movements are slowly compromised and patients may experience severe spasticity (muscle weakness), rigidity, loss of muscle

bulk and strength, as well as the slowness of movement. Some patients with MJD can develop difficulties of speech and swallow as well as visual problems (such as double vision or limitations of eye movement). Other symptoms may comprise involuntary movement disorders, including dystonia (repetitive muscle contractions) and parkinsonian features, rigidity (stiffness), and/or bradykinesia (slowness of movement). Some patients may develop pyramidal syndrome (an increase in the muscle tone in the lower extremities, brisk deep tendon reflexes, Babinski sign and a decrease in fine motor coordination), peripheral neuropathy with amyotrophy and other oculomotor abnormalities (with nystagmus, eyelid retraction, progressive external ophthalmoplegia, ophthalmoparesis, and bulging eyes). Other patients may experience facial and lingual fasciculations (muscle twitches), postural instability, loss of proprioceptive, amyotrophy, corticospinal, autonomic nervous system dysfunctions and sleep disorders as well as weight loss. Interestingly, the intellect remains mostly unaffected (5,7,38–44), although some recent studies suggested a mild cognitive involvement (45–47).

Another important variable is the age of disease onset. Usually, patients with MJD are presymptomatic during most of their lives, followed by a period of progressive decline and premature death (5). Even so, some patients can experience the symptoms early in adolescence or late in life (up to 70 years of age) (48,49). Noteworthy, a negative correlation was established between age at onset of the disease and the clinical presentation: the earlier the first symptoms appear, the more severe and quickly is the progression of the disease (5,50). In severe cases, the cause of death is often related to complications that arise from lack of mobility and/or poor coordination of swallowing and breathing. Other causes of death may include urinary tract infection and cachexia (a disorder characterized by an extensive weight loss and muscle deteriorating that cannot be reversed even with nutritional supplementation) (51,52). Regarding life expectancy, it is thought that patients have a mean of 21 years of surviving time (ranging from 7 to 29 years) (5,49).

Herewith, it was possible to define a clinical classification with subtypes of the disease (5,6,38). The first type (also called “Joseph” type, the most severe) is characterized by cerebellar ataxia and dominance of pyramidal and extrapyramidal anomalies (mostly dystonia). The symptoms appear early in life (10-30 years) and the disease progresses more quickly. In the “Thomas” type, that is the most common form, symptoms include cerebellar ataxia, progressive external ophthalmoplegia, and with or without pyramidal signs. The symptoms manifest at an intermediate age (20-50 years). Next, the third type (also termed “Machado” type, whichever is the mildest form) is marked by a late-onset (40-75 years) and slow progression of the disease. Symptoms include cerebellar deficits and peripheral alterations (such as loss of proprioception and muscle atrophies), with or without pyramidal signs (5,53–56). Some

authors may include a fourth and rare type, which is characterized by peripheral neuropathy, fasciculations, and slowly progressive parkinsonism features. The age of disease onset is variable (54,56–58). Remarkably, different subtypes can be present in the same family (5,6,54).

1.1.3. Neuropathological features

Compared to healthy individuals, the brains of patients with advanced MJD have substantially less weight (ranges between 1.000 and 1.300 g), due to the progressive neuronal loss (59,60). Magnetic resonance imaging and neuroimaging studies demonstrated that the cerebellum and the brainstem are atrophic and an enlargement of the fourth ventricle is present (61).

The most affected brain areas in MJD patients are the cerebellum, the brainstem, and some cranial nerves as well as the spinal cord. However, the extent of the damage is not only spread through the central nervous system but also in the peripheral nervous system. More specifically, it has been observed that neuronal loss is frequent in the cerebellar dentate nucleus, *substantia nigra*, striatum, thalamus, pontine nuclei, and motor nuclei as well as cranial nerves (the oculomotor, the dorsal nucleus of the vagus, the vestibular nuclei), and in subregions of the basal ganglia (such as globus pallidus, subthalamic nuclei). Additionally, the nerve motor nuclei, Clarke's column nuclei, anterior roots, the medial longitudinal bundle and the anterior horn of the medulla are similarly affected in MJD (3,40,43,53,62–69). Other brain systems were also found to be affected, such as the cholinergic and dopaminergic midbrain, the somatosensory (visual, auditory, and vestibular) as well as the ingestion and urination-related systems (6,41,70–72).

Interestingly, it has also been reported the presence of gliosis associated with neuronal loss since the first pathological descriptions of MJD patients. Gliosis is a process that involves a coordinated cellular and molecular event in response to central nervous system (CNS) damage, leading to glial cells proliferation and/or glial scar formation in the site that occurred the cell damage (40,63,68).

Hence, diagnosing patients with MJD was not a straightforward task since, without genetic diagnoses tests, physicians based their conclusions on the patient's physical history together with the family history (73,74).

1.1.4. Aetiology: the Ataxin-3 (*ATXN3*) gene product

It was in 1993 that the locus responsible for MJD was mapped on the long arm of the chromosome 14q32.1 (75). One year later, the gene associated with the disease was identified: *MJD1,* now termed *ATXN3* (76). The *ATXN3* gene has a length of approximately 48 kb and contains 13 exons with a cytosine-adenine-guanidine (CAG) tract located at exon 10 (76,77).

MJD is caused by an unstable expansion of a (CAG)n tract in the *ATXN3* gene encoding a polyglutamine (polyQ) repeat near the C-terminus of the wild-type protein – ataxin-3 (ATXN3) (75,78). MJD is also associated with a group of human disorders known as polyQ diseases because they share the same genetic feature: a pathological expansion of a CAG trinucleotide repeat in their respective genes (79). In normal individuals, the number of CAG repeats varies between 12 and 44 CAGs, whereas in MJD patients it contains between 61 and 87 repeats units. The gap ranges from 45 to 60 and is associated with incomplete phenotype penetrance. With this evidence, it was possible to develop and improve the molecular diagnosis for MJD, based on the determination of the CAG repeat number in the MJD-causing gene (50,73,74,80–88). Additionally, it was possible to understand that the mutation was quite unstable, with the occurrence of both expansion and/or reduction in the size throughout generations (89). The discovery of the dynamic expansion of the CAG repeat helped to clarify some features of MJD. Firstly, the variability of MJD clinical spectrum can be partially explained by the presence of different CAG repeat sizes in affected individuals (90). Secondly, it was possible to understand why some cases presented more severe clinical manifestations even within the family. Particularly, it was described that in comparison to parents, some descendants tend to develop symptoms of the disease earlier in life, experience them in a more severe form and have a faster progression of the disease. This biological phenomenon, called anticipation, was explained in a molecular perspective: with successive generations, there is a tendency to increase the number of CAG repetitions, which leads to an increase in the severity of symptoms. Hence, not only the size of the expanded CAG repeat number is inversely correlated with the age of disease onset but it is also correlated with the frequency of other clinical features. Unfortunately, this information cannot provide accurate information about the disease course or define at what age the symptoms will manifest for each individual (49,75,90–92).

ATXN3 belongs to the cysteine proteases family and is composed of a catalytic Josephin domain (a structured globular N-terminal with a papain-like fold), a polyQ tract and a flexible C-terminal tail. The C-terminal tail sequence contains 2 or 3 motifs that interact with ubiquitin (78,93,94). Concerning expression, ATXN3 is ubiquitously expressed in neuronal and non-neuronal tissues (such as spleen, liver,

heart, kidney, and testis). This pattern of expression was observed in both healthy individuals and patients, although with some regional and cellular differences. In healthy human brains, the *ATXN3* mRNA levels are widely distributed across the brain, with considerable high levels in the cerebellum, hippocampus, and *substantia nigra*, and intermediate levels in the striatum and cerebral cortex. Additionally, in patients' brains, *ATXN3* is expressed predominantly in the nuclei of neurons, but it can be found in the cytoplasm as well as in neuronal processes. These findings were also observed in animal models of the disease. The distribution and differential localization of *ATXN3* in disease is still poorly understood. Despite the predominance in neurons, it was also found at low levels of expression in glial cells: mainly in astroglia and oligodendroglia (both in normal and diseased brains) (52,77,95,96).

Regarding its physiological function, it is known that ATXN3 takes part in different cellular pathways such as protein homeostasis (96), transcription (97,98), membrane dynamics, cell motility, endocytosis (99,100), and autophagy (101), and to play an important role in the ubiquitin-proteasome pathway (reviewed in (102)). As a deubiquitinating (DUB) enzyme, ATXN3 binds to polyubiquitylated proteins (preferably with four or more ubiquitin moieties) through its ubiquitin-interaction motifs (UIMs)(96,103,104). Since the *ATXN3* gene is alternatively spliced, different protein isoforms can be produced with a variable number of UIMs. Hence, ATXN3 isoforms behave differently withing the cell and may be involved in the regulation of inclusion bodies, given their propensity to aggregate(105).

It is also known that ATXN3 is modified to post-translation modifications (such as phosphorylation (106–108), ubiquitylation (109,110), and SUMOylation (111,112)), which influence its function, stability, interaction affinity with other molecules, and regulate its subcellular localization (102). It is also known that ATXN3 can physically interact with several proteins, and the presence of the expanded CAG repeat may perturb the normal protein-protein interactions and cause abnormal protein function (113–115). For example, it has been shown that only mutant ATXN3 can bind to the type 1 inositol 1,4,5-trisphosphate receptor (IP_3R1) and modulate intracellular calcium (Ca^{2+}) release levels, destabilizing neuronal Ca^{2+} signalling (116).

1.1.5. ATXN3 aggregation and intranuclear inclusions in MJD

A hallmark of several neurodegenerative diseases, including MJD, is the high propensity of the respective mutant proteins to form intracellular aggregates. The expansion of the glutamine repeat may induce conformational changes and alter protein interactions, causing the mutant protein to adopt stable structures that resist unfolding and proper clearance by the proteasome (115). Theoretical models have

been generated as an attempt to unravel the pathogenesis process in many polyQ disorders. A model suggests that, when mutated, Atxn3 may interact with other proteins in an abnormal manner inducing selective degeneration. The expansion is thought to confer a toxic gain of function as well as loss-of-function to the expanded ataxin-3 (117,118). Most compelling evidence has shown that the C-terminal fragment of expanded mutant ataxin-3 is more toxic than the full-length protein that contains the polyQ stretch, within a threshold concentration (119). It is suspected that a toxic C-terminal fragment is required for neuropathology, by triggering the aggregation process and inducing other toxic events such as cell death and formation of intranuclear inclusions in neurons (120,121).

Ubiquitinated intranuclear inclusions containing mutant ataxin-3 were observed in neurons of MJD-affected brain regions as well as in spared areas (122). This was also observed in cultured cells and transgenic mouse models (119). However, no direct correlation was found between the occurrence of these protein structures and neuronal demise (95,120). While these molecular structures are considered a central feature of pathogenesis, the mechanisms leading to the neurodegenerative process in affected areas are largely unknown (120,123–125).

1.1.6. Therapeutic strategies for MJD

Although research in many laboratories worldwide is progressively leading to a better understanding of the disease mechanism(s) in MJD, there is no cure or specific treatment to delay or halt the progression of the disease. The current treatment approach for MJD patients is the therapeutic management of the symptoms, to ameliorate neurological symptoms and increase patient's quality of life. As part of the non-pharmacological treatments, patients can receive genetic counselling as well as do speech therapy, physical exercise and physiotherapy (73,126,127). The pharmacological approach includes specific drugs to treat parkinsonian signs, restless legs syndrome and other motor-related symptoms (57,128,129).

The major goal of the current research in MJD is to find disease-modifying therapies. To accomplish that it is necessary to understand the pathological mechanisms underlying the disease, overcome research challenges, and explore possible therapeutic strategies.

1.1.7. The CMVMJD135 mouse model, a suitable model to study MJD

In the last years, research on MJD has been boosted by the development of transgenic mouse models (130). Even though several transgenic mouse models have been generated to study MJD, it is difficult to develop an animal model showing significant analogy to the heterogeneous and complex symptoms and neuropathological features of the human disorder (131), reviewed in (132).

Some years ago, our lab has developed the CMVMJD135 mouse model to study MJD. To introduce human ATXN3 in mice, a full-length *ATXN3* cDNA carrying a repeat tract ((CAG)2CAAAAGCAGCAA(CAG)124, coding for 135 glutamines) was converted in the *ATXN3c* variant into the pCMV vector. After the plasmid (pF25B3.3::AT3Q130::YFP, called pCMVAT3Q135_1.5) was linearized by total digestion with PaeI (Fermentas), the fragment of interest (3150 bp) was purified from an agarose gel and microinjected into fertilized murine oocytes of the C57Bl/6 mouse strain (QTRN, Canada). The CMVMJD135 lineage was established by breeding the founder C with C57Bl/6 wild type females **(Figure 1)** (133).

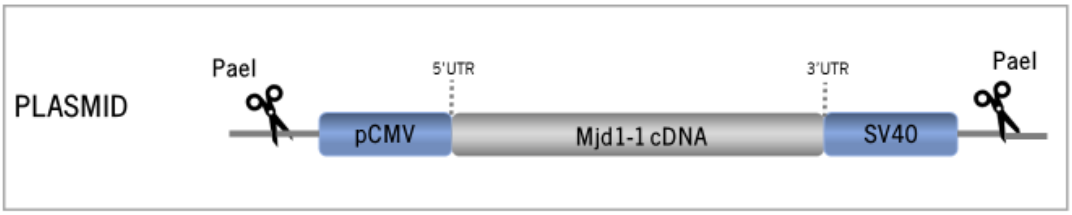

Figure 1 – Schematic diagram of the plasmid CMVMJDAT3Q135_1.5 used for the generation of a transgenic mouse model of MJD carrying the expanded *ataxin-3* with 135 CAGs. The expression of *ATXN3c* cDNA variant is under the regulation of the CMV promoter. *Adapted from* (133,134).

The CMVMJD135 mouse model ubiquitously expresses the human 3-UIMs version of ATNX3 protein, with 135 glutamines. In the brain, *ATXN3* mRNA expression was detected at near-endogenous levels in the cerebellum, brainstem, forebrain, peripheral tissues, and spinal cord (133).

As in MJD patients, both somatic and intergenerational instability was observed in the CMVMJD135 mice (133,134). Regarding phenotypic features, the MJD mice display progressive neurological deficits that overlap with the core clinical features of MJD patients. More specifically, starting at 6 weeks of age, CMVMJD135 mice show the first sign of the disease - loss of muscle strength. Motor abnormalities gradually appear and progress with time, such as lack of balance and coordination, abnormal gait and decrease of locomotor and exploratory activity as well as the loss of hindlimb tonus resistance, limb

clasping, and grasping. Also, transgenic mice demonstrate with time an unhealthy appearance, abnormal body posture, loss of gain weight and tremors.

Pathologically, the CMVMJD135 mice (at 20-35 weeks of age) display ATXN3 inclusions in the nucleus of neuronal cells in different regions, also known to be affected in MJD patients (133). More precisely, these inclusions are found in the pontine nuclei, reticulotegmental nucleus of the pons, spinal cord neurons, the facial nuclei, anterior olfactory nuclei, ventral tenia tecta, inferior olive, the dentate nuclei, locus coeruleus, and the cuneate nuclei. It is also possible to observe a reduction in the volume without cell loss in the dentate nuclei as well as reduction of the brain weight (at 20 weeks of age) **(Figure 2)**(133).

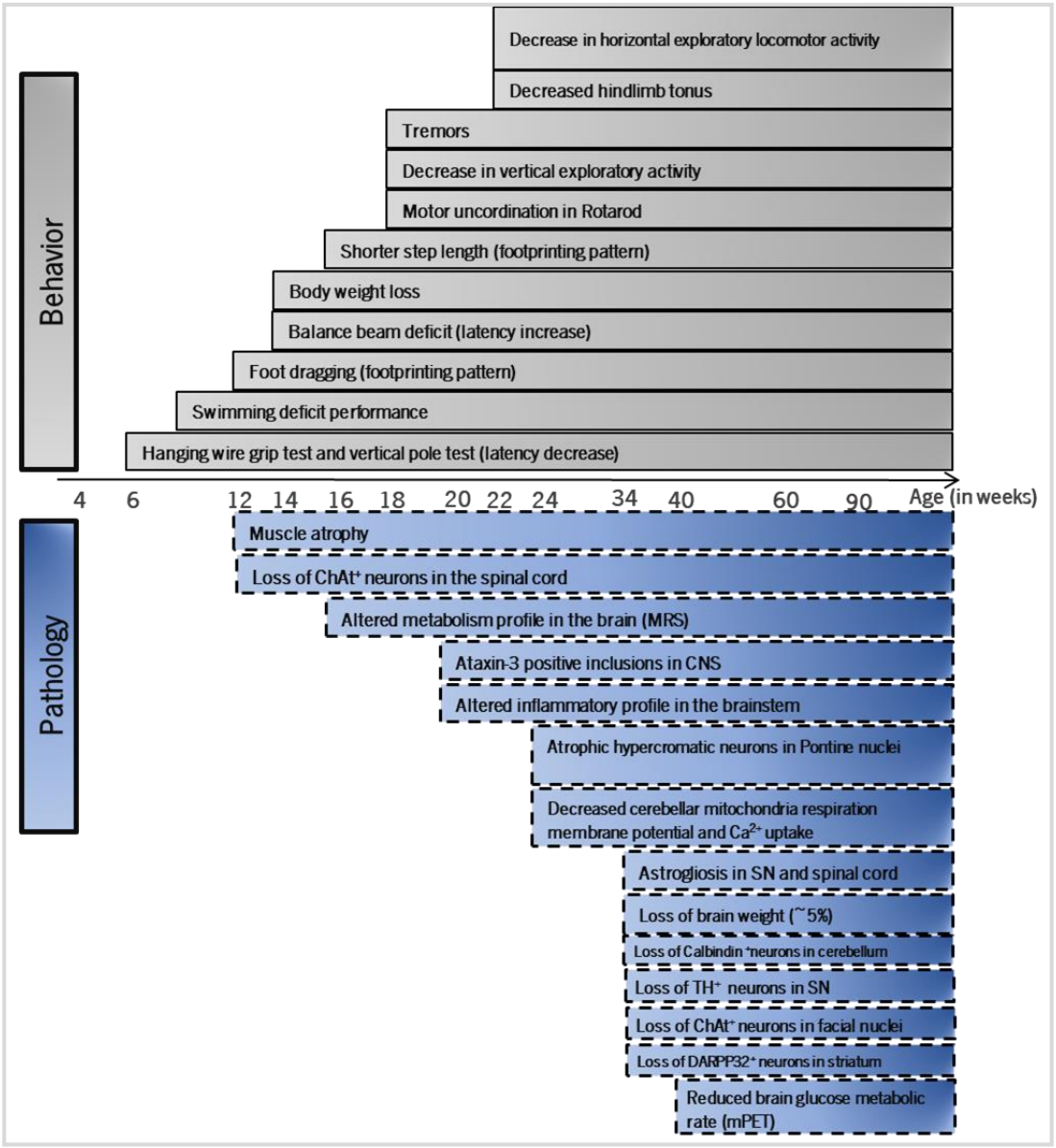

Figure 2 – Schematic diagram of CMVMJD135 mouse model phenotypically features. The first symptoms observed appear around 6 weeks of age in the mice and the pathological features gradually worsen with time. *Adapted from* (133,135) and Duarte-Silva *et al., unpublished*.

In summary, the CMVMJD135 mouse model displays quantifiable traits that mimic the human condition both at the phenotypic and neuropathologic levels, which makes it a powerful tool for the study of pathogenic mechanisms associated with MJD as well as to explore novel therapeutic strategies (133).

1.1.8. Astrogliosis, a consistent pathological finding in MJD

Astrogliosis has been observed in patients with MJD, but it has been considered as a reaction to damage in neurons. In response to CNS insult, astrocytes are stimulated to undergo molecular and morphological changes that induce their proliferation and the release of toxic and/or neuroprotective molecules (136,137).

In MJD patients, reactive astrogliosis is present in both spared (such as cortex) and affected brain regions (internal segment of the pallidum, *substantia nigra,* lateral reticular nucleus, pontine, pre-cerebellar nuclei and subthalamic nuclei) (40,66,138).

In the CMVMJD135 mouse model, astrogliosis is present and appears to be region-specific, since an increased GFAP intensity was observed in the *substantia nigra* (133) and the spinal cord, but not in the pontine nuclei (a key affected brain area, unpublished observations). Additionally, 3D reconstruction revealed an altered astrocytic morphology in these brain areas. Furthermore, the evaluation of the expression levels of astrocytes-related molecules showed an increased of pro-inflammatory as well as a decreased of anti-inflammatory molecules in the brainstem and in the spinal cord of 34 weeks old CMVMJD135 animals, where the symptoms are well stablish (Duarte-Silva *et al.,* unpublished results).

Altogether, these findings point to the potential involvement of astrocytes in the progression of MJD pathogenesis, alone or through the interaction with neuronal and microglial cells.

1.2. Astrocytes: the star-shaped cells of our brain

The human brain is composed of two broad categories of cells: neurons and glial cells. For many years, neurons were considered the main types of cells in the brain, responsible for processing and transmitting information through electrical impulses. At the same time, it was thought that glial cells were structural and supportive cells that occupied the space between neurons. However, a growing body of evidence is showing that these cells are active players in brain circuits and signal processing (139–141).

In the CNS, the main glial cell types are astrocytes, microglial cells and oligodendrocytes, while in the peripheral nervous system the predominant ones are the Schwann cells, Enteric glial cells and

Satellite cells (139,140). Astrocytes, the focus of this study, are the most numerous glial cell type on the CNS and their name was coined by Michael von Lenhossek due to their star-shaped morphology (139).

1.2.1 Astrocyte structure and morphology: a heterogeneous cell population

To appreciate the complex heterogeneity of astrocytes it is necessary to comprehend their formation and development.

During embryogenesis, radial glial cells develop from early neuroepithelial cells. At the early stages of embryogenesis, these cells generate several types of neurons. With time, radial cells withdraw their committed process and became glial-committed precursor cells. These precursors proliferate and are converted into astrocytes in the subventricular zone. Astrocytes mature throughout the development, overlapping with synaptogenesis and angiogenesis. After birth, these cells continue to proliferate and participate in different cellular processes, according to brain's requirements (142–145).

The properties and functional roles of astrocytes depend on a combination of several factors, mainly the site of origin, extrinsic signals during development and intrinsic signalling cascades induced by the surrounding cells or molecules. Therefore, astrocytic cells can be classified in two types: (i) the protoplasmic astrocytes of the grey matter, that display highly branched bushy processes, and (ii) the fibrous astrocytes of the white matter, which have straight and long processes (145–148).

1.2.2. Astrocyte functions in the brain

Astrocytes are responsible for numerous functions in the brain, including the maintenance of homeostasis and the modulation of brain circuits (148–150) **(Figure 3)**. In contrast to neurons, astrocytes cannot generate action potentials and therefore, do not exhibit electrical excitability. Nevertheless, these cells have voltage-gated ion channels on the membrane surface that allow interaction with other cells via intracellular signalling pathways. (How astrocytes sense and modulate their communication via intercellular calcium waves is further explored in 1.2.3). Astrocytes have a distinct morphological organization that favors specific responses important for regulation of the activity of a specific brain area. For instance, by maintaining close contact with neuronal cell bodies, dendrites, axons and synapses, these cells can modulate the neurovascular connection and communication between neurons (148,151,152). Interestingly, a single synapse can be modulated by an astrocyte, but one astrocyte can establish contact with thousands of synapses at the same time. Also, the cell-cell communication occurs

through gap junction channels that allow the diffusion of small molecules such as ions, neurotransmitters and energy substrates. Astrocytes are involved in immune responses and in the enwrapping of endothelial cells and pericytes with endfeet (specialized structure) in order to modulate and repair the blood-brain barrier as well as uptake nutrients from the bloodstream (149,141,153,154).

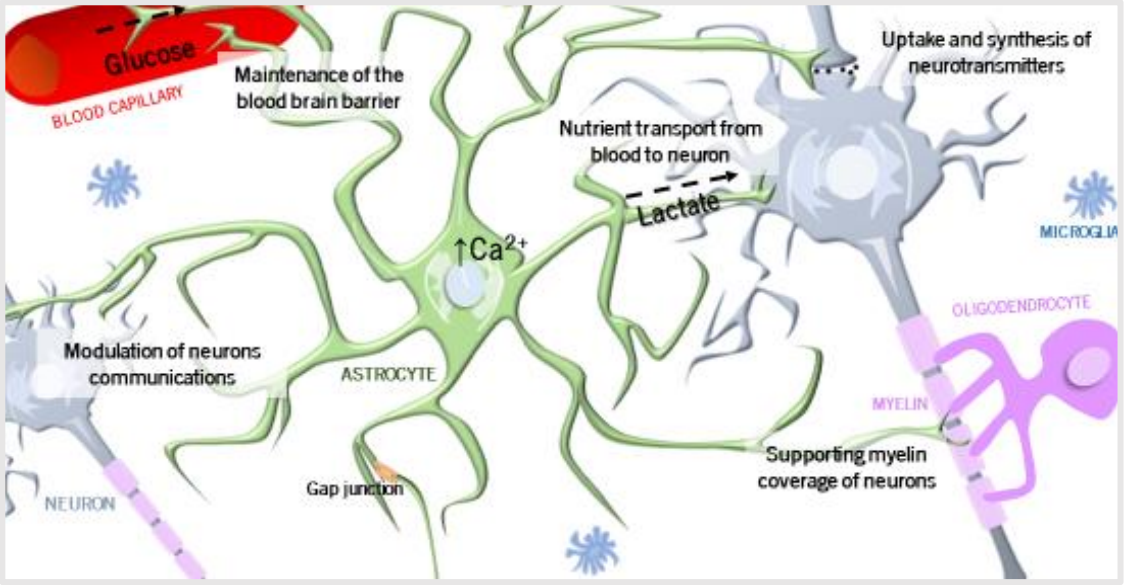

Figure 3 – The physiological roles of astrocytes cells. The brain homeostasis and architecture depend on the functionality of astrocytes. Astrocytes are involved in many brain's functional processes such as a vasomodulator, regulator of the blood-brain barrier, metabolic control (149,141,153,154), modulation of neurotransmission as well as are responsible for the uptake and synthesis of neurotransmitters and ionic balance (150,152,154).

1.2.3 Astrocytic calcium signalling mechanism and its functional role in the brain

Recent studies have shown that astrocytes can sense, integrate and respond to neuronal activity, by raising the intracellular Ca^{2+} ion concentration. It has also been demonstrated that the astrocytic Ca^{2+} elevations may occur spontaneously or via elicitation of neuronal activity (148,151,155,156). The Ca^{2+} influx is dependent on Ca^{2+} release from the extracellular space, but also from the intracellular stores of the endoplasmic reticulum (ER) and mitochondria. While Ca^{2+} from mitochondria is released via the mitochondrial permeability transition pore, Ca^{2+} released from the ER occurs via ryanodine receptor type 3 (RyR3) and inositol 1,4,5-trisphosphate receptors (IP_3Rs). In this dissertation we will focus on the IP_3Rs, since these receptors has been recognized as major players in the Ca^{2+} signalling in astrocytes, and because the physiological function of RyR3 remains unclear in these cells (157–162).

In more detail, Ca^{2+} intracellular signalling **(Figure 4)** begins with the activation of G protein-coupled receptors that trigger a signalling cascade, which allows the production and accumulation of inositol

1,4,5-trisphosphate in the endoplasmic reticulum (ER). Next, the inositol-1,4,5-trisphosphate receptor type 2 (IP_3R2), present in the ER, releases Ca^{2+} to the cytosol. The reduction of Ca^{2+} in ER induces the activation of a regulatory Ca^{2+} mechanism, through plasma membrane Ca^{2+} channels, ionotropic receptors or store-operated channels. Ca^{2+} interacts with the intracellular targets and triggers an orchestrated gliotransmitter release, that leads to (multi)synaptic responses. Remarkably, the activation of G-protein-coupled receptors in astrocytes always lead to intracellular Ca^{2+} elevation (148,156,157,163,164).

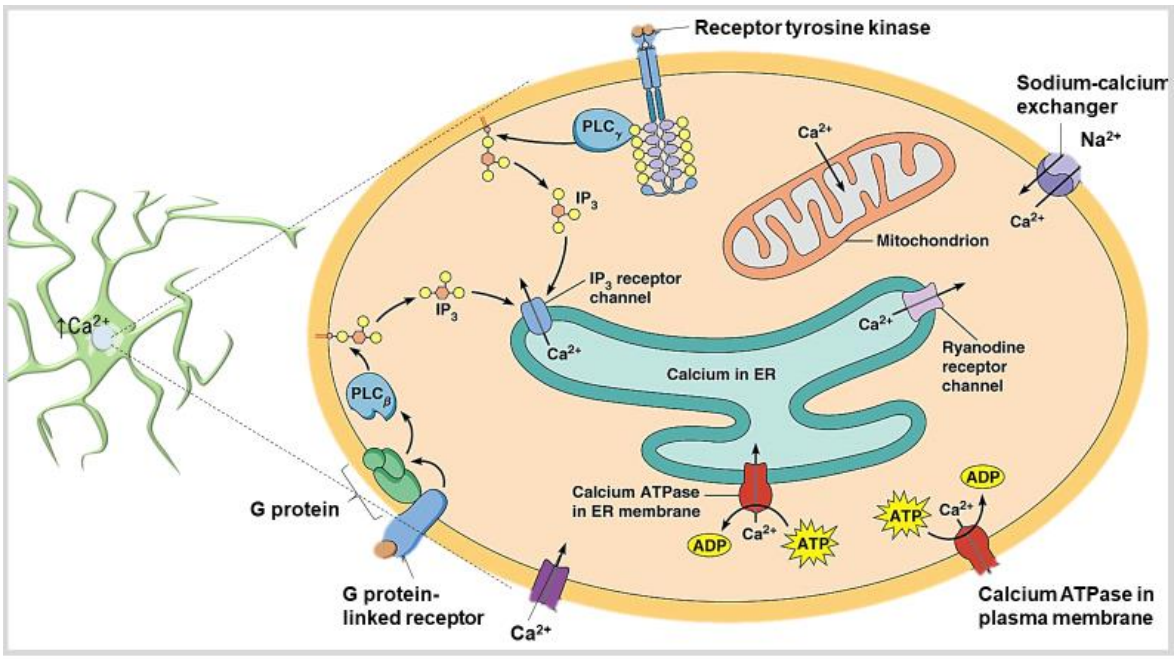

Figure 4 – Ca^{2+} intracellular signalling pathway. Ca^{2+} signalling occurs similarly in neurons and astrocytes and is dependent on inositol 1,4,5-triphosphate (IP_3). An extracellular molecular signal binds to protein receptors and induce a cascade of events, which allow the IP_3 connection to Ca^{2+} channels at the endoplasmic reticulum. This binding leads to the release of Ca^{2+} to the extracellular space. *Adapted from* (148,156,157,163,164) and *Pearson Education Inc.*

In spite of the increasing evidence emerging in the last years, the functional consequences of Ca^{2+} signalling to the brain circuits and behaviour is still growing. It seems that astrocytic Ca^{2+} elevation induces the release of chemical transmitters (such as glutamate, ATP, D-serine, GABA and peptides) to dynamically respond to changes in the surroundings or CNS insults (154,156,165,166) **(Figure 5).**

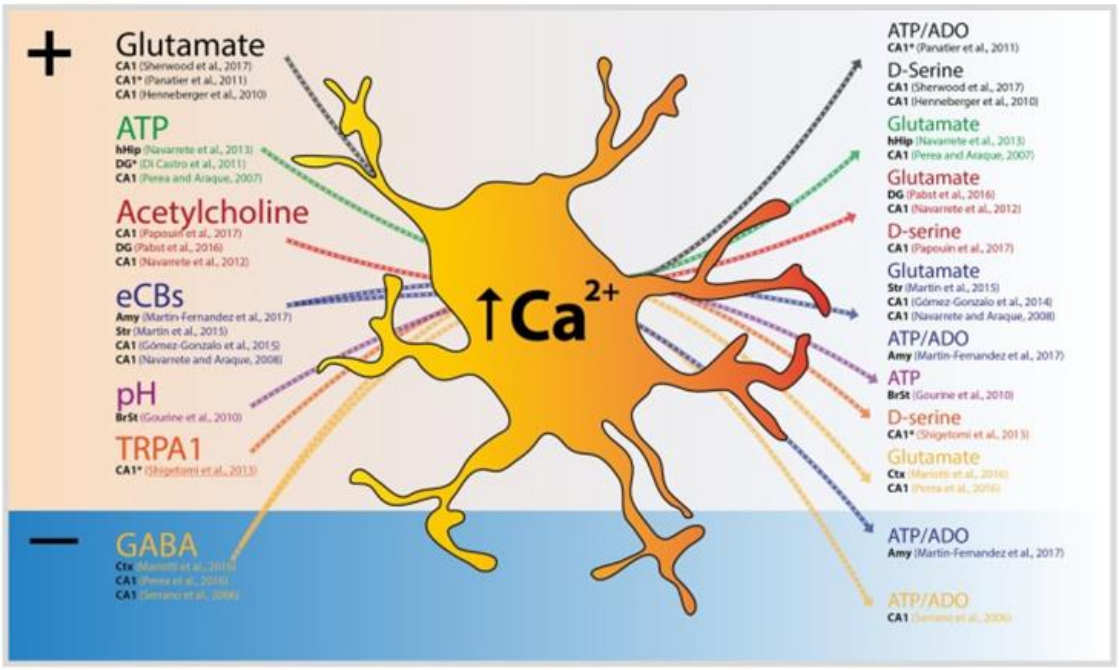

Figure 5 – Excitatory and/or inhibitory signals trigger Ca^{2+} elevations in astrocytes and neurons and lead to gliotransmitter release. Input signals (on the left) triggers astrocytes Ca^{2+} elevations, which induce orchestrated transmitter release that leads to (multi)synaptic responses (on the right). The regions of the brain affected are indicated in black: Amy, Amygdala; BrST, brainstem; CA1, CA1 subfield of the hippocampus; Ctx, cortex; DG, dentate gyrus; hHIP, human hippocampus; Str, Striatum). *Adapted from* (167).

Astrocytic Ca^{2+} elevation can be observed in the soma and in the main processes – global or restricted to thin processes and microdomains – focal. The global response activation occurs above a certain threshold of neuronal activity that triggers the G coupled protein and the signalling cascade leads to the production of IP_3 and increase gliotransmitter release. On the other hand, the focal response may happen spontaneously, via pharmacological influence or through genetic ablation of IP_3Rs, and allow the cell to selectively respond to one stimulus. The functional implications of local increase in cytosolic calcium concentration are not known, but it is thought to promote stabilization or control of synaptic events, cell survival, gene transcription and many other processes related to membrane excitability (168–170). Also, astrocytes appear to control plasticity not only in local neuronal circuits but also in synapses that occur between neurons in the long-distance. This suggests that the release of transmitters occurs with specific spatial and temporal properties. Indeed, low-frequency neuronal activity is associated with an astrocytic Ca^{2+} response that triggers the local release of transmitters. In contrast, high-frequency synaptic activity induces long-range effects at different synapses (171–173).

Accordingly, the Ca^{2+} signalling pathway is thought to be significant for the healthy function of neuronal networks and dysregulation of Ca^{2+} signalling components has been widely implicated in the pathogenesis of brain disorders.

1.3. The IP_3R2 KO mouse model

The use of genetic tools to modulate astrocytic Ca^{2+} signalling is a promising strategy to assess the role of Ca^{2+} elevation in different behavioral dimensions: cognition, emotion, sensory processes and motor behaviours. The IP_3R2 knockout mouse model (IP_3R2 KO) has the IP_3 signalling inhibited by the deletion of the IP_3R2 receptor. Among the IP_3 receptors, the IP_3R2 is primarily and predominantly expressed in astrocytes in the rodent brain (174,175)

Despite the suppression of the global Ca^{2+} signalling, the IP_3R2 KO mice still have IP_3R2-independent Ca^{2+} signals through alternative Ca^{2+} sources, such as the plasmalemma Ca^{2+} influx or the mitochondria (158,163). In the IP_3R2 KO mice the ER Ca^{2+} is globally supressed in astrocytes but not in neurons, making the IP_3R2 KO mouse model a suitable tool to study the role of astrocytes in many pathological conditions (176). In fact, previous studies demonstrated the impact of the astrocytic IP_3R2 suppression in the ischemic brain. In the IP_3R2 KO brain, no change was observed in the neuronal population nor in the glial fibrillary acidic protein (GFAP, an intermediate filament protein from the cytoskeleton that is used as a molecular marker to identify astrocytic cell populations but also to study morphology), suggesting normal brain cell populations. The lack of Ca^{2+} waves in the astrocyte network of these mice has also been demonstrated experimentally (161,175). Interestingly, after stroke induction, the IP_3R2 KO mice displayed reduced brain damage, neuronal death and tissue loss when compared with wild type (WT) mice. Furthermore, at the functional level, genetic ablation of this receptor in the context of ischemic stroke led to a significantly improved neurological outcome, increasing the strength and sensorimotor skills of the IP_3R2 KO mice. This might suggest that suppressing Ca^{2+} signalling can be protective against neuronal death and/or brain damage (175). Another study focusing on the effect of astrocytes on ageing has shown that, unlike aged WT mice, the IP_3R2 KO does not display deficits in spatial recognition memory nor in exploratory activity. In the prefrontal cortex of aged IP_3R2 KO mice, a decrease of $NeuN^+$ cells (a marker for post-mitotic neurons) as well as an increase in $S100\beta^+$ astrocyte densities (a marker for astrocytes) were detected. In parallel with a marked reduction of dendritic tree complexity, these findings suggest that the IP_3R2 may be involved in age-related events (167). Additionally, it was recently demonstrated that deletion of the IP_3R2 receptor in mice does not interfere with the normal acquisition

of mice's developmental milestones; both male and female mice displayed regular somatic and neurological development, healthy physical maturation as well as a normal motor function and exploratory behaviour in adulthood (176).

Altogether, the IP_3R2 KO mouse seems to be a suitable tool to study the functional impact of global IP_3R2-dependent astrocytic Ca^{2+} signalling.

1.4. Astrocytes and neurodegenerative diseases

The relevance of neuron-glia interaction and the involvement of astrocytes in several neurodegenerative diseases, including Alzheimer's, Parkinson's and Huntington's diseases, has been extensively recognized and studied worldwide (177,178).

Despite the progress of the past decades, the relevance of glial cells, mainly astrocytes, in the disease context is still controversial and poorly understood. For instance, "reactive" astrocytes may release both protective and toxic molecules that affect neuronal survival. Similar to the nomenclature proposed for microglia, astrocytes were also classified according to different activation states, in which astrocytes can acquire a pro-inflammatory (A1) or anti-inflammatory (A2) phenotypes accordingly to the surrounding environment (179). In human neurodegenerative diseases including Alzheimer's, Huntington's, Parkinson's, Amyotrophic lateral sclerosis and Multiple sclerosis, it was shown that the A1-like astrocytes lose their normal function and gain a new toxic function. These findings suggest that in some cases, astrogliosis may result in a combination of a loss of astrocytes beneficial roles and a gain of harmful functions during CNS insults (178,179). Therefore, understanding the molecular changes that occur in astrocytes in response to CNS insults holds great potential to identify possible therapeutic targets (144,180).

In many neurodegenerative diseases, not only is astrogliosis observed but astrocytic glutamate uptake is also known to be impaired. In Huntington's disease, the presence of mutant huntingtin aggregates in astrocytes is associated with a marked decreased expression of glutamate transporters, leading to a reduction in glutamate uptake early in the disease. Consequently, alterations in this function may contribute to a progressive and severe phenotype of reactive astrocytes (181).

Since astrocytes promote brain homeostasis and modulate neuronal circuits via Ca^{2+}-related signalling pathways, it is not surprising that aberrant neuronal Ca^{2+} signalling can contribute to the pathogenesis of neurodegenerative disorders. Studies in young and old rodents have shown that the neuronal Ca^{2+} signalling machinery undergoes significant age-dependent changes. However, the

mechanisms behind those changes are not entirely understood (182). In Alzheimer's disease, mitochondrial impairments induce Aβ oligomers to form Ca^{2+}-permeable channels in neuronal membranes. The influx of Ca^{2+} into neurons creates an excessive metabolic load on neurons, making them particularly vulnerable to mitochondrial secondary insults and cell death (183). Also, in Parkinson's disease and amyotrophic lateral sclerosis, this mechanism of Ca^{2+} influx is presumed, although with some functional differences (184). Since astrocytes have a direct influence in neuronal circuits, these cells may be critical players in disease onset and progression. Therefore, the astrocytic calcium signalling mechanism may represent a promising therapeutic target to modulate neuronal circuits and understand disease course (184,185).

In summary, overall, the data support the possibility that abnormal neuronal Ca^{2+} signalling might contribute to the pathogenesis of MJD. The SCA3-YAC-84Q mice, a mouse model of MJD, was treated with a Ca^{2+} signalling inhibitor called dantrolene, which lead to motor performance improvement and reduction of neuronal loss in the pontine nuclei and *substantia nigra* (116). Importantly, mutant ATXN3, but not endogenous WT ataxin-3, was shown to interact with the IP_3R1 receptor (at C-terminal region of ataxin-3), increasing neuronal Ca^{2+} influx (116). Considering the homology at the amino acids level between IP_3R1 and IP_3R2 (around 70%), it is reasonable to hypothesize that mutant ATXN3 may also interact with IP_3R2 and thus contribute to altered astrocytic signalling. Also, inhibition of calpains, proteases belonging to the calcium-dependent proteases family, were previously shown to suppress the formation of intranuclear inclusions in cells containing pathological ataxin-3 (186). Altogether, these observations suggest a possible involvement of IP_3R2 in abnormal Ca^{2+} signalling in MJD, unexplored to date.

2. AIMS

In the last decades, a large body of evidence emerged to support the relevance of neuron-glial interactions and the importance of glial cells in the healthy brain as well as in neurodegenerative disease, including Alzheimer's disease, Parkinson's disease, Huntington's disease, amyotrophic lateral sclerosis and spinocerebellar ataxias. However, the involvement of glial cells, namely astrocytes, in MJD is poorly understood.

Given that ATXN3 is expressed ubiquitously in brain cells, including neurons and glial cells and that mutant ATXN3 interacts with IP_3R1 and hypothetically with IP_3R2 receptors (116), we hypothesized that abnormal Ca^{2+} signalling in astrocytes may be contributing to MJD disease process.

Although previously results showed that Ca^{2+} signalling suppressors administration improved the motor phenotype of the SCA3-YAC-84Q mice, until now, no studies related to the astrocytic Ca^{2+} signalling pathway were performed in the CMVMJD135 mouse model. Consequently, more studies are needed to dissect the contribution of dysfunctional astrocytes in the progression of MJD, focusing on the role of the IP_3R2 receptor.

Hence, the main goal of this dissertation was to understand the contribution of astrocytic (dys)function to the onset and progression of MJD. To achieve this, the study was divided into three main goals:

i. **To determine the levels of *IP_3R* isoforms and Ca^{2+} signalling related components in the CMVMJD135 mouse model:** by assessing the IP_3R receptors gene expression in affected brain areas of the CMVMJD135 mice (by quantitative real-time PCR).

ii. **To define the impact of IP_3R2 ablation on MJD onset and progression:**
   - Longitudinal characterization of IP_3R2 KO mice motor function.
   - Motor function evaluation of the double mutant mice (genetic ablation of the IP_3R2 in the CMVMJD135 model).

iii. **To evaluate the role of IP_3R2 ablation on biomarkers of MJD neuropathology:** by assessing gene expression levels of inflammatory genes in affected brain regions of MJD mice with and without *IP_3R2* gene expression.

3. MATERIALS AND METHODS

3.1. Ethics Statement

This project and all animal protocols were approved by the national authority for animal experimentation (DGAV020317, 28-09-2016) and by the Animal Ethics Committee of the Life and Health Sciences Research Institute, University of Minho (Braga, Portugal). Animal facility and the people that worked directly in animal procedures were certified by the Portuguese regulatory – Direção Geral de Alimentação e Veterinária (DGAV).

All animal procedures were conducted in consonance with the European Union Directive 2010/63/EU. The experiments were designed under the principles of refinement, reduction and replacement. Health monitoring was performed according to (Federation of European Laboratory Animal Science Associations) FELASA guidelines, where the Specified Pathogen Free health status was confirmed by sentinel mice maintained in the same animal housing room. To minimize discomfort, stress and pain to the animals, humane endpoints were defined and included a 20% reduction of the body weight, incapacity to reach food and/or water, presence of wounds in the body or signs of dehydration (133). In this study, humane endpoints were applied to 2 animals: one that had a rectal prolapse (genotype: IP_3R2-/-; Q135) and the other that had body wounds (genotype: Q135). The last animal was attacked by the homecage littermates and the wounds failed to heal despite our efforts. Furthermore, animal euthanasia protocols were established according to the final purpose: decapitation or exsanguination perfusion with saline or 4% PFA. In the second case, the mice were deeply anaesthetized with a mixture of ketamine hydrochloride (150 mg/kg) and medetomidine (0.3 mg/kg).

3.2. Animal maintenance

Animals were maintained in a conventional animal facility and under standard laboratory conditions, which includes an artificial 12 h light/dark cycle, lights on from 8:00 am to 8:00 pm, an ambient temperature of 21± 1°C and relative humidity of 50–60%. The mice were given a standard 4RF25 diet during the gestation and postnatal periods, and 4RF21 diet after weaning (3 weeks of age; Mucedola SRL) as well as water *ad libitum*. At weaning, mice were housed in groups of six animals, in filter topped polysulfone cages 267 × 207 × 140 mm (370 cm^2 floor area) (Tecniplast), using corncob bedding (Scobis Due, Mucedola SRL). Environmental enrichment consisted of soft tissue paper and shredded paper to stimulate the natural behaviour of nesting.

3.3. Mouse models and generation of experimental groups

In this dissertation, two mouse models (*Mus musculus*, strain C57BL/6) were used to understand the potential involvement of astrocytes in MJD progression. The CMVMJD135 mouse model is a well-established transgenic MJD line generated in our lab (133,134). This mouse model expresses the human ATXN3 (cDNA, isoform 3c) under the control of the CMV promoter (ubiquitous expression) at near-endogenous levels. Thus, the cDNA variant of the *ATXN3* gene carries a repeat tract with the sequence (CAG)2CAAAAGCAGCAA(CAG)129, coding for 135 glutamines. To study the impact of astrocytic Ca^{2+} signalling suppression in MJD, the IP_3R2 KO mouse model was used (kindly provided by Dr. João F. Oliveira, University of Minho, Braga, with the consent of the original authors). The IP_3R2 KO has a targeted deletion of the *Itpr2* gene that suppresses globally the Ca^{2+} signalling. The *Itpr2* gene belongs to the inositol 1,4,5-triphosphate receptor family type 2 (IP_3R2), a secondary messenger that regulates the astrocytic Ca^{2+} signalling (174).

The experimental groups were obtained in house **(Figure 6).** Firstly, the heterozygous CMVMJD135 mice were crossed with homozygous IP_3R2 KO mice and the following genotypes were obtained: wild-type (WT), heterozygous CMVMJD135 (Q135), homozygous IP_3R2 KO (IP_3R2 -/-) and heterozygous IP_3R2 KO (IP_3R2 +/-) mice as well as a double mutant of heterozygous CMVMJD135 and heterozygous IP_3R2 KO (Q135; IP_3R2 +/-). To generate the experimental groups used in this study, the obtained double mutants (Q135; IP_3R2 +/-) were crossed with the heterozygous IP_3R2 KO (IP_3R2 +/-). As a result, the following genotypes of interest were obtained: WT, Q135, IP_3R2 -/- and IP_3R2 -/-; Q135. Animals with other possible genotypes (not needed within the scope of this study) were either euthanized or shared with other lab members, as recommended in the European Union Directive 2010/63/EU, to avoid waste of experimental animals.

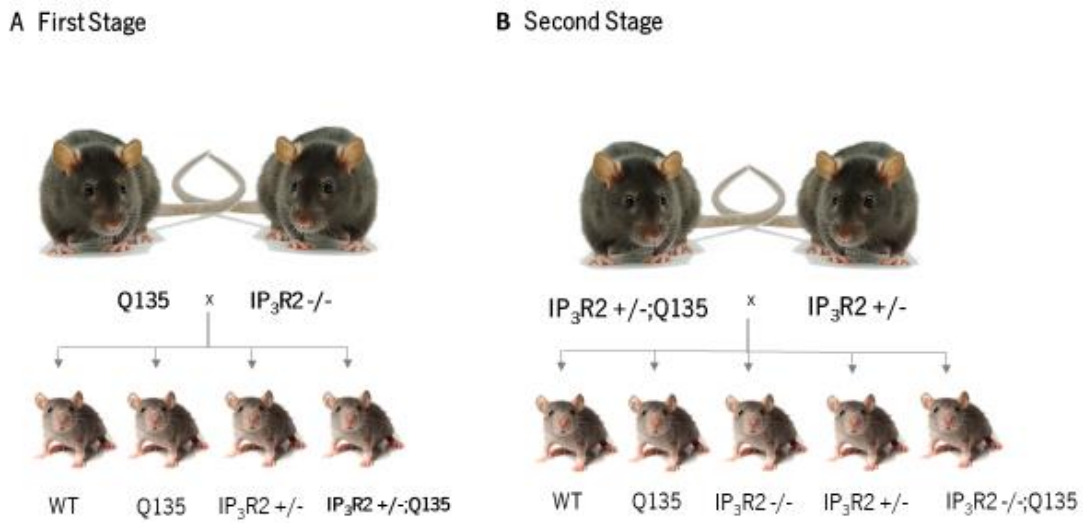

Figure 6 – Schematic diagram of mice breedings. The heterozygous CMVMJD135 mouse model was crossed with null-IP_3R2 mutant **(A).** Next, the heterozygous IP_3R2 KO (Q135; IP_3R2 +/-) was crossed with the heterozygous IP_3R2 KO **(B)** and their progeny (double mutants, wildtype and single transgenics/KO) was used in the behavioural characterization.

3.4. Mice genotyping protocols

3.4.1. Animal identification and tail biopsy

At weaning, the animals were identified with an ear punch (using an ear clip) and tail tissue (2-3mm) was collected for further DNA isolation and genotyping procedures (MJD and IP_3R2 KO genotyping protocols).

3.4.2. DNA extraction

Two chemical methods were used in this study to isolate DNA. The Citogene (Citomed) DNA isolation kit was used for the MJD genotyping protocols. To disrupt the cell membranes and release the DNA along with the broken proteins, 300 µl of Cell Lysis solution and 2 µl of Proteinase K (Novagene) were added to the tail tissue, followed by incubation overnight at 55°C (Binder, Inc.). After centrifugation at 13000 rpm, for 8 minutes, the supernatant (containing the DNA) was transferred to a new tube containing 300 µl of 100% isopropanol for precipitation, followed by centrifugation at 1300 rpm for 8 minutes. After removing the supernatant, 300 µl of 70% ethanol were added to the pellet and the samples were centrifuged at 1300rpm for 5 minutes. The supernatant was discarded and 30 µl of DNA Hydration solution was added to the pellet. The isolated DNA was stored at 4°C and used for the MJD genotyping protocols.

For the IP_3R2 KO genotyping protocol, another chemical method to extract the DNA was used. Briefly, 300 µL of 50 mM sodium hydroxide (NaOH) was added to each tail sample, followed by incubation at 98°C in a heating block for 50 minutes. This step allowed the dissociation of the tissue and released of the cell contents. After the samples were homogenized for 15 seconds using a vortex, the reaction was neutralized with 30 µL of 1 M Tris. Next, the samples were centrifuged at 14000 rpm for 6 minutes, in which the supernatant was transferred to a new tube and maintained at 4°C for further use.

3.4.3. CMVMJD135 mice genotyping protocols

In the case of MJD genotyping, two different protocols were used: firstly, to determine mice's genotype and, secondly, to determine the CAG repeat length of transgenic animals.

These protocols were established and described previously in P. Maciel Lab (134) . The primers TR1((5′-GAAGACACCGGGACCGATCCAG3′) and TR2 (5′-CCAGAAGGCTGCTGTAAAAACGTGC-3′) were used to amplify the transgene (454bp) and the primers mmMJD89 (5′- CAAAGTAGGCTTCTCGTCTCCT-3′) and mmMJD24 (5′-AGTGCTGAGAACACTCCAAG-3′) were used to amplify the mouse endogenous *Atxn3* gene (800 bp), which was used as an internal control for the PCR.

Briefly, for the identification of transgenic animals, 12 µl of the reaction mixture and 0.5 µl of each DNA were added to respectively PCR tube. The reaction mixture was composed by nuclease free-water, the primers mentioned above (TR1, TR2, mmMJD89 and mmMJD24; 66ng/ µl) and Taq Supreme NZYTech (a ready-to-use solution containing a robust DNA polymerase derived from Taq DNA polymerase, dNTPs, $MgCl_2$, reaction buffer and additives at optimal concentrations for the amplification of DNA templates up to 6 kb). PCR cycling conditions were as follows: 95°C for 5 minutes followed by 35 cycles of denaturing at 95°C for 1 minute, annealing at 64°C for 1 minute, extension at 72°C for 1 minute and a final extension at 72°C for 5 minutes.

For the determination of the CAG repeat, fragment analysis was used (Stab Vida). Briefly, 48 µl of another reaction mixture and 2 µl of each DNA were added to each PCR tube. This reaction mixture was composed by nuclease free-water, Mytaq reaction buffer and Mytaq HS DNA polymerase (Bioline) as well as both pairs of the primers: MJD25a (5′-GCTGGCCTTTCACATGGAT-3′) and MJDcDNA (5′-CGGAAGAGACGAGAAGCCTAC-3′, with 5′ 6-FAM modification). The buffer solution contained dNTPs, MgCl2 and enhancers at optimal concentrations. PCR cycling conditions were as followed: 30 cycles of denaturing at 95°C for 3 minutes, annealing at 95°C for 15 minutes, extension at 55°C for 15 minutes and a final extension at 72°C for 15 minutes.

3.4.4. IP_3R2 KO mice genotyping protocol

To determine the animal's genotype, PCR analysis was performed using a pair of primers to amplify the endogenous IP_3R2 (IP_3R2 WT Forward 5'-ACC CTG ATG AGG GAA GGT CT-3' and IP_3R2 WT Reverse 5'-ATC GAT TCA TAG GGC ACA CC-3') as well as the mutant allele-specific primers (IP_3R2 NEO Forward 5'-AAT GGG CTG ACC GCT TCC TCG T -3' and IP_3R2 NEO Reverse 5'-TCT GAG AGT GCC TGG CTT TT-3') as previously described 166 . PCR cycling conditions were the following: 95°C for 4 minutes, followed by 35 cycles of denaturing at 95°C for 30 seconds, annealing at 55°C for 1 minute, extension at 72°C for 45 seconds and a final extension at 72°C for 15 minutes. PCR products were visualized by green safe staining.

3.4.5. Agarose gel electrophoresis for the separation of DNA fragments

A solution with 1,5% agarose powder and Tris Acetate-EDTA 1x buffer (TAE, used as a running buffer in the electrophoresis process) was heated in a microwavable flask until the agarose was completely dissolved in the TAE buffer. Greensafe Premium fluorescent dye (NzyTech), was added to acid nucleic visualization. These dyes bind to the DNA and afterwards allow the visualization of the DNA under ultraviolet (UV) light. The solution was placed into a gel tray with the well(s) comb(s) in place until the gel completely solidified. Next, the agarose gel was transfer to the electrophoresis unit and TAE 1x were added to the unit until covered the gel. The DNA molecular weight ladder Gene Ruler TM 1kb (ThermoFisher Scientific) was loaded into the first lane of the gel, while each sample was loaded very carefully in the other wells. Gels were visualized with GelDoc Go Imaging (Biorad), using the ImageLab software.

3.5. Behavioural analysis

Male animals (n=7-12 per genotype) were used in this study. Behaviour tests were performed during the diurnal period and the animals were tested at 6, 8, 12, 16, 20, 24 and 30 weeks of age **(Figure 7A).** Motor behaviour was assessed using the balance beam walk test (12-mm square and 11-mm round beams) and the motor swimming test. The stride length of each mice was evaluated by footprint analysis (187). Furthermore, a general health assessment was performed using a modified SHIRPA protocol (133,188,189), enriched with the adhesive removal test (190,191) **(Figure 7B).** The behavioural tests used in this study are briefly described below.

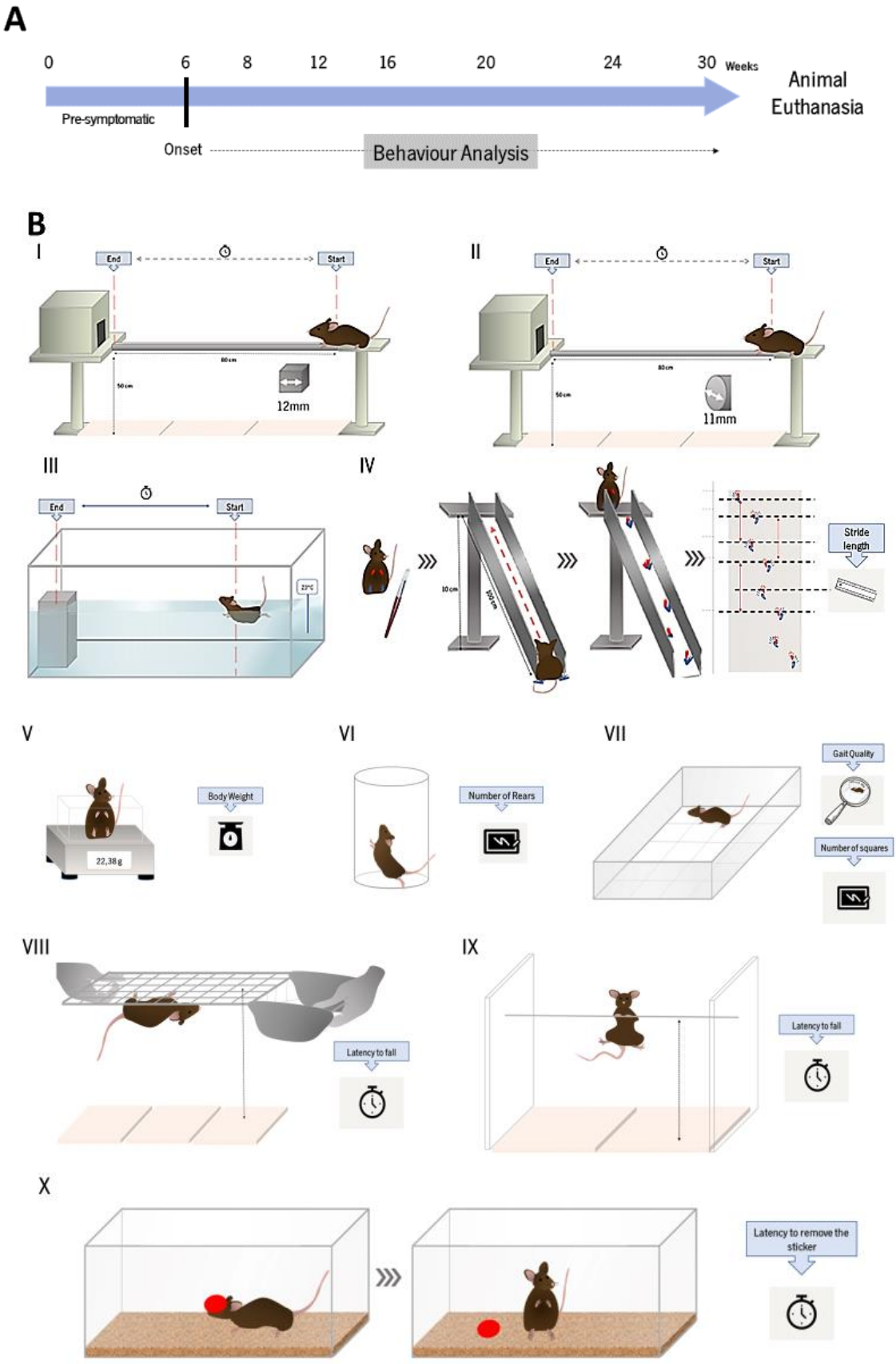
A
0
6
8
12
16
20
24
30
Weeks
Pre-symptomatic
Onset
Behaviour Analysis
Animal
Euthanasia
B
I
End
Start
12mm
II
End
Start
11mm
III
End
Start
IV
Stride length
V
22,38 g
Body Weight
VI
Number of Rears
VII
Gait Quality
Number of squares
VIII
Latency to fall
IX
Latency to fall
X
Latency to remove the sticker

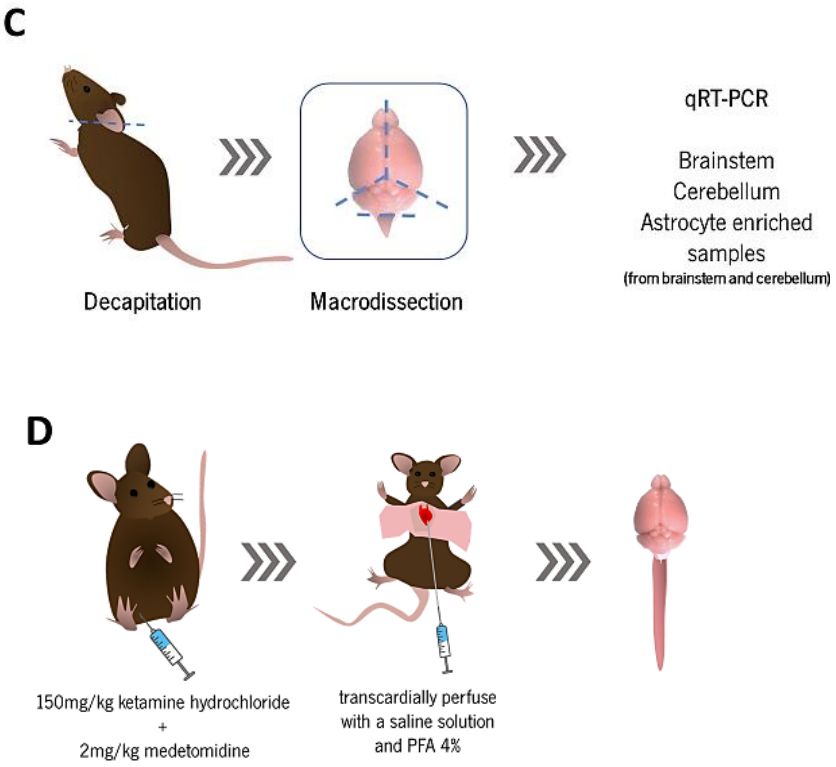

Figure 7 – Experimental design. (A) Animals were tested at 6, 8, 12, 16, 20, 24 and 30 weeks of age and euthanized at 30 weeks of age. **(B)** Behaviour tests used in this study. **(C)** At 30 weeks of age, some animals were euthanized by decapitation, their brains harvested and the brainstem and cerebellum macrodissected, while others were deeply anaesthetized, transcardially perfused with saline solution followed by 4% PFA and their brains and spinal cord harvested. These samples were used to perform pathological/molecular analyses.

3.5.1. Beam balance test

Balance and fine motor coordination were evaluated by the latency of each mouse to traverse elevated narrow beams to a safe platform. The beams consisted of long strips of PVC (1 m) with a 12 mm square cross-section or 11 mm round diameter. The beams were placed horizontally, 50 cm above the bench surface (protected with soft sponges to protect mice from falls), with one end mounted on narrow support and the other end attached to an enclosed dark box (20 cm square), into which the mouse could escape.

Mice were trained during 3 consecutive days in the squared beam (3 trials/animal) and in the fourth day the animals were tested in both beams (2 trials/animal). The time each mouse took to cross the beams were recorded and discounted if the animal stops in the beam. A failed trial was considered when an animal fell from the beam. Each animal had the opportunity to fail twice in each beam (187) **(Figure 7B.I and. II)**.

3.5.2. Motor swimming test

This test was used to evaluates voluntary locomotion, by taking in the advantage of the survival instinct of mice in water environments. Each mouse was gently placed at one end of a 100 cm clear acrylic tank filled with water (15 cm depth) and trained during 2 consecutive days (3 trials/animal), to reach a visible black platform at the opposite end. In the following 3 days (2 trials/mouse), the animals were tested and the time that took each mouse to cross the water tank was recorded. The tank was labelled with a blue line to mark the starting position and the mice swam the distance of 60 cm to complete the trial. The water temperature was maintained at 23°C by a thermostat (187) **(Figure 7B.III)**.

3.5.3. Footprint analysis

Mice hind and forepaws were coated with black and red non-toxic ink, respectively, and encouraged to walk an inclined corridor (over absorbent paper) in direction of an enclosed black box. The footprint patterns obtained for each mouse were used to analyze motor performance. The corridor had 100 cm long × 4.2 cm width × 10 cm height and a clean rectangular paper sheet were placed on the floor of the runway for each mouse run.

In this test, an inclined runway was used, instead of a horizontal one, since mice tend to run upwards to escape. Three values were measured, for six consecutive steps, to evaluate mice stride length (187) **(Figure 7B.IV)**.

3.5.4. SHIRPA protocol (SmithKline Beecham Pharmaceuticals; Harwell, MRC Mouse Genome Centre and Mammalian Genetics Unit; Imperial College School of Medicine at St Mary's; Royal London Hospital, St Bartholomew's and the Royal London School of Medicine; Phenotype, Assessment)

The SHIRPA protocol is a standardized three-stage protocol used to characterize genetically modified mice at a behavioural and neurological level in a systematic and standardized manner.

In the primary stage, the behavioural and functional profile was observed, in which defects in gait and motor control or coordination can be perceived.

Furthermore, a more extensive behavioural assessment and phenotypic analysis were performed at the secondary screening. This includes the evaluation of spontaneous locomotor activity in the horizontal and vertical planes, balance and coordination. The combination of the primary and secondary

screens provides a phenotypic characterization by detecting abnormalities or variation between mice (between groups and/or time points).

In the tertiary stage, neurological reflexes were analyzed to identify potential models of neurological disease. These tests were used to analyze the phenotypic variability of transgenic and knockout phenotypes that may result from gene-targeted phenotype profile.

In this study, we enriched the SHIRPA protocol with the adhesive removal test to assess movement initiation in the mice (133,188,189).

3.5.4.1 Body weight

Mice were weighed at 6, 8,12,16, 20, 24, and 30 weeks of age, using a dynamic range scale. The dynamic range scale allowed the measurement of the body weight while mice were freely moving. **(Figure 7B.V).**

3.5.4.2. Vertical movement assessment (Rears)

Mice were placed in a viewing jar (15 cm diameter) for 3 minutes, and the number of vertical movements (including movements on and off-the-wall) was registered (192,193) **(Figure 7B.VI).**

3.5.4.3. Horizontal locomotor activity

Mice were transferred to a 15-labelled-squares arena (55×33×18 cm), and the number of squares travelled in for 1 minute were recorded. The gait quality was also evaluated, by scores as fluid, fluid but abnormal and unable to walk (194) **(Figure 7B.VII).**

3.5.4.4. Hanging wire grid test

Mice were placed on the top of a metallic horizontal grid and inverted 180° towards the surface of the bench (protected with soft sponges to protect mice from falls). With this test, the mice latency to fall off a metal grid upon exhaustion were evaluated. The maximum time of the test allowed was 120 seconds (195) **(Figure 7B.VIII).**

3.5.4.5. Wire manoeuvre

Mice were picked by the tail and the forelimbs placed to a fixed wire (where underneath soft sponges were placed to protect mice from falls). This test is based on the latency of a mouse to fall off a

metal wire upon exhaustion. The maximum allowed time of the test was 120 seconds (195) **(Figure 7B.IX).**

3.5.4.6. Adhesive Removal test

After proper restraining, the experimenter softly placed a round adhesive (8 mm diameter) on the head of the mouse and transfer the animal to a cage. The time the animal took to remove the adhesive was registered and measurement of sensorimotor ability (190,191) **(Figure 7B.X).**

3.6. Quantitative real-time PCR (qRT-PCR)

In this study, the qRT-PCRs analysis was performed to evaluate i) the relative expression of the IP_3R receptor genes in the brainstem and cerebellum of the CMVMJD135 mouse model and ii) the inflammatory profile of the double mutant animals euthanized (after behavioural assessment).

3.6.1. Tissue processing

WT (n=5) and CMVMJD135 (n=4) animals were anaesthetized with a mixture of ketamine hydrochloride (150 mg/kg) and medetomidine (0.3 mg/kg). After the withdrawal reflexes were checked to be absent, the animals were euthanized by transcardiac perfusion with a saline solution, their brain was harvested, and the brainstem and cerebellum were macrodissected. Part of the brainstem and cerebellum collected were further used to isolate astrocytes using magnetic beads (MACs; the protocol is described in detail in 3.5.2)

After behaviour assessment, WT (n=6), Q135 (n=4) IP_3R2 -/- (n=5), IP_3R2 +/- (n=4) and IP_3R2-/-; Q135(n=6) mice were euthanized by exsanguination perfusion with saline or PFA 4%, their brain harvested and the brainstem macrodissected.

3.6.2. Astrocyte isolation using magnetic beads (MACS)

Astrocytes were isolated from brainstem + cerebellum of 34-weeks-old WT and Q135 mice (n=3-4).

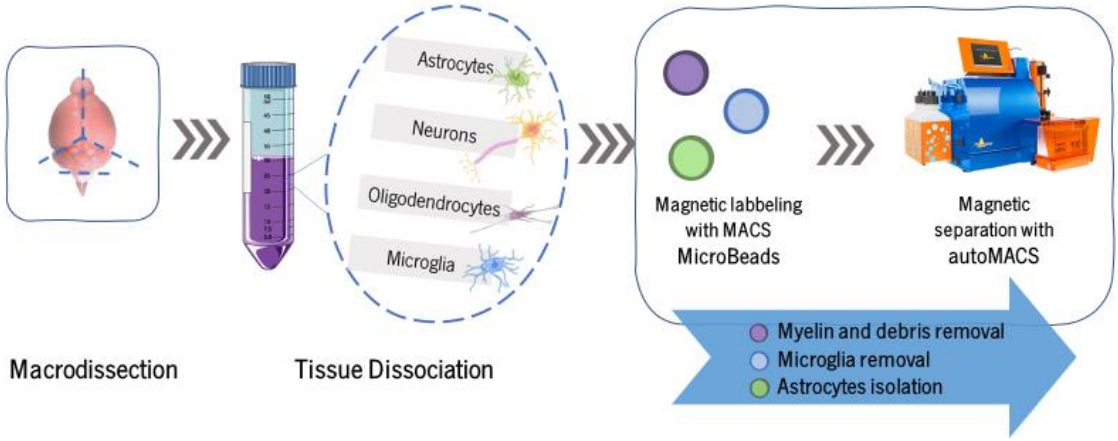

Figure 8 – Automatic cell separation technology using magnetic-activated sorting (MACS) technology (Miltenyi Biotec). The mice's brains were macrodissected and the cerebellum and brainstem were dissociated. The isolation of astrocytes was performed in a three-step procedure: i) myelin and debris removal, ii) microglia removal and iii) astrocyte isolation. In each step, the cells of interest were labelled with MACS Microbeads and placed in the autoMACS. The autoMACS magnetically separated the labelled cells in the cell suspension and transfered the unlabelled fraction to a new tube.

3.6.2.1 Tissue dissociation

The Neural tissue dissociation kit (P) (Miltenyi Biotec) was used to dissociate the brain regions of interest according to manufacturer's instructions. All steps were performed at 4°C.

Briefly, the brainstem and the cerebellum were cut in small pieces and transferred to a falcon tube containing Hanks's Balanced Salt solution without Ca^{2+} and Mg^{2+} (HBSS w/o, Sigma-Aldrich). Next, the solution was centrifuged at 4°C, for 2 minutes, and the supernatant discarded. After that, 50 µL of enzyme P and 1900 µL of Buffer X (Enzyme mix 1) was pre-heated at 37°C for 10-15 minutes. The enzyme mix 1, was added to the pellet and the solution was incubated at 37°C for 10-15 minutes.

A second enzyme mix composed by Buffer Y + 10 µL Enzyme A (-20°C) was added to the sample and the tissue was mechanically dissociated. In the first step of dissociation, a 1mL syringe and a 20G needle were used and the cell suspension was incubated at 37°C for 10 minutes under slow continuous rotation.

Lastly, a fire-polished glass Pasteur pipette was used to fully dissociate the tissue by pipetting up and down. The cell suspension was incubated again at 37°C for 10 minutes (under slow continuous rotations), before pass-through a 70 µm cell strainer. Finally, a Hanks's Balanced Salt Solution with Ca^{2+} and Mg^{2+} (HBSS w, Sigma-Aldrich) was added to the strainer. The solution was centrifuged at 300 g for 10 minutes at 4°C and the supernatant discard. Before the process of myelin removal, the cells (in the pellet) were resuspended in 0.5% BSA in PBS.

3.6.2.2. Myelin and debris removal

For this procedure, the Miltenyi Biotec's Myelin removal kit was used, according to manufacturer's instructions. Briefly, myelin-removal beads were added to the previous solution. After incubation at 2-8°C, for 15 minutes, cells were washed with 10X 0.5% BSA in PBS and the non-myelin cell debris along with the unbound beads were removed by centrifugation at 300 g at 4°C for 10 minutes, followed supernatant discard.

To each pellet was added 2 mL of 0.5% BSA in PBS and the tube was placed in the autoMACs (Miltenyi Biotec). During the automatic procedure, the autoMACs magnetically separate the labelled myelin cells in the cell suspension and transfer the myelin to a new tube.

3.6.8.3. Microglial removal

After the myelin removal, the myelin negative fraction was centrifuged at 300 g at 4°C for 10 minutes and the supernatant discard. The pellet was resuspended in 90 µl of 0.5% BSA in PBS and the microglia beads ($CD11b^+$ microbeads) were added. Next, the solution was incubated for 15 minutes at 2-8°C. The solution was washed with 1 mL of 0.5% BSA in PBS and the unbound beads, as well as debris, were discarded after centrifuging at 300 g for 10 minutes at 4°C.

After the pellet was resuspended in 500 µl of the 0.5% BSA in PBS, the cell suspension was placed in the autoMACS. In the end, the labelled and unlabelled cell fractions were collected.

3.6.2.4 Astrocyte isolation

For the isolation of astrocytes, the Miltenyi Biotec's anti-ACSA-2 kit was used according to manufacturer's instructions. Briefly, the cells suspension was centrifuged at 300 g at 4°C for 10 minutes and the pellet resuspended in 80 µL of BSA. After, the addition of 10 µL of FcR blocking reagent, the cell suspension was incubated at 2-8°C, for 10 minutes. The same procedure was conducted as in 3.5.1.3: the astrocytes-specific microbeads (anti-ACSA-2 microbeads) were added and the cell suspension was incubated at 2-8°C for 15 minutes.

Then, a wash with 1 mL of 0.5% BSA in PBS was performed, followed a centrifugation 300 g at 4°C for 10 minutes. Finally, the pellet was resuspended in 500 µL of 0.5% BSA in PBS the tube place in the autoMacs to isolate the astrocytes.

3.6.3. RNA Extraction

Total RNA was isolated from WT, Q135, IP_3R2 -/-, IP_3R2 +/- and IP_3R2-/-; Q135 littermates tissues using TRIzol (Invitrogen, USA) according to the manufacturer's protocol. Briefly, 1 mL of TRIzol was added to the samples and the tissue dissociated using a 20G needle and 1mL syringe. After incubation at room temperature (RT) for 5 min, 200 µl of chloroform was added to each tube. Chloroform separated the different nucleic acids and protein into different layers, upon centrifugation. Therefore, the samples were firstly incubated at RT for 2 minutes and then centrifuged at 8000rpm, 4°C, for 15 minutes. Next, the upper clear and aqueous phase that contains mainly RNA was carefully transferred to a new 1.5 mL tubes containing 2-propanol and the tubes were gently inverted to allow RNA precipitation. After incubation at RT for 10 minutes and centrifugation at 9000 rpm, 4°C, for 10 minutes, the RNA precipitated forming a pellet.

The supernatant was discarded, and the pellets were washed with 1mL of ethanol 70%. Followed by a centrifugation at 5000 rpm, 4°C, for 5 minutes, the RNA was eluted with RNAse free water, incubated at 65°C for 10 minutes in a thermoblock and stored at -80°C until further analysis.

3.6.4. cDNA synthesis

First-strand complementary DNA (cDNA) was synthesized using the iScript™ cDNA Synthesis Kit (Biorad). Briefly, the RNA was quantified using the Spectrophotometer NanoDrop™ (ThermoFisher Scientific). RNA quality/integrity was verified by the A260/A280 ratio and by running a small amount of RNA on a 1% agarose gel (the visualization of the 28S/18S RNA subunits in a ratio of 2:1 is indicative of intact RNA). Based on the RNA quantification, the volume of nuclease-free water and RNA used for each sample was calculated. Afterwards, 4 µl of 5x iScript Reaction Mix and 1 µl of iScript Reverse Transcriptase (RTase) was added to each reaction tube, along with the respective volume of RNA and nuclease-free water.

PCR cycling conditions used: priming at 25°C for 5 minutes, reverse transcription at 46°C for 20 minutes and RTase inactivation at 95°C for 1 minute. The synthesized cDNAs were stored at -20°C.

3.6.5. Quantitative Real-time Polymerase Chain Reaction (qRT-PCR)

Quantitative gene expression was assessed by qRT-PCR. Gene expression quantification was performed in a CFX 96TM real-time system instrument (Bio-Rad Laboratories), using SoFast Eva Green® RT-PCR reagent kit (Bio-Rad) according to the manufacturer's instructions and using equal amounts of cDNA from each sample.

To proceed with the evaluation of IP_3R gene expression in the CMVMJD135 mouse model, the amplification efficiency of *Itpr1* and *Itpr2* primers sets **(Table 1)** was determined.

Table 1 – Primers sequences used for analysis of gene expression (qRT-PCR).

Gene	Primer sequence	
	Forward (5´to 3´)	Reverse (5´to 3´)
Itpr1	CTCTGTATGCGGAGGGATCTAC	GCGGAGTATCGATTCATAGGAC
Itpr2	CTTCCTCTACATTGGGGACATC	GGCAGAGTATCGATTCATAGGG

For that, a series of 1:2 dilutions of cDNA were performed and the values of efficacy for each gene (see Supplementary information, Table 5).

Target genes primers used to characterize the inflammatory profile of the double mutants' animals (in the context of MJD) are represented in **(Table 3)**.

Table 2 – Primers sequences for each gene of interest and their product size (qRT-PCR).

Gene	Primer sequence		Product Size
	Forward (5´to 3´)	Reverse (5´to 3´)	
Gfap	AAACCGCATCACCATTCCTG	TCTGGTGAGCCTGTATTGGG	143
Ccl2	AGCTGTAGTTTTTGTCACCAAGC	GTGCTGAAGACCTTAGGGCA	155
Tnfa	GCCACCACGCTCTTCTGTCT	TGAGGGTCTGGGCCATAGAAC	106
Serping1	ACAGCCCCCTCTGAATTCTT	GGATGCTCTCCAAGTTGCTC	299
Fbln5	CTTCAGATGCAAGCAACAA	AGGCAGTGTCAGAGGCCTTA	281
Amigo2	GAGGCGACCATAATGTCGTT	GCATCCAACAGTCCGATTCT	263
Ggta1	GTGAACAGCATGAGGGGTTT	GTTTTGTTGCCTCTGGGTGT	115
S100a10	CCTCTGGCTGTGGACAAAAT	CTGCTCACAAGAAGCAGTGG	238

B3gnt5	CGTGGGGCAATGAGAACTAT	CCCAGCTGAACTGAAGAAGG	207
Sphk1	GATGCATGAGGTGGTGAATG	TGCTCGTACCCAGCATAGTG	135
Ptgs2	GCTGTACAAGCAGTGGCAAA	CCCCAAAGATAGCATCTGGA	232

The housekeeping beta-2-microglobulin (*B2m*) gene was used as an internal control. The relative gene expression was determined using the $2^{-\Delta\Delta_{Ct}}$ relative quantification method and represented as fold change normalized to the mean of the relative expression of the control group.

The PCR cycling conditions used were: denaturation at 95°C for 30 seconds, 30 cycles at 95°C for 5 seconds, annealing at 60°C for 30 seconds, plus an extension at 65°C for 5 seconds and a final extension at 95°C for 5 seconds.

3.7. Histopathological analysis

After behaviour assessment, mice (n=4-5 per group) were deeply anaesthetized and transcardially perfused with PBS and subsequently by 4% PFA (in PBS). Brains were sliced in the sagittal plan using Vibrating-blade microtome Leica VT 1000S. Slides with 40 µm-thick sections were stained with hematoxylin and eosin, according to standard procedures.

Quantification of pyknotic cells as well as $GFAP^+$ cells were performed in the pontine and deep cerebellar nuclei. The cell counting was performed using a stereology Microscope (Olympus) and the Visiopharm integrator system software (Visiopharm). The delineation of the areas of interest was made using a 4x objective to draw the mask, while a 40x 1.0 numerical aperture oil immersion objective was used to count the cells in a random counting frames of 80 µm x 80 µm in 100% of pontine nuclei and 50% of deep cerebellar nuclei.

All quantifications were carried out in the following genotypes of interest: WT, Q135, IP_3R2 KO and double mutant mice.

3.8. Statistics

The G*Power 3.1.9.2 software was used to calculate the sample size, based on a power of 0.8 (obtained from previous data) (135) and a significance level of 0.05 was used for all statistical tests.

All statistical analyses were performed using SPSS 22.0. Behavioural data were analyzed by a repeated-measures ANOVA when variables were continuous or presented a normal distribution. Values that deviated more than 1.5 interquartile ranges from the mean were considered outliers and excluded from further analyses. The assumption of normality was assessed by qualitative analysis of Q-Q plots and frequency distributions (z-score of skewness and kurtosis) as well as by the Kolmogorov-Smirnov and Shapiro-Wilk tests. The assumption of homogeneity of variances was evaluated by Levene's test.

Regarding Repeated Measurements, sphericity was tested using Mauchly's test, and assumed for all tested variables. For the comparison of means between 5 groups, the one-way analysis of variance (ANOVA) was used, followed by Tukey HSD or Dunnett T3's test (when data passed on the assumption of homogeneity of variances or when the populations variances were not equal, respectively).

Regarding non-normally distributed data and/or for the comparison of medians of discrete variables across time-points, a Friedman's ANOVA was carried out, with pairwise comparisons through the Kruskal-Wallis statistic test.

For other mean comparisons between 2 groups, the two-tailed unpaired Student's t-test was used. Effect size measurements are reported for all analyses (Cohen's d for t-tests and eta square- η^2-for ANOVAs). GraphPad Prism 8 was used to create graphs. All statistical information is reported in the supplementary data.

4. RESULTS

4.1. Longitudinal behavioural characterization of the IP3R2 KO mice

We have recently shown that the IP_3R2 KO mouse model has a normal acquisition of neurodevelopmental milestones and showed no motor deficits (176). However, the motor behavioral dimension of these mice was for that purpose evaluated at a single adult life stage (12 weeks of age). As there were no longitudinal studies on the motor behavioural characterization of the IP_3R2 KO mouse model, we sought to understand whether the constitutive deletion of the IP_3R2 interferes on the motor performance of these mice along ageing. For this, we submitted the IP_3R2 KO mouse model to various tests to evaluated different components of the behavioural motor dimension, such as motor coordination and balance, muscular strength and gait **(Figure 7B)**. Importantly, motor behaviour assessment was performed at various stages of the young adult/adult life, more precisely at 6, 8, 12, 16, 20, 24 and 30 weeks of age **(Figure 7A)**. To our knowledge, no descriptions are available for the heterozygous IP_3R2 mice (IP_3R2 HET), thus we also included these animals in our behavioral analyses.

To understand whether the suppression of global Ca^{2+} waves in astrocytes affects motor coordination, we used the motor swimming test. No significant differences were found between WT and IP_3R2 KO mice in their swimming performance **(Figure 9A)**.

Next, we performed the beam walking test, in which mice need to maintain their balance while traversing narrow beams to reach a safe dark box. When using the 12-mm square beam (the training beam), no significant differences were found in animals' performance **(Figure 9B and C).** Also, the IP_3R2 KO/HET performance did not differ statistically from their WT-littermates when difficulty was increased by using a 11-mm circle beam. **(Figure 9D).** Hence, neither IP_3R2 KO nor HET mice display balance deficits throughout age.

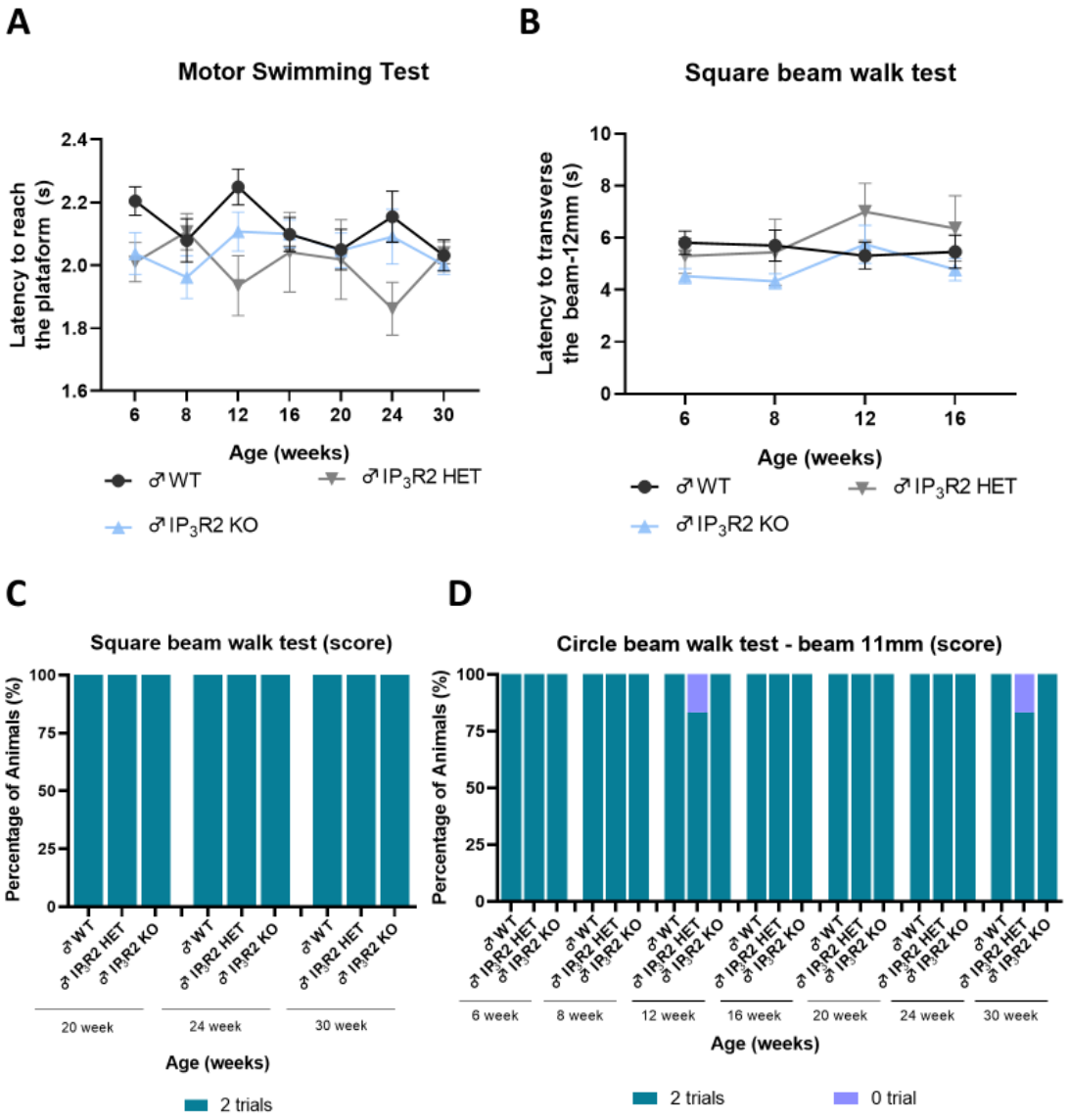

Figure 9 – The IP₃R2 KO mouse model showed normal motor function. (A) In the motor swimming test, the mice latency to reach the safe platform was measured during three consecutive days. Analysis of the total mean revealed no significant differences between WT (n=9-12), IP₃R2 HET (n=5-7) and IP₃R2 KO mice (n=7-10). *Repeated Measures ANOVA and One-way ANOVA using Dunnett T3 Post-Hoc analysis*. In the beam walk test, two types of beams were used to increase the test difficulty and evaluate fine motor coordination and balance: a square beam with 12-mm of diameter **(B and C)** and a circular beam with 11-mm of diameter **(D).** The latency to cross the square or circle beams were recorded**. In the square beam (B)** no significant interactions between genotype and age were found, more specifically between WT (n=11-12), IP₃R2 HET (n=5-6) and IP₃R2 KO (n=8-10). *Repeated Measures ANOVA and One-way ANOVA using Dunnett T3 Post-Hoc analysis*. The animal's performance was also analyzed based on the following scores: 0- 2 trials (performed the test by traverse the beam twice, as expected), 1- 1 trial (completed only one crossing of the beam) and 2- 0 trials (unable to complete the task). In both **(C) square beam and (D) circle beam (score),** no significant differences were found between mice regarding their performance. *Friedman test and Kruskal-Wallis test with pairwise comparisons.* Values are presented as mean ± SEM or as percentage of animals (%) (for the continuous and non-continuous variables, respectively).

To assess gait quality of the IP$_3$R2 KO mouse model, footprint patterns were obtained and analyzed. The distance between the front and hind footprint - stride length - can be obtained from the mean of three values in six consecutive steps. The IP$_3$R2 HET mice showed normal stride length when compared to WT-littermates. In IP$_3$R2 KO mice, the stride length differed significantly from WT only at 6 weeks, in which the IP$_3$R2 KO displayed a longer difference between the front and the hind footprint **(Figure 10A).**

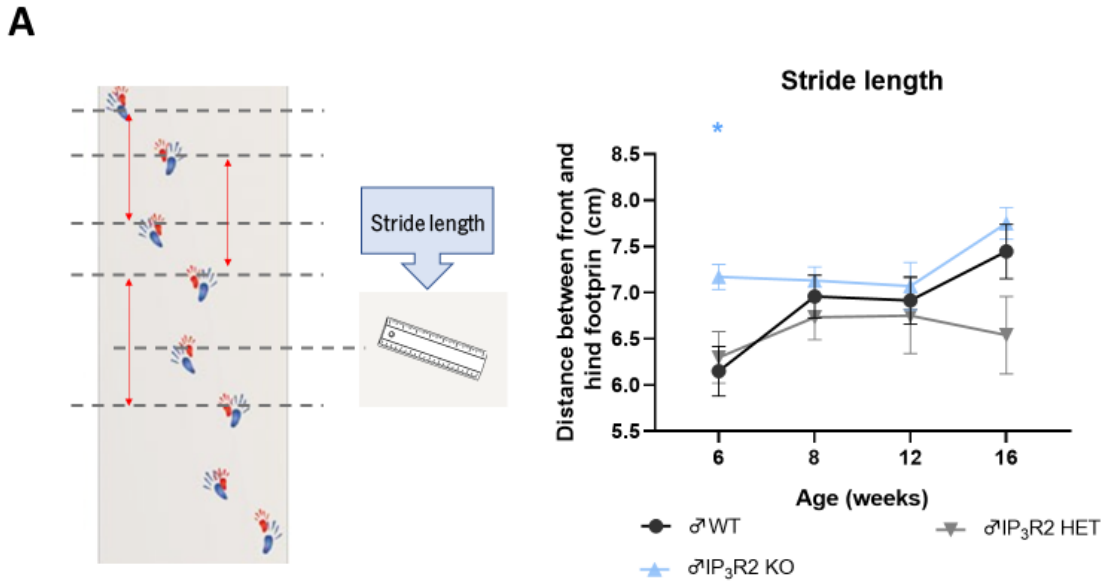

Figure 10 – The IP$_3$R2 KO mouse model presents normal gait. Footprint pattern analysis can provide information about stride length**. (A) Analysis of mice stride length** revealed significant differences between the stride length of the IP$_3$R2 KO (n=8-10) and the WT (n=11-12) mice but only at 6 weeks of age. No significant differences were found between the step alternations of these mice after this time point, indicating a uniformity of stride length among genotypes. *Repeat Measures ANOVA and One-way ANOVA using Dunnett T3 Post-hoc analysis.* Asterisks indicate significant differences between mice genotypes: * WT vs IP$_3$R2 KO. Means were considered statistically significant at a p-value *p< 0.05.

Body weight was registered at the beginning of each week in all time-points analyzed. No differences were found among genotypes, with the IP$_3$R2 KO showing a body weight gain similar to WT and IP$_3$R2 HET mice **(Figure 11A).** To measure vertical spontaneous activity (assessed by the number of vertical movements - rears), mice were transferred to a viewing jar and allowed to explore for 3 minutes. Within this clear object, it was possible to observe mice natural behaviour without disturbances. Rearing behaviour did not differ between genotypes at any time points analyzed, suggesting a normal exploratory activity and limb strength **(Figure 11B)**. Horizontal movement, assessed by the number of squares

travelled in an arena, was similar for all mice, and no significant differences were found between genotypes **(Figure 11C)**.

Altogether, these findings suggest that the IP$_3$R2 KO mouse model has a normal body weight gain as well as similar spontaneous locomotor performance when compared to control animals.

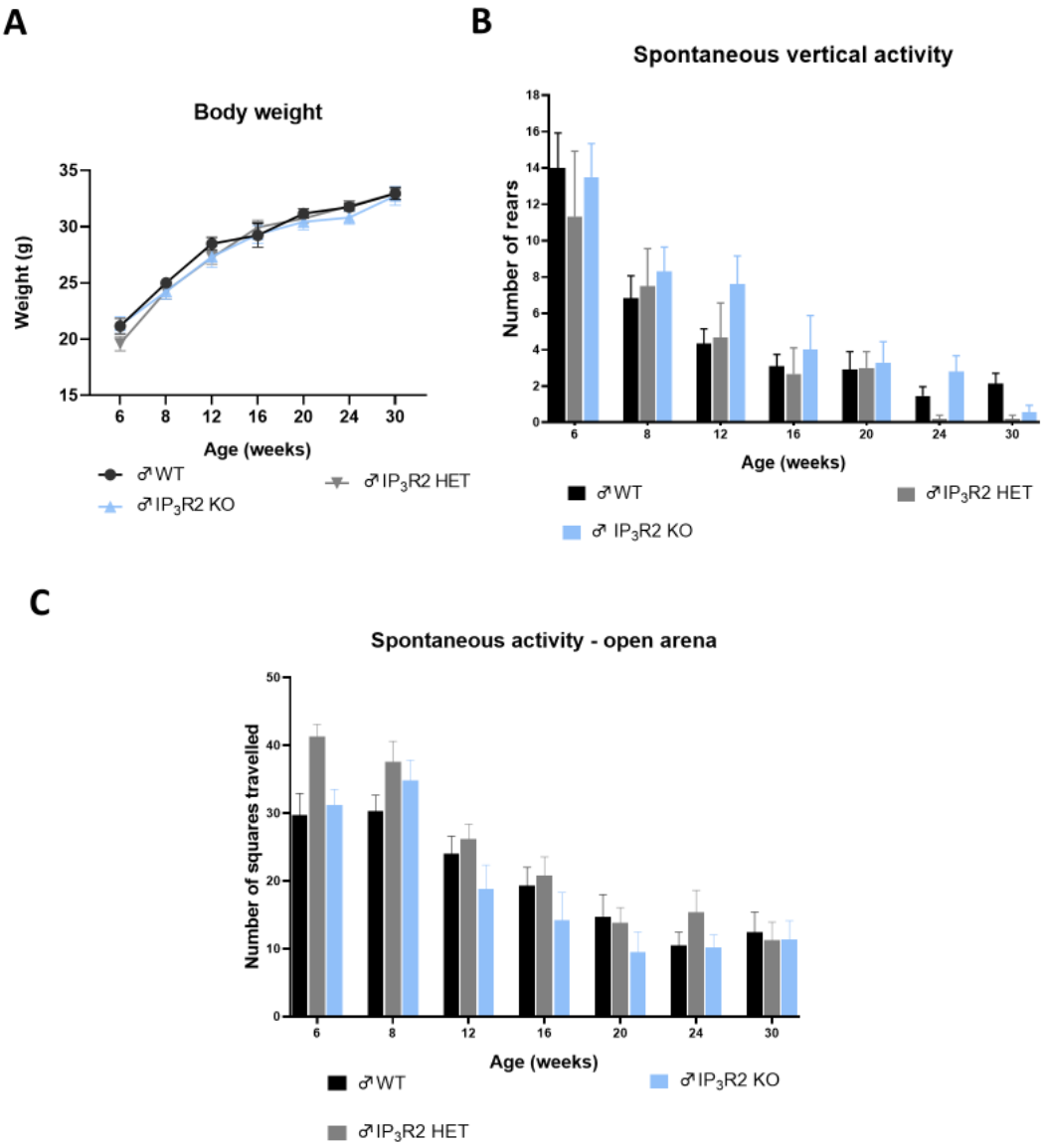

Figure 11– The IP$_3$R2 KO mouse model displayed normal body weight gain and exploratory activity. (A) Assessment of body weight with age revealed no statistical difference between WT (n=9-12), IP$_3$R2 KO (n=9-10), IP$_3$R2 HET (n=6). *Repeated Measures ANOVA and One-way ANOVA using Dunnett T3 Post-hoc analysis.* **(B) The number of vertical movements** was analyzed in a cylindrical clear perspex viewing jar. The spontaneous vertical activity was similar among genotypes [WT (n=8-12), IP$_3$R2 KO (n=7-10), IP$_3$R2 HET (n=5-6)] in all the timepoints analyzed. *Repeated Measures ANOVA and One-way ANOVA with Dunnett T3 Post-Hoc analyses.* **(C)** The **horizontal spontaneous locomotor activity** was analyzed in a squared arena. No significant differences were found between IP$_3$R2 KO (n=8-10) and WT (n=9-12) as well as with IP$_3$R2 HET (n=5-6). *Repeated Measures ANOVA and One-Way ANOVA using Dunnett T3. Post-Hoc analyses.* Values are presented as mean ± SEM.

Following, we performed a sequence of additional and more challenging tests to measure muscular strength. First, mice were placed in a metal grid that was inverted 180°. In this test, the four-limb muscular strength was evaluated. A similar limb strength was observed for both genotypes, which suggests that IP_3R2 KO mouse does not have impairments in fine coordination and muscular strength **(Figure 12A).** To evaluate the forelimb strength, the wire manoeuvre test was performed**,** which revealed no differences between genotypes, indicating that the animals also displayed similar forelimb strength **(Figure 12B)**.

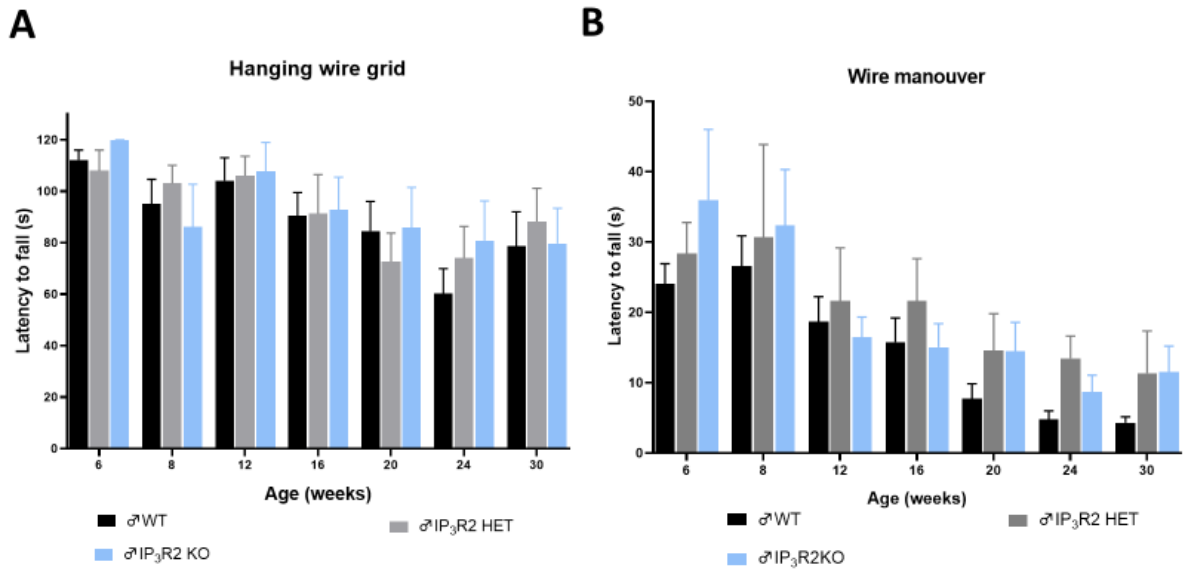

Figure 12 – The IP_3R2 KO mouse model showed no muscular strength abnormalities. (A) In the hanging wire grid test, the IP_3R2 KO (n=9-10) displayed a similar performance when compared to the WT (n=9-12) and IP_3R2 HET (n=5-6). *Friedman test and Kruskal-Wallis analysis*. **(B)** The IP_3R2 KO (n=8-10) also exhibited similar forelimb strength as the WT (n=8-12) and the IP_3R2 HET (n=5-7) **in the wire manoeuvre test**, where no statistical differences were found among genotypes. *Repeated Measures ANOVA and One-Way ANOVA*. Values are presented as mean ± SEM.

To evaluate the ability of animals to initiate movement, the adhesive removal test was performed. The animals learned the task from week 6 to week 8 since the latency to remove the sticker was lower between these two-initial time-points. Overall, no differences were observed between genotypes. (**Figure 13A and B**).

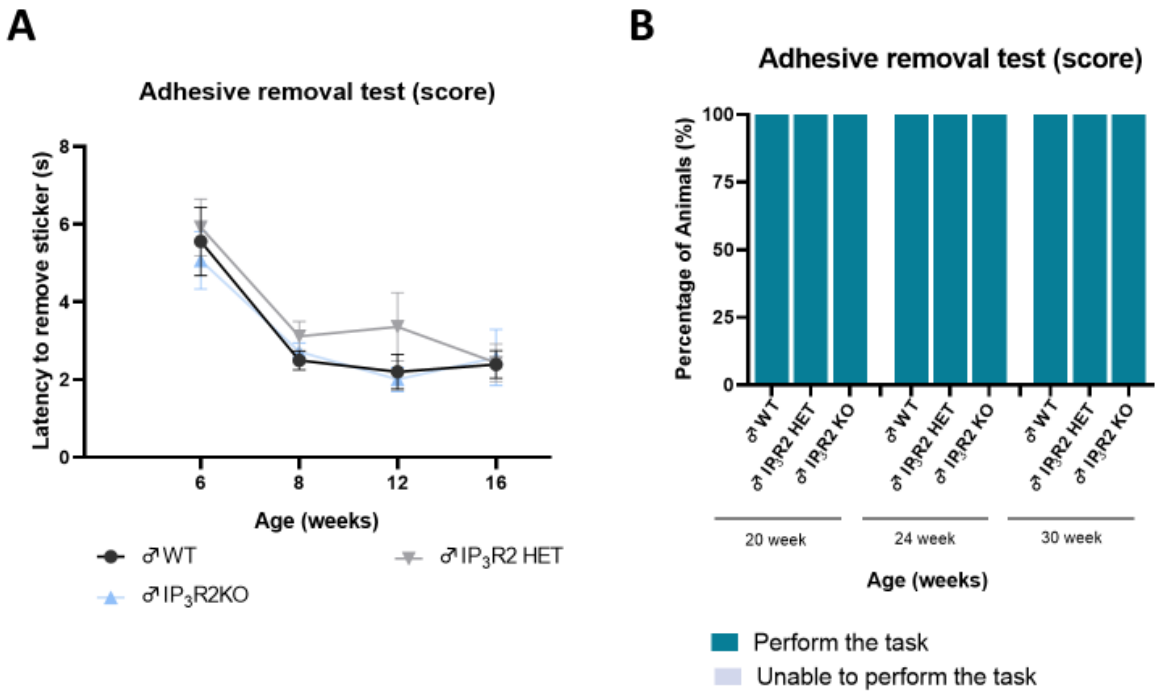

Figure 13 – The IP₃R2KO mouse model displayed normal sensorimotor ability and ability to initiate movement. (A) In the adhesive removal test, no differences were found in the mice performance to remove the sticker. *Repeated Measures ANOVA and One-WAY ANOVA with Dunnett T3 post-doc analyses.* **(D)** From 16 weeks of age on, the animals were evaluated according to their ability to remove the sticker before reaching the time limit of 120 seconds. For that, the following score was given to evaluate mice's performance: 0 – Performed the test (removed the sticker before reaching 120 seconds) and 1 – Unable to perform the test (more than 120 seconds to remove the sticker or was unable to perform the test). No significant differences were found among genotypes in the adhesive removal test. *Friedman Test and Kruskal-Wallis analysis*. Values are presented as mean ± SEM or as percentage of animals (%) (for the continuous and non-continuous variables, respectively).

This longitudinal motor characterization demonstrated that the IP₃R2 KO mouse model has normal motor coordination and sensory motor ability as well as balance and strength. Altogether, these findings suggest that the IP₃R2 KO mouse model is a reliable tool to study the functional impact of global IP₃R2-dependent astrocytic Ca^{2+} signalling in adult mice, since IP₃R2 KO mice showed normal motor function through age.

4.2. Relative expression of the IP₃ receptors in the CMVMJD135 mouse brain

The main goal of this study was to understand the contribution of astrocytic (dys)function in the onset and progression of MJD. Because no previous studies addressed the influence of IP₃R2 genetic deletion in the context of MJD, the first step was to understand if the expression levels of the *IP₃Rs* were

altered in affected brain areas of the CMVMJD135 mice. For that, we evaluated the expression levels of *Itpr1* for the IP_3R1 (receptor known to be enriched in neurons) and *Itpr2* for the IP_3R2 (receptor mostly present in astrocytes). After validating primers' efficiency (Supplementary information: Table 3 – Primers efficiency for the *Itpr1* for the IP_3R1 and *Itpr2* for the IP_3R2), we proceeded to analyse the expression of these genes in the brainstem and cerebellum.

In the brainstem, the CMVMJD135 mice (Q135) displayed a similar expression of *Itpr1* and *Itpr2* when compared to the WT mice **(Figure 14A and B, respectively)**.

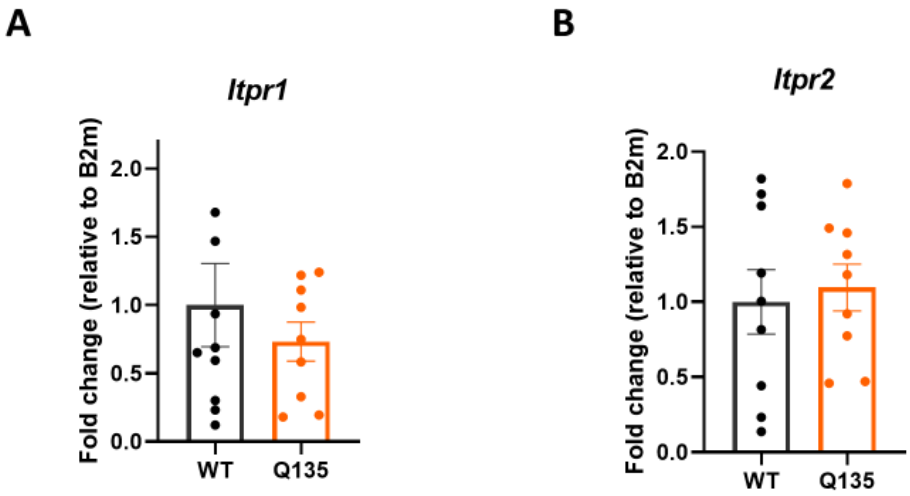

Figure 14 – The *Itpr1 and Itpr2* expression levels are not altered in the brainstem of CMVMJD135 mice. Relative expression of *Itpr1* **(A)** and *Itpr2* **(B)** are equal between WT and Q135 mice. *B2m* was used as a housekeeping and the *Itpr1* gene as a negative control. Data shown are mean values Mean ± SEM (N=6 technical replicates and n=9 animals/group) and the relative gene expression was calculated using the $2^{-\Delta\Delta Ct}$ relative quantification method and represented as fold change of gene expression. *Independent Student's t-test.*

Similarly, the relative expression of *Itpr1 and Itpr2* expression levels were identical in both genotypes in the cerebellum, as observed in **Figure 15A** and **Figure15B,** respectively.

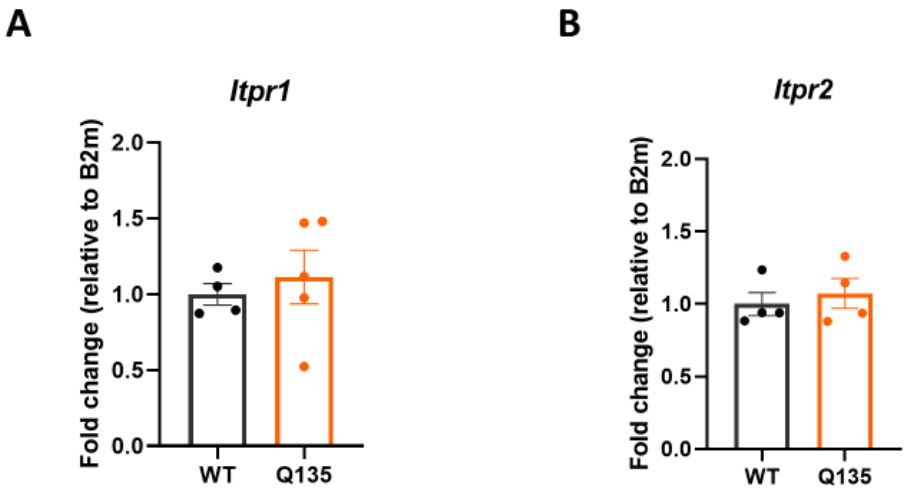

Figure 15 – The *Itpr1 and Itpr2* expression levels were not altered in the cerebellum of CMVMJD135 mice. Relative expression of *Itpr1* **(A)** and *Itpr2* **(B)** are equal between WT and Q135 mice. *B2m* was used as a housekeeping gene. Data shown are mean values Mean± SEM (N=2 technical replicates and n=3-5 animals/group) and the relative gene expression was calculated using the $2^{-\Delta\Delta Ct}$ relative quantification method and represented as fold change of gene expression. *Independent Student's t-test*. Means were considered statistically significant at a p-value *p<0.05.

Furthermore, we aimed to understand if the expression of *Itpr2* was altered in astrocyte-enriched samples, isolated from affected brain regions of the CMVMJD135 mice **(Figure 16).**

The relative expression of *Itpr2* seems to be similar among genotypes **(Figure 16A)**. Because contamination with other cell types may occur during the astrocyte isolation protocol, we analyzed the mRNA expression levels of 3 genes known to be mostly expressed in neurons (*Itpr1*, *Slc2a3* and *Reln*).

The relative expression of the *Itpr1, Slc2a3* and *Reln* were considerably high in the astrocyte samples of the CMVMJD135 mice, suggesting contamination of the astrocyte samples with neuronal cells **(Figure 16B-E)**. Thus, these results are deemed inconclusive due to sample contamination with other cell types and, therefore, a further optimization of the astrocyte enriched samples preparation protocol is needed in order to ascertain the mRNA levels of *Itpr2*.

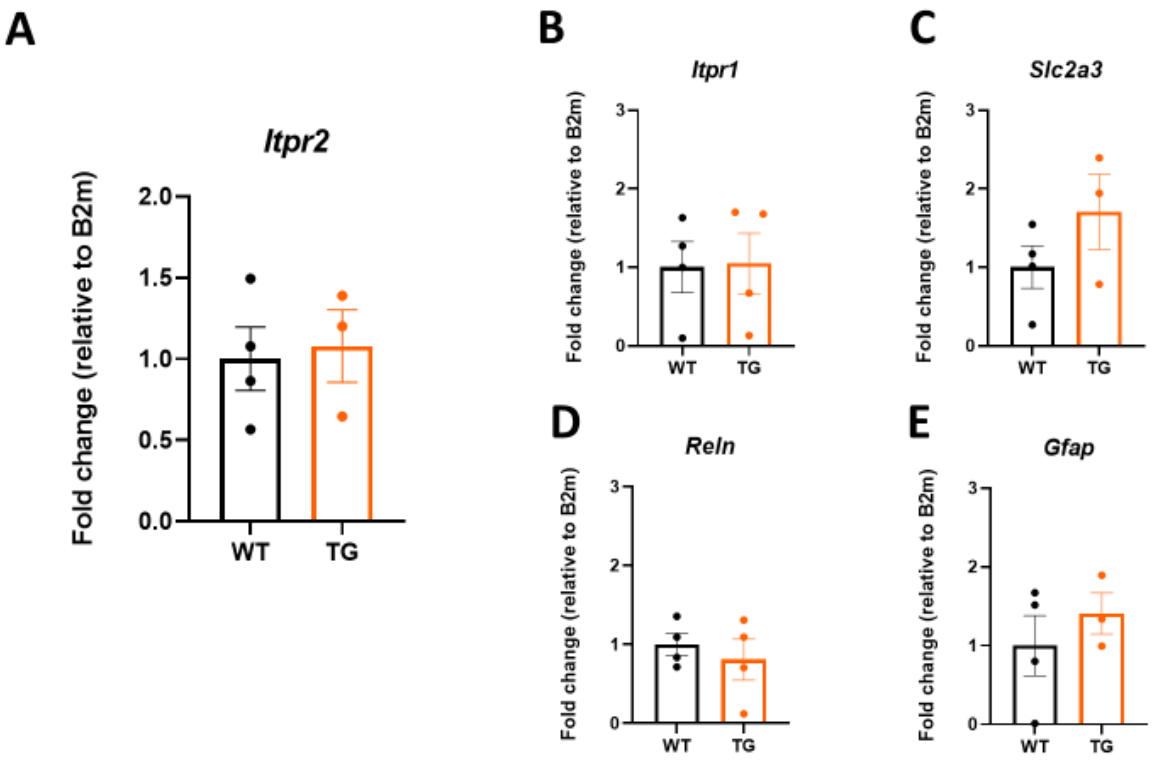

Figure 16 – *Itpr1, Slc2a3*, *Reln* and *Gfap* genes are expressed in the astrocytes enriched-samples. The selected neuron-specific genes were found to be expressed in the "astrocyte-enriched" samples, indicating that these samples were contaminated with neurons. *B2m* was used as a housekeeping gene. Data shown are mean values Mean± SEM (N= 1-4 technical replicates and n=3-4 animals/group) and the relative gene expression was calculated using the $2^{-\Delta\Delta Ct}$ relative quantification method and represented as fold change of gene expression. *Independent Student's t-test*.

In summary, assessment of gene expression of the two IP_3R isoforms by RT-qPCR demonstrates that *Itpr1* and *Itpr2* gene expression is not altered in the brainstem and cerebellum of the CMVMJD135 mice at the mRNA levels.

Nevertheless, assuming that astrocytic Ca^{2+} signalling plays a critical role in synaptic circuits, it could be expected that the depletion of the *Itpr2* gene and the suppression of the global astrocytic Ca^{2+} signalling would lead to marked changes in the mouse behaviour.

Therefore, we considered relevant to assess the impact of IP_3R2 receptor depletion in the onset and progression of MJD.

4.3. The role of IP_3R2 receptor in the pathogenesis of MJD

In this part of the work, we sought to understand if deletion of IP_3R2 receptor and consequent blockage of global astrocytic Ca^{2+} signalling impact MJD onset and progression. To achieve this, we crossed the CMVMJD135 with the IP_3R2 KO mouse. Since we have firstly characterized the IP_3R2 KO at the motor behavioural level, we confirmed that the IP_3R2 KO mice does not show motor problems or other motor deficits that could bias our results. Therefore, we crossed the two mouse models to obtain littermates of the following genotypes of interest: WT, IP_3R2 KO, IP_3R2 HET, Q135 and the double mutant (Q135;IP_3R2 KO). In this longitudinal behavioural characterization, we used the previously described and validated behaviour tests **(Figure 7B)** and we tested the animals at 6, 8, 12, 16, 20, 24 and 30 weeks of age **(Figure 7A)**.

Firstly, we analyzed the swimming ability of the double mutant and no differences were found between Q135 and Q135;IP_3R2 KO, suggesting that the differences observed are relative to the motor problems of the Q135 mouse alone (**Figure 17A).**

As disease progresses, CMVMJD135 mice have difficulties in maintaining balance and show progressive impairments in fine motor control. Therefore, we wanted to understand if ablation of IP_3R2 modified this phenotype. For this, we tested the animals in the beam walking test. No significant differences were found between the double mutant and Q135 mice (**Figure 17B**). Because Q135 mice showed a worsening of the phenotype at 16 weeks of age, that affects the ability to perform the task causing them to fall off the beams very frequently, we analyzed the data by attributing performance scores to the animals as follows: 0- performed 2 trials, 1- performed 1 trial, 2-can't walk on the beam. As expected, results showed that from 20 weeks of age onwards, the double mutant and the Q135 mice performed significantly worse than WT mice. However, no differences were found between the Q135 and the double mutant in the square beam test (**Figure 17C)**. Furthermore, a circle beam was used to increase the difficulty of the task. Difficulties in traversing the circle beam were observed starting at 8 weeks of age. After 8 weeks of age, the Q135 mice and the double mutant performed significantly worse than the WT mice, increasing the percentage of animals that cannot perform the 2 trials in the beam (**Figure 17D)**. Consistently, there were no significant differences between the double mutant and the Q135 animals' performance, suggesting that the motor and balance deficits observed in the double mutant animals can be attributed to the Q135 mouse phenotype.

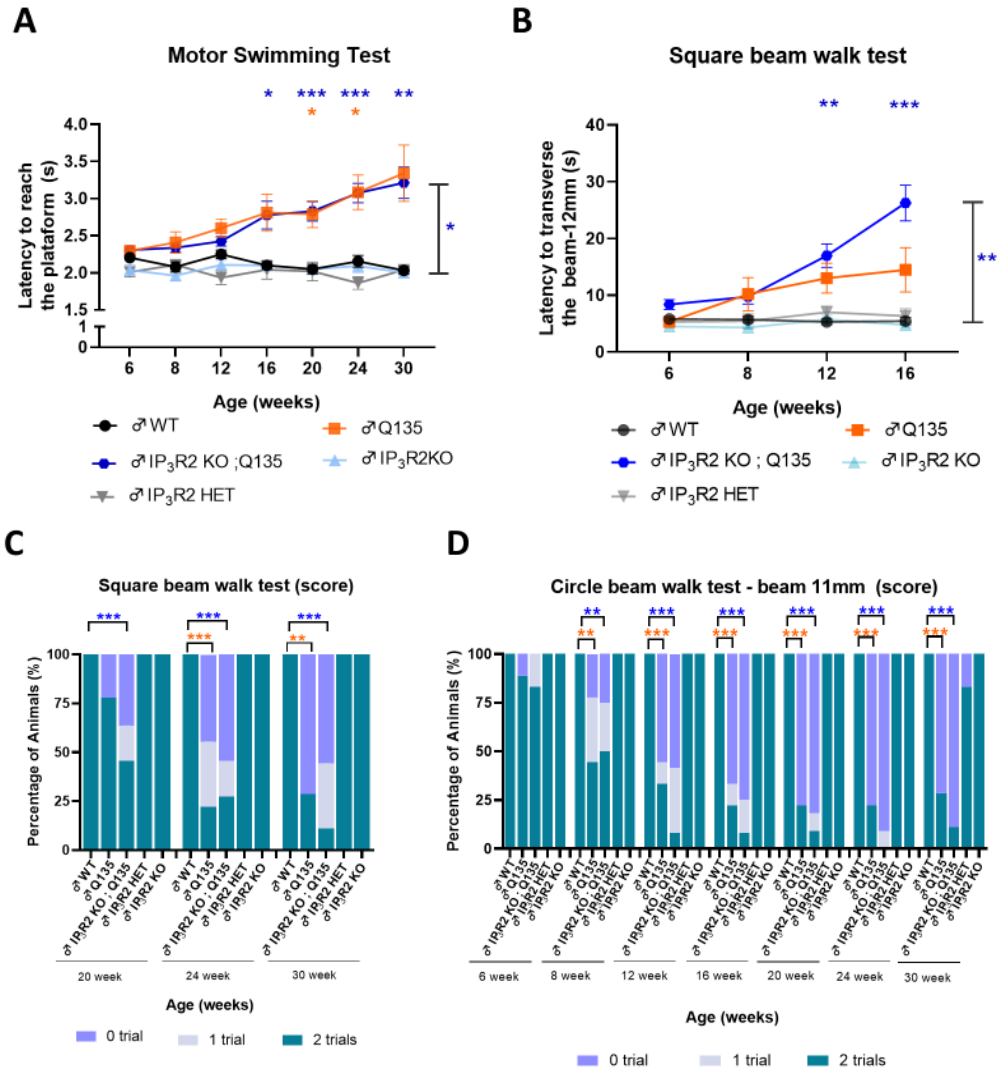

Figure 17 – The double mutant showed similar motor performance when compared to Q135 mice. (A) Motor swimming test showed that the double mutant (n=9-12) spent more time swimming to reach the safe platform than the WT (n=9-12) mice, throughout ageing. The IP₃R2 KO;Q135 mice showed no differences when compared to the Q135 mice (n=7-9). *Repeated measures ANOVA with One-way ANOVA using Dunnett T3 Post-Hoc analysis.* **(B) In the square beam test**, significant differences were found between WT mice (n=11-12) and double mutants (n=10-12) at 12 and 16 weeks of age. No differences were found between the Q135 and the IP₃R2 KO;Q135. *Repeated Measures ANOVA with Dunnett T3 multiple comparisons and One-way ANOVA with Dunnett T3 Post-Hoc analyses*. From 16 weeks of age onwards, we analyzed the square and circle beams by scoring the animals. **(C) In the square beam (score)**, significant differences were found between the double mutant and the WT mice as well as between the Q135 and the WT mice. No significant differences were found between the double mutant and the Q135 mice at 20, 24 and 30 weeks of age. *Friedman test with Kruskal-Wallis analysis*. **(D) In the circle beam walk test (score)**, results also showed significant differences between the double mutant or Q135 mice and the WT mice at 8, 12, 16, 20,24 and 30 weeks of age. However, no differences were found between the Q135 and the double mutant. *Friedman test with Kruskal-Wallis analysis*. Values are presented as mean ± SEM or as percentage of animals (%) (for the continuous and non-continuous variables, respectively). Asterisks indicate significant differences between * WT and double mutant and * WT and Q135. Means were considered statistically significant at a p-value ** p< 0.01 and *** p< 0.001.

We next used some parameters of the SHIRPA protocol to assess motor and neurological dysfunction. Footprint patterns revealed an abnormal stride length of double mutant mice throughout time, where the distance between the front and hind footprint was significantly narrower in comparison to the WT mice **(Figure 18A)**. Interestingly, at 6 weeks of age the Q135 mice displayed a significantly different stride (larger) than the double mutant, which may suggest a modest worsening of the gait deficits in these animals.

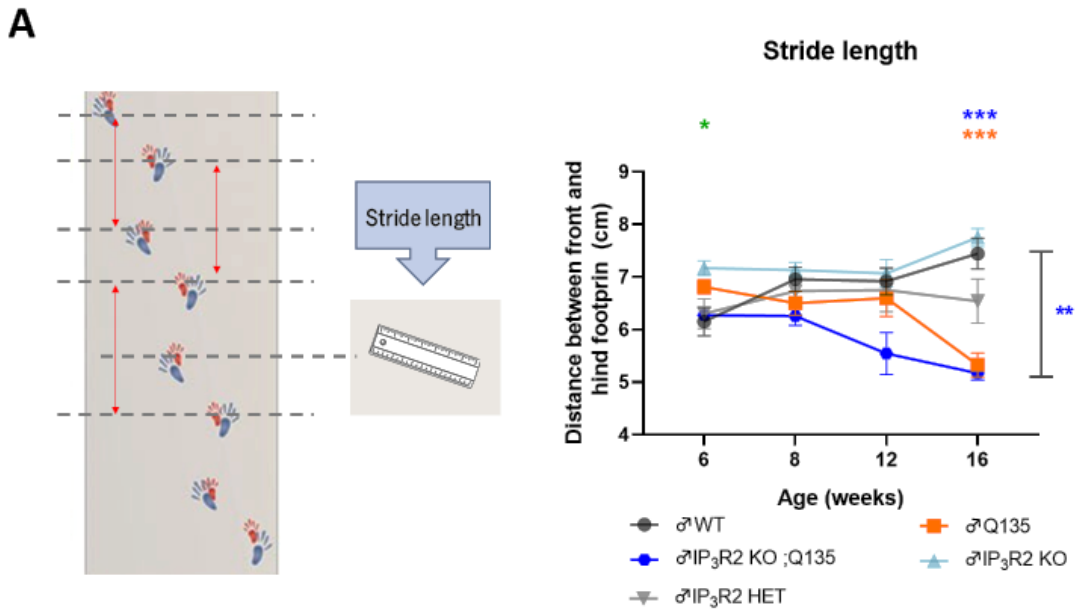

Figure 18 – Gait is modestly affected in the double mutant mice. (A) In the stride length, results showed significant differences between the double mutant (n=6-12) and the WT mice (n=11-12) throughout age. At 6 weeks of age, the stride length of the double mutant was shorter than the Q135 mice (n=4-9). *Repeated Measures ANOVA with Dunnett T3 multiple comparisons and One-way ANOVA with Dunnett T3 Post-Hoc analysis*. Asterisks indicate significant differences between * WT and $IP_3R2KO;Q135$, * WT and Q135 * Q135 and IP_3R2 KO;Q135. Means were considered statistically significant at a p-value *p< 0.05 and *** p< 0.001.

All mice gained weight at a similar rate until 12 weeks of age **(Figure 19A).** The double mutant and the Q135 mice displayed significantly lower body weight gain than the WT mice throughout time. As expected, the spontaneous vertical activity decreased with time, with the Q135 and the double mutant mice performing significantly fewer vertical movements when compared to WT mice. Nevertheless, no differences were found between Q135 and the double mutant animals **(Figure 19B)**.

In the squared open arena, the double mutant and the Q135 animals travelled significantly less than the control littermates over a 1-minute period. However, no significant difference was found between the transgenic mice and the double mutant **(Figure 19C)**.

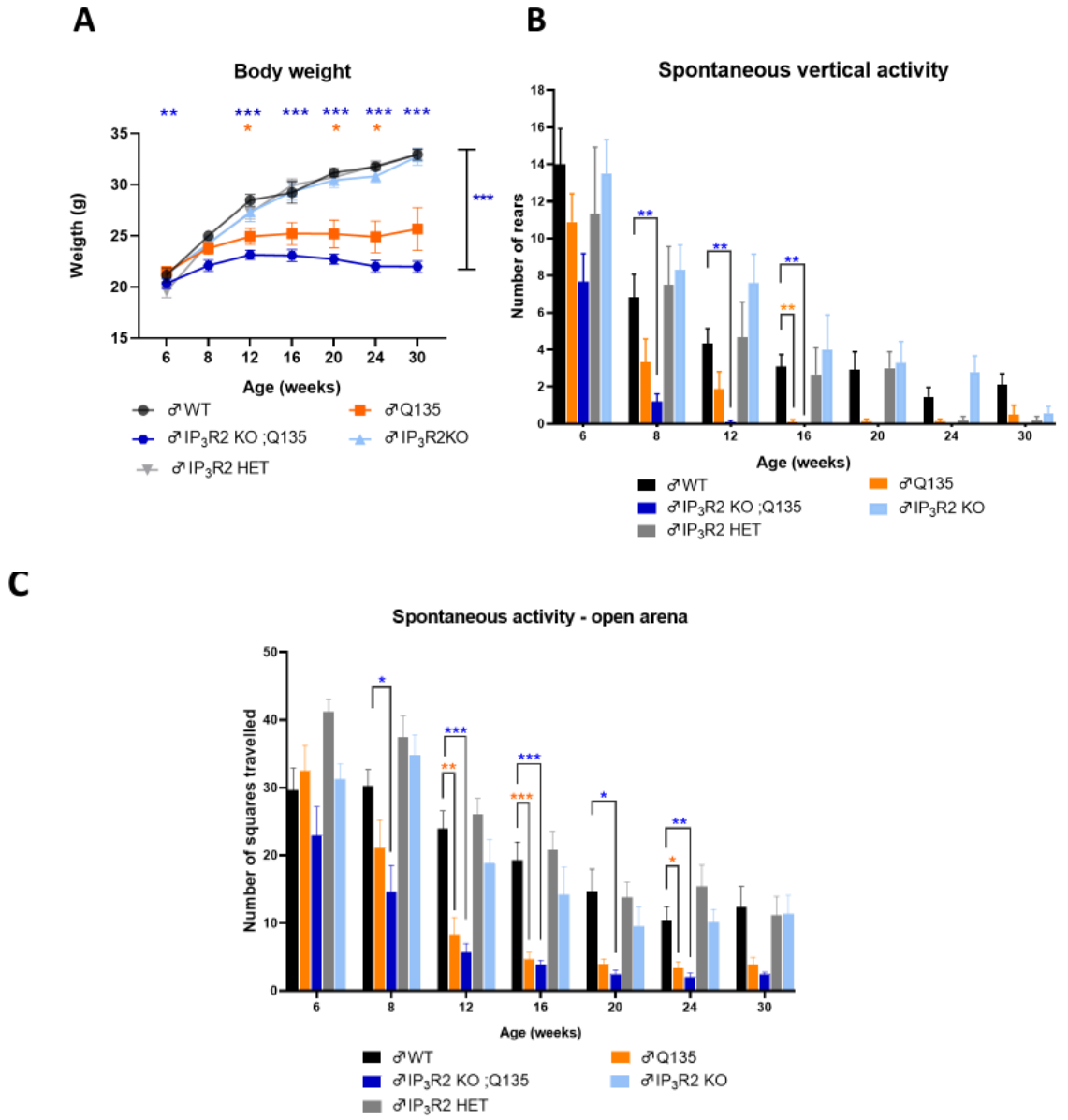

Figure 19 – Double mutant mice showed similar spontaneous exploratory behaviour when compared to Q135 mice. (A) Assessment of body weight showed significant differences between the double mutant (n=11-12) and WT mice (n=9-12). This difference was found at 8, 12, 16, 20, 24 and 30 weeks of age. *Repeated Measures ANOVA with Dunnett T3 multiple comparisons and One-way ANOVA with Dunnett T3 Post-Hoc analysis.* **(B) Regarding the number of rears,** results showed significant differences between WT (n=8-12) and double mutant (n=10-12) at 8, 12 and 16 weeks of age. It was also found differences between Q135 mice (n=6-9) and WT mice at week 16 of age. *Repeated Measures ANOVA with Dunnett T3 multiple comparisons and One-way ANOVA with Dunnett T3 Post-Hoc analysis.* **(C) In the squared open arena**, the double mutant mice (n=10-12) travelled a lower number of squares in comparison to the control mice (n=9-12), showing lower horizontal spontaneous activity**.** Results revealed significant differences at 8, 12, 16, 20 and 24 weeks of age. *Repeated Measures ANOVA with Dunnett T3 multiple comparisons and One- way ANOVA with Dunnett T3 Post-Hoc analysis.* Values are presented as mean ± SEM or as percentage of animals (%) (for the continuous and non-continuous variables, respectively). Asterisks indicate significant differences between * WT and double mutants and * WT and Q135. Means were considered statistically significant at a p-value *p< 0.05, ** p< 0.01 and *** p< 0.001.

Loss of muscular strength is a very early and severe symptom observed in the Q135 mice. Thus, forelimb and hindlimb strength were also evaluated. In the hanging wire grid both Q135 mice and double mutant showed a significantly lower latency to fall from the grid when compared to WT-littermates **(Figure 20A)**, suggesting that limb muscular strength is diminished in these animals, but is not altered by the absence of the IP_3R2, being the phenotype attributed to the Q135 animals. Accordingly, both Q135 mice and double mutant displayed less forelimb strength in the wire manoeuvre test **(Figure 20B).**

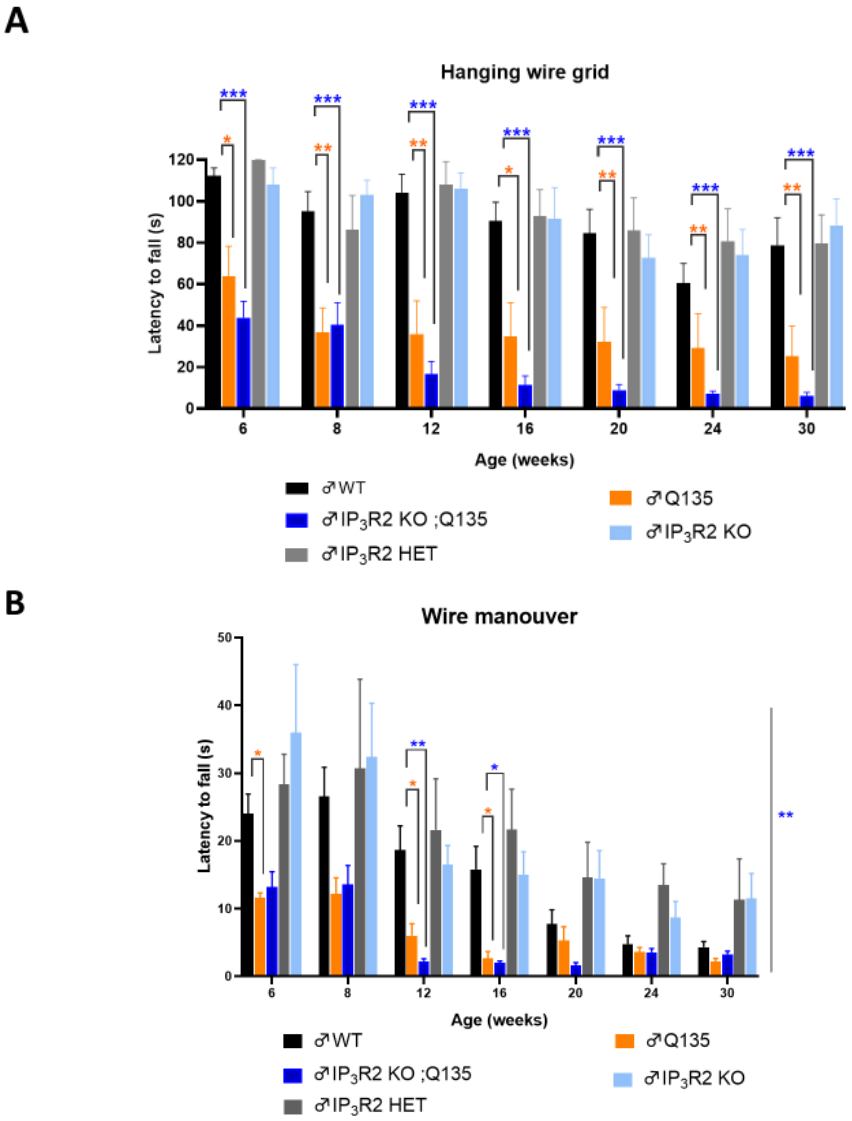

Figure 20 – The double mutant displayed loss of limb muscular strength similarly to Q135 mice (A) In the hanging wire grid test, significant differences were found between the double mutant (n=11-12) and the WT mice (n= 9-12) at 6, 8, 12,16, 20, 24 and 30 weeks of age. *Repeated Measures ANOVA with Dunnett T3 multiple comparisons and One-way ANOVA using Dunnett T3 Post-Hoc analyses* **(B) Regarding the wire manoeuvre test**, similar results were found. The double mutant (n=10-12) have less forelimb strength than WT mice (n=8-12) at 6, 8, 12 and 16 weeks of age. *Friedman test with Kruskal-Wallis analysis*. Values are presented as mean ± SEM or as percentage of animals (%) (for the continuous and non-continuous variables, respectively). Means were considered statistically significant at a p-value *p< 0.05, ** p< 0.01 and *** p< 0.001.

Lastly, we evaluated whether the double mutant showed any sign of movement initiation deficits. Both Q135 and double mutant animals showed an increased latency to remove the nose sticker when compared to WT-littermates, suggesting movement initiation deficits **(Figure 21A and B)**, but no statistically significant differences were found between Q135 and the double mutant, suggesting no impact of IP_3R2 ablation on this phenotype.

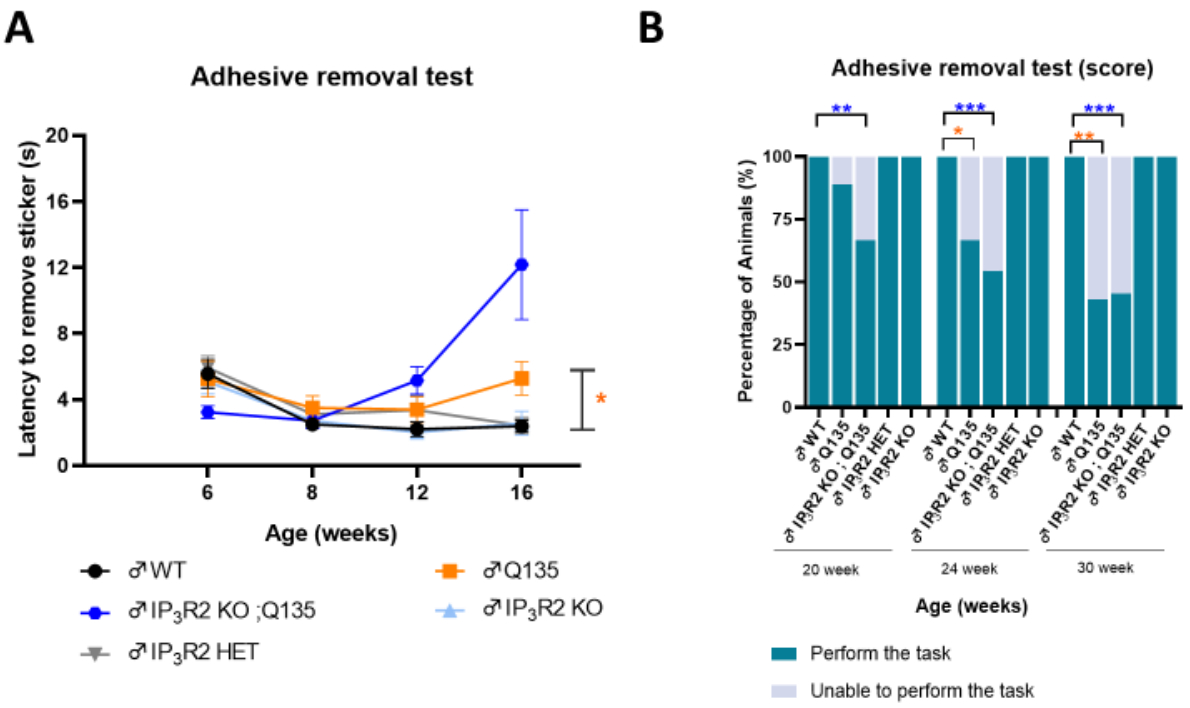

Figure 21 – The double mutant performed as the Q135 in the adhesive removal test. ***(A)*** **In the adhesive removal test**, the double mutant and the CMVMJD135 mice showed a worsening of their performance over time. *Repeated Measures ANOVA with Dunnett T3 multiple comparisons and One-way ANOVA with Dunnett T3 Post-Hoc analyses.* **(B)** From 16 weeks of age on**,** the animals were evaluated according to their ability to remove the sticker before reaching the time limit of 120 seconds. For that, the following score was given to evaluate the mice performance: 0 – Performed the test (removed the sticker before reaching 120 seconds) and 1- Unable to perform the test (more than 120 seconds to remove the sticker or was unable to perform the test). Results also indicated that the double mutant latency to remove the sticker differs significantly from WT mice at 20, 24 and 30 weeks of age. *Friedman Test and Kruskal-Wallis analysis*. Values are presented as mean ± SEM or as percentage of animals (%) (for the continuous and non-continuous variables, respectively). Asterisks indicate significant differences between * WT and double mutants and * WT mice and Q135. Means were considered statistically significant at a p-value *p< 0.05, ** p< 0.01 and *** p< 0.001.

4.4. Relative expression of specific genes in the brainstem of double mutant animals

Following behaviour characterization, the relative expression levels of *Itpr1* and *Itpr2* genes was assessed in the brainstem of IP$_3$R2KO;Q135 mice and respective littermates by qRT-PCR. Besides the IP$_3$R isoforms, the relative expression levels of inflammation-related molecules were evaluated.

As shown previously (section 4.2, above) the relative expression of *Itpr1* in the brainstem was similar among genotypes **(Figure 22A)**. Accordingly, the mRNA levels of *Itpr2* were not altered in the Q135 when compared to WT mice **(Figure 22B).** As expected, expression of *Itpr2* was not detected in the IP$_3$R2 KO nor in the IP$_3$R2KO;Q135 mice **(Figure 22B).**

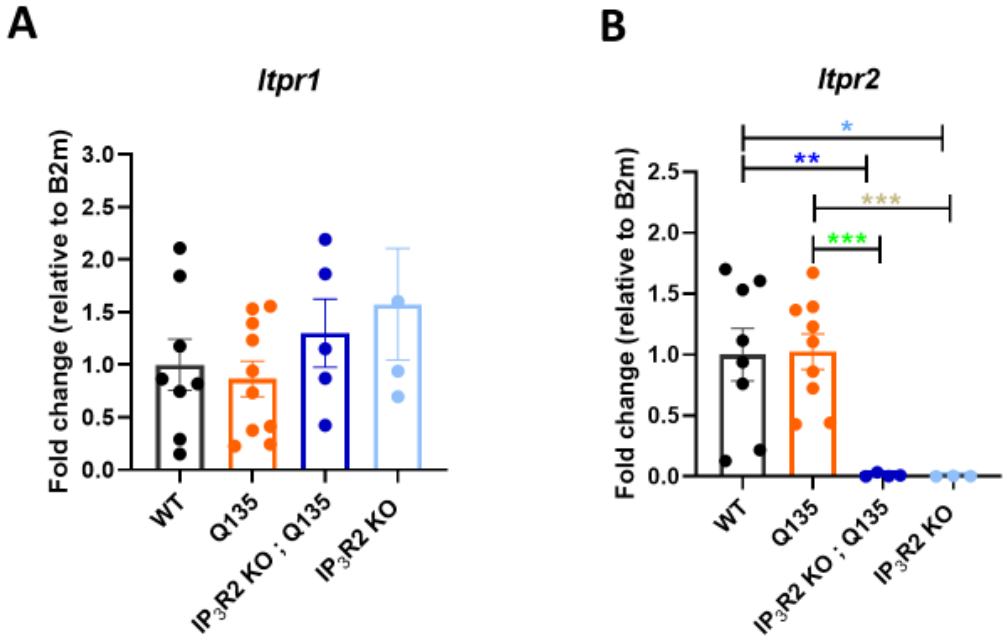

Figure 22 – Expression levels of *Itpr1 and Itpr2* in the brainstem. The relative expression of *Itpr1* (N= 2-4 technical replicates, n=3-9 animals/group) are not altered in the brainstem of IP$_3$R2KO;Q135 mice, while the expression of *Itpr2* (N=2-5 technical replicates, n=4-9 animals/group), is absent in the IP$_3$R2 KO mice and double mutant. Relative gene expression was calculated using the $2^{-\Delta\Delta Ct}$ relative quantification method. *One-way ANOVA using Post-Hoc analyses Tukey HSD or with Dunnett T3 Post-Hoc analyses.* Values are presented as mean ± SEM. Asterisks indicate significant differences between * WT and double mutants and * WT and IP$_3$R2 KO, * Q135 and double mutants and * Q135 and IP$_3$R2 KO. Means were considered statistically significant at a p-value *p<0.05 and *** p< 0.001.

Regarding the inflammatory profile of these animals, results showed no significant differences in the levels of several inflammation-related genes among genotypes, including *Gfap, Ccl2 and Tnfa* **(Figure 23A-C)**.

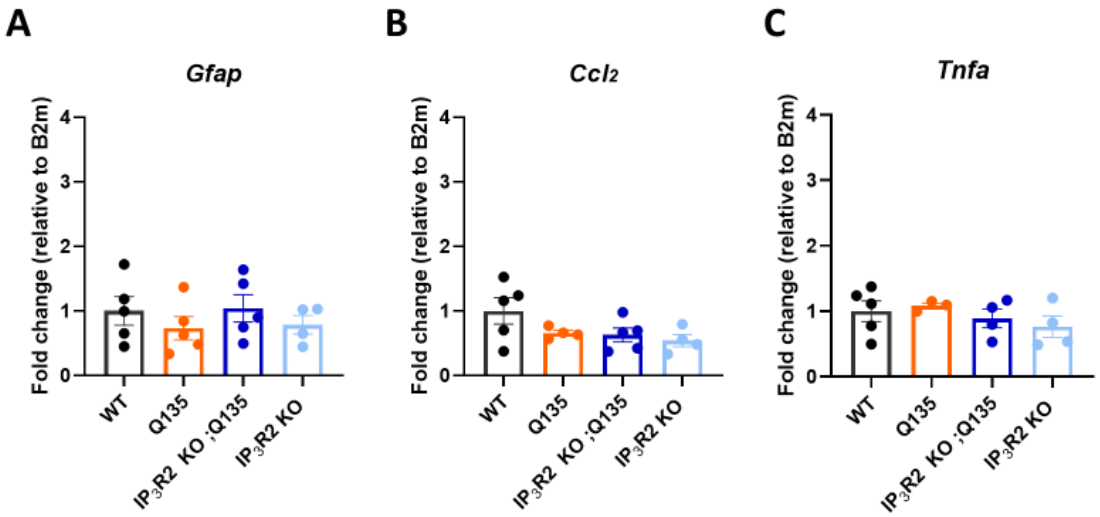

Figure 23 – The IP₃R2 KO; Q135 showed similar levels of *Gfap, Ccl2 and Tnfa* expression genes when compared to WT mice. Relative gene expression was calculated using the $2^{-\Delta\Delta ct}$ relative quantification method. *One-way ANOVA using Post-Hoc analyses Tukey HSD or with Dunnett T3 Post-Hoc analyses.* Values are presented as mean ± SEM ([A-E] (N=3-5 technical replicates and n=3-5 animals/group). The relative gene expression was calculated using the $2^{-\Delta\Delta ct}$ relative quantification method and represented as fold change of gene expression.

Recently, Liddelow, S. *et al.*(179), defined two distinct groups of reactive astrocytes based on their transcriptional profile: "A1" reactive astrocytes - astrocytes more predisposed to inflammatory and neurotoxic related functions, and "A2" reactive astrocytes - known to be more prone to anti-inflammatory and neuroprotective functions.

Based on this information, we have performed qRT-PCR analysis for some of those genes. No statistical differences were found regarding the relative expression levels of A1-associated **(Figure 24A-D)** and A2-associated **(Figure 24E-H)** genes, among genotypes.

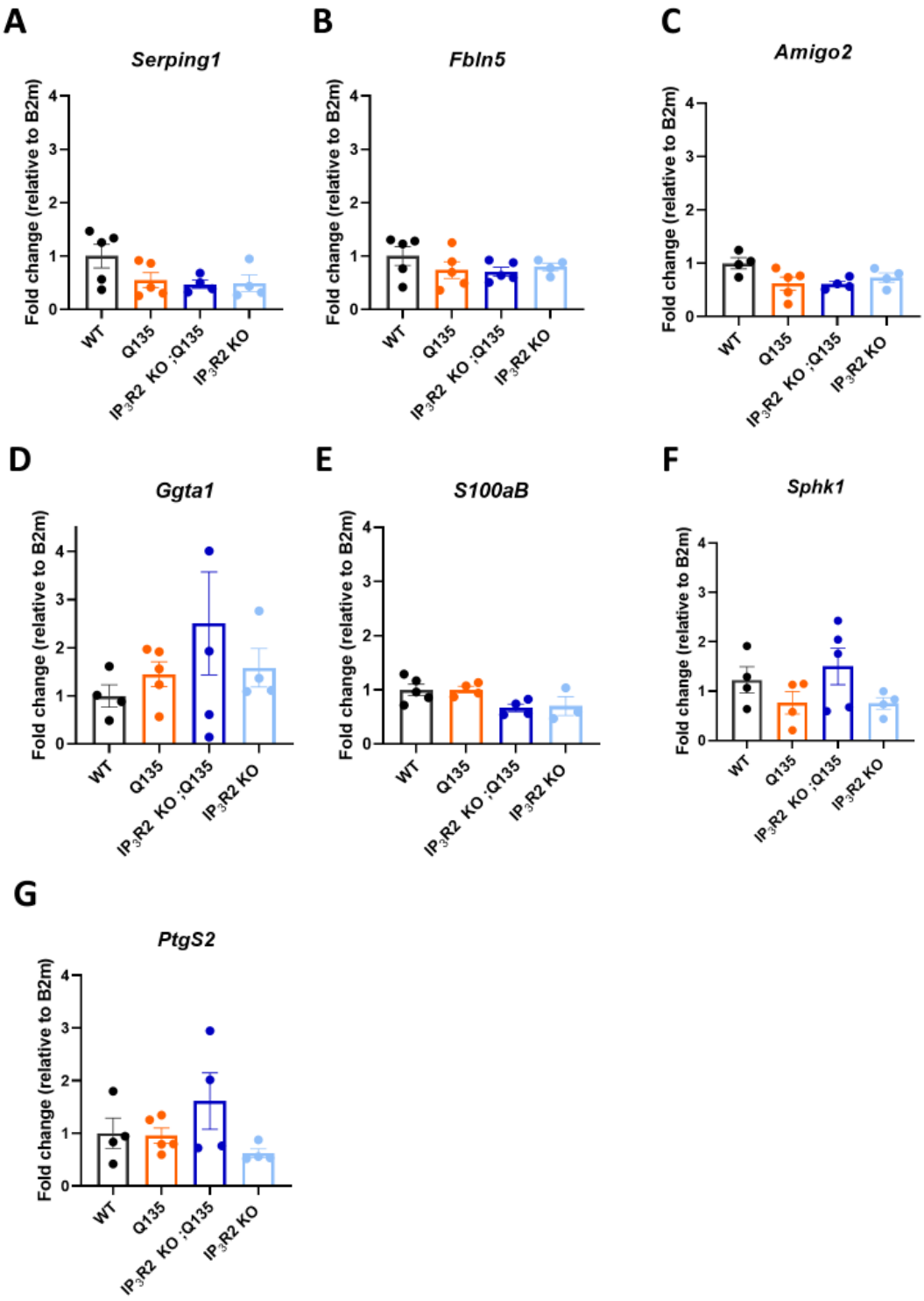

Figure 24 – The double mutant mice displayed similar expression levels of A1 and A2 "astrocytic genes" when compared to Q135 mice. Relative gene expression of (A) *Serping1*, (B) *Fbln5*, (C) *Amigo2*, (D) *Ggta1*, (E) *S100aB*, (F) *Sphk1* and (G) *PtgS2* were calculated using the $2^{\Delta\Delta ct}$ relative quantification method. *B2m was used as housekeeping gene. One-way ANOVA using Post-Hoc analyses Tukey HSD or with Dunnett T3 Post-Hoc analyses.* Values are presented as mean ± SEM ([A-D] (N=2-4 technical replicates and n=3-5 animals/group). The relative gene expression was calculated using the $2^{\Delta\Delta ct}$ relative quantification method and represented as fold change of gene expression.

4.5. Histopathological observation of brain sections of double mutant mice

The behaviour assessment and analyses of the inflammatory profile of the animals did not reveal major differences among the CMVMJD135 and double mutant mice. Although we observed that the stride length of the double mutant mice was shorter when compared to Q135 at 6 weeks of age, the biological relevance of this subtle difference is not clear. Therefore, we sought to understand whether the IP_3R2 ablation had any impact on MJD neuropathology.

Therefore, we examined histologically brain sections of WT, Q135, IP_3R2 KO and IP_3R2 KO; Q135 in the pontine nuclei **(Figure 25A)** and in the deep cerebellar nuclei **(Figure 25B)** to evaluate the presence of pyknotic cells. It was previously described that the Q135 mice showed increased number of pyknotic cells (133). No differences, however, were found between the number of these hyperchromatic cells between IP_3R2 KO; Q135 and Q135 mice (**Figure 25**).

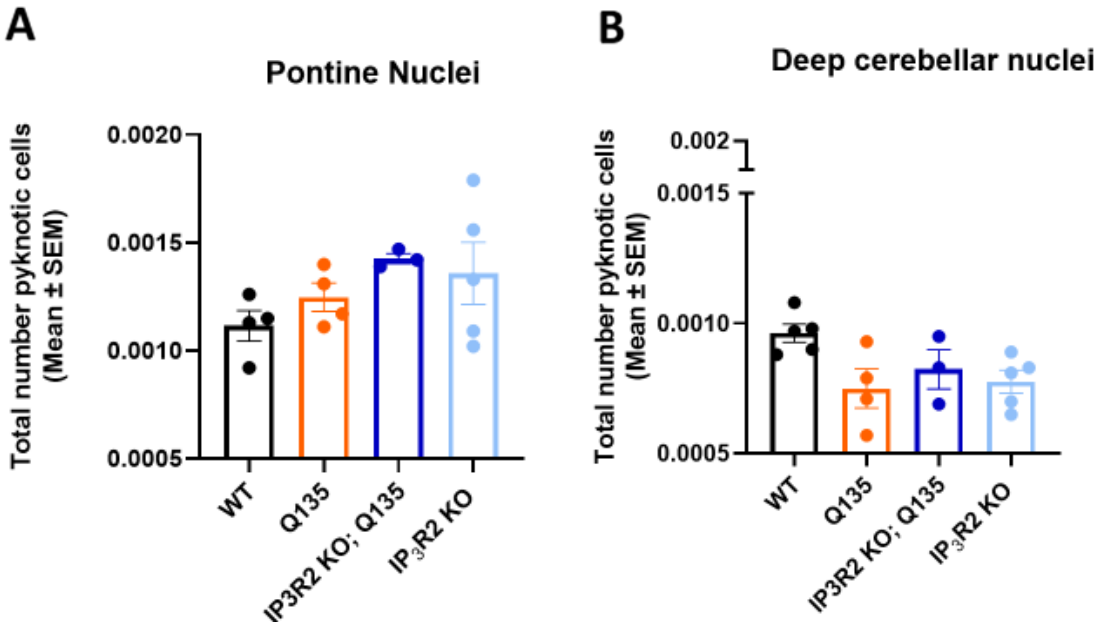

Figure 25 – The double mutant mice display similar number of pyknotic cells when compared to Q135 mice. **(A)** Quantification of pyknotic cells of the sagittal brain sections (N=3-6 sections/animal; n=3-5 animals, per group) did not reveal significant differences among genotypes. *One-way ANOVA using Dunnett T3 Post-Hoc analyses.* Values are presented as Mean ± SEM.

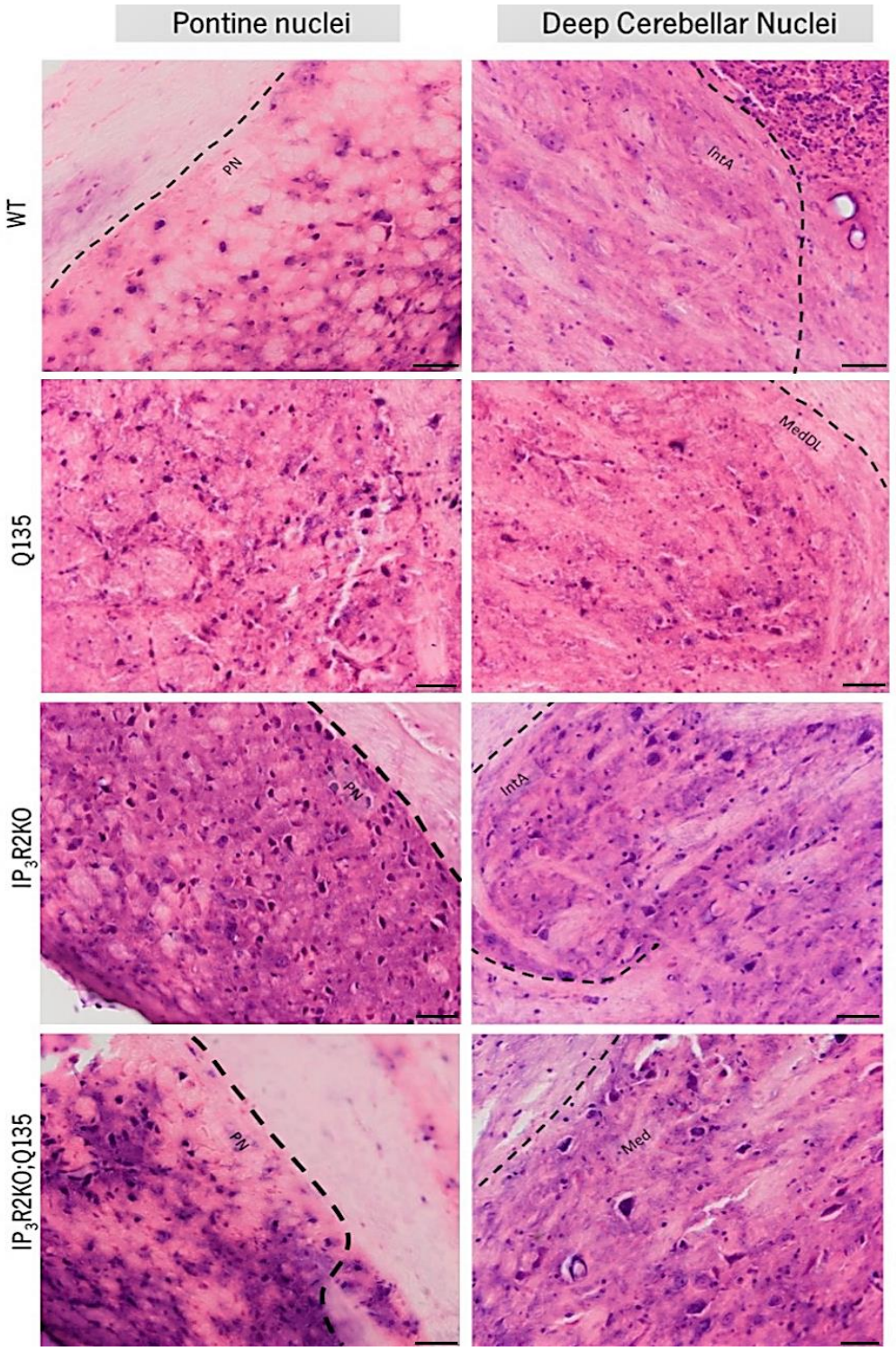

Figure 26 – Representative sections stained with H&E of WT, Q135, IP₃R2 KO and IP₃R2 KO; Q135 mouse brains. The neuropathological analysis revealed the presence of pyknotic cells in the pontine nuclei and deep cerebellar nuclei of the Q135 mice. Scale bar (black): 50 μm. PN- Pontine nuclei, IntA- interposed cerebellar nucleus, anterior part; Med- medial (fastigial) cerebellar nucleus; MedDL- medial cerebellar nucleus, dorsolateral protuberance.

5. DISCUSSION

The contribution of glial cells, mainly astrocytes, to neurodegenerative diseases has recently been suggested, with a large body of findings supporting the relevance of neuron-glia interactions and the involvement of astrocytes in the progression of several neurodegenerative diseases, including Alzheimer's, Parkinson's and Huntington diseases. Until now, the possible role of astrocytes in MJD was not been fully pursued, which generates an important gap on the field. Therefore, in this study, we aimed to further understand the involvement of astrocytes in MJD pathogenesis using a well-established mouse model of the disease (133). In this mouse model, astrocytes morphology and inflammatory profile have been shown to be altered in specific brain regions (*Duarte-Silva et al., unpublished results*). Considering these findings, we took advantage of a genetically modified mouse strain that lacks the IP_3R2, known to be enriched in astrocytes. The choice of the IP_3R2 KO mouse model relied on previous findings describing the alteration of Ca^{2+} signalling in MJD: i) the modulation of the Ca^{2+} signalling pathway (for example, using pharmacological drugs) was described to ameliorate motor impairments as well as reduce neuronal loss and astrogliosis in another MJD mouse model ii) given the fact that the IP_3R1 interacts with mutant Atxn3, and because the IP_3R1 and IP_3R2 share considerable homology between them (around 70%), it is possible that the IP_3R2 also interact with mutant Atxn3, a hypothesis that we will further pursue. [(116),(175)]. Considering that Ca^{2+} alterations were previously described in the neurons, we sought to understand if these alterations could be also occurring in the astrocytes – already shown to be involved in MJD pathology –, and since we had the IP_3R2 KO mouse available at our laboratory, this seemed a good strategy to pursue our research questions. Based on this, we crossed a well characterized MJD mouse model with the IP_3R2 KO mice to gain insight on astrocytic and the IP_3/ Ca^{2+} signalling involvement in MJD disease progression.

The IP_3R2 KO adult mice showed normal motor behaviour throughout age

The first step of this study was to characterize the motor function of the IP_3R2 KO mouse model at baseline. Indeed, we have recently described that IP_3R2 KO mice showed normal neurodevelopment milestones and normal motor function in adulthood (evaluated at 12 weeks of age). Our current results are in accordance and further expand those previous descriptions, where it was shown that IP_3R2 KO mice showed normal muscular strength, exploratory activity and time to reach the ground in the pole test

(176). Nevertheless, we performed, for the first time, a full motor characterization across ageing of the IP_3R2 KO mouse model.

Overall, our detailed behaviour assessment showed that the IP_3R2 KO mouse model does not display motor impairments or neurological reflex deficits. This longitudinal characterization is important to our study, because if the IP_3R2 KO mouse model displayed motor impairments, when we crossed with the CMVMJD135 mice, the progeny would have motor defects arising from the mouse models background and not from the direct effect of the receptor ablation.

Moreover, these findings support that the IP_3R2 KO mouse model seems to be a reliable tool to genetically address the astrocytic function in healthy and diseased brains.

The IP_3R isoforms mRNA levels are not altered in the brainstem and cerebellum of the CMVMJD135 mice

Assessment of gene expression levels of the two IP_3R isoforms revealed that *Itpr1* and *Itpr2* are not altered in the brainstem of the CMVMJD135 mouse model, a well-known affected brain region, at least at the mRNA level. In contrast, a higher expression of *Itpr2* was observed in patients and models of amyotrophic lateral sclerosis (ALS) as well as in models of acute and chronic neurodegeneration. Moreover, upregulation of IP_3R2 during inflammation in ALS can be linked to the stimulation of metabotropic glutamate receptors (mGluRs) that ultimately leads to the block of MAPK activation and cytokine/chemokine transcription, which suggest an anti-inflammatory function of *Itpr2* (196,197). Considering that inflammation-related molecules are altered in the CMVMJD135 mice only at very late stages of disease (unpublished data) and that the behavioural deficits occur prior to this observation, inflammation seems to be a consequence of several insults during disease progression, which may explain the unaltered levels of *Itpr2* in the CMVMJD135 mice used in this study. Previous data from our lab have demonstrated a decrease on several neurotoxic/neuroprotective astrocyte-specific markers in the brainstem, which suggests a dysfunction of the astrocytes in this brain area, when the symptoms are already well stablished. [Duarte-Silva *et al.,* unpublished data). On the other hand, the altered inflammatory profile could be explained by changes in the interaction between IP_3R2 and other targets (176). Hypothetically, it is possible that IP_3R2 interact with mutant ataxin-3 during inflammation in MJD and induce alterations in astrocytes function with the course of the disease. Nevertheless, further studies should be performed to i) confirm the interaction of mutant ataxin-3 with the IP_3R2; ii) unravel the involvement of Ca^{2+} signalling in the observed altered inflammatory profile in MJD.

In the CMVMJD135 mice the relative expression of *Itpr1* is not altered, which is not in accordance to what was described for several other ataxias, such as SCA1, SCA2, SCA3, SCA7, SCA15 and SCA16 (reviewed in (198)). Studies have shown that *Itpr2 is* expressed in deep cerebellar nuclei (before the second postnatal week), in a fraction of Purkinje cells and some parts of granule cells (199). Since IP_3R2 appears to play an important role the differentiation and development of postnatal cerebellum, it would be expected that alteration of *Itpr2* expression levels would leave to marked cellular changes in the cerebellum. On the other hand, it is known that the *Itpr1* is enriched in Purkinje cells. Moreover, it was also described that disruption of the intracellular Ca^{2+} signalling in Purkinje cells leads to ataxia in the mouse and human patients (199,200). Based on this, it would be interesting to explore if the expression of *Itpr1* is abundant in Purkinje cells of our MJD mouse model. If this is true, it is possible that Ca^{2+} homeostasis can be disrupted in these cells, and the integration of signals from other neuronal cells could be compromised and lead to other complications such as cerebellar dysfunction and cell death. Considering this, pursuing the functional role of the *Itpr1* in the onset and progression of MJD seems to be a promising path to explore in the future.

In our astrocytic enriched samples, no differences were found in the levels of *Itpr2* between the WT mice and the CMVMJD135 mice. However, unexpectable, we were also able to detect expression of the *Itpr1 gene*. As we did not expect to detect such higher levels of expression of the *Itpr1* gene in these samples (as this receptor is described to be mainly expressed in neurons), we assessed the expression levels of other known neuron-specific genes, *Slc2a3 and Reln,* to assess the purity of the astrocyte-enriched samples. In fact, we detected higher levels than expected of these neuronal markers in our samples, suggesting contamination with neurons. Nevertheless, some other studies have also reported a high expression of *Itpr1* in purified astrocytes (201,202). Therefore, in order to confirm these findings, further optimization of the astrocyte isolation protocol should be considered. Also, it could be reasonable to use primary astrocytes cultures or other procedures for the isolation of these cell types such as fluorescence-activated cell sorting.

Genetic ablation of IP_3R2 has mild detrimental effects in MJD

To investigate the functional relevance of the *Itpr2* ablation in MJD, we crossbred the IP_3R2 KO mice with the CMVMJD135 mice and performed an extensive motor behaviour characterization. Globally, no major differences regarding motor function were found in the double mutant animals when compared the single transgenic single, suggesting no major role of this receptor in the onset and progression of

MJD. Nevertheless, the double mutant animals had a transient slightly worse performance than the CMVMJD135 mouse model in gait parameters, suggesting that *Itpr2* genetic ablation in the context of MJD might have some mild detrimental effects, other than the ones we have tested in this study. Interestingly, similar results were described in ALS models, where genetic ablation of IP_3R2 showed no impact on disease onset and motor coordination but worsened muscular strength and decreased survival of the $SOD1^{G23A}$ mice(196). At a first glance, the detrimental effects of ablation of IP_3R2 in MJD seems contra-intuitive, as higher levels of *Itpr2* could, in theory, lead to an increased excitotoxicity damage in neurons. Indeed, it was previously demonstrated that neuronal overexpression of IP_3R2 is detrimental in ALS model (203). Thus, it would be expected that ablation of this receptor could have beneficial effects; nevertheless, and as we showed no differences in the levels of *Itpr2* in affected brain regions of MJD, the small detrimental effects observed may be caused by other effects (such as abnormal protein-protein interactions) rather than the expression levels of this gene. Contrarily to our observations, the ablation of this receptor in ischemic brain as well as in then aged brains showed to be neuroprotective (175–177,204). These are very interesting observations that indicate a distinct role of astrocytes in different contexts and disease aetiologies.

Relative expression of specific genes in the brainstem of double mutant animals

Assessment of gene expression levels of IP_3R isoforms type 1 and type 2 by qRT-PCR validates that *Itpr2* expression is depleted, as expected, in the IP_3R2 KO and in the double mutant animals. The analysis of the inflammatory profile of the animals revealed no significant differences among genotypes, indicating that the constitutive depletion of IP_3R2 did not induce neuroinflammatory changes. As mentioned before, we used a panel of genes that was previously proposed as useful to classify the phenotype of astrocytes into A1 and A2 astrocytes subtypes (as parallel to the M1/M2 phenotypes if macrophages and microglia (179), which has been widely used to characterize the phenotype of reactive astrocytes in many brain disorders. Nevertheless, our results suggest a mixed profile with an overall reduction of expression of astrocyte-specific genes in the context of MJD. Based on this, it is plausible to question whether there is a compensatory response to control the inflammatory process and maintain the cellular function.

Double mutant mice showed no alterations in pyknotic cell numbers

In order to clarify the role of IP_3R2 ablation in MJD neuropathology, we also analysed H&E stained brain sections of WT, Q135, IP_3R2 KO and IP_3R2 KO; Q135, to analyse the presence of pyknotic cells. The presence of scattered dark and shrunken cells is well demonstrated in several affected brain regions, such as the dentate and pontine nuclei, and the thalamus in MJD animal models' brains (133,134). However, we did not find any differences in H&E staining among genotypes, despite a trend towards an increase in pyknotic cells in the Q135 and double mutant mice, which are not different between them, suggesting that the genetic ablation of the IP_3R2 had no significant impact on this pathological feature.

In models of ALS, the ablation of IP_3R2 also showed no major impact on the number of motor neurons loss in the spinal cord and had no impact on microgliosis and astrogliosis (196). The observations were not similar in models of ischemia, where the genetic ablation of IP_3R2 improved the observed neuropathology, such as astrogliosis, infarction volume and neuronal loss (175). These different effects of IP_3R2 absence on neuropathology suggest that the disease context is a very relevant variable.

6. CONCLUSIONS AND FUTURE PERSPECTIVES

In this dissertation, we showed for the first time that suppression of Ca^{2+} signalling in astrocytes had no impact in several behavioural dimensions of MJD, with IP_3R2 KO;Q135 displaying a similar behavioural motor phenotype as compared to the CMVMJD135 mouse model.

Nonetheless, it is important to understand the role of the IP_3R2 ablation in the animals' neuropathology. Although no major differences were found between the double mutant and the CMVMJD135 mice, the double mutant had slightly smaller stride length when compared to the transgenic mice for MJD, suggesting mild gait abnormalities.

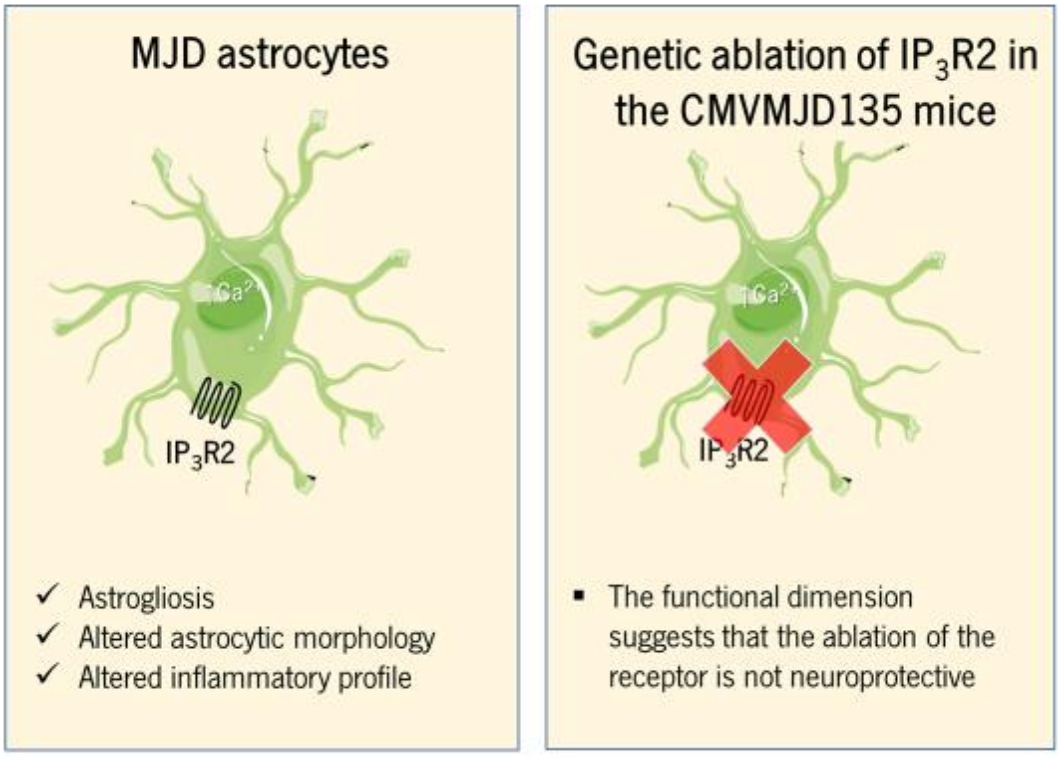

Thus, in the near future, we propose to:

1) Assess the IP_3R isoform expression at the protein level

Assess the expression levels these genes at the protein level by Western Blot, in the brain regions mentioned above as well as in the astrocyte-enriched samples. This would allow us to understand if our astrocytic-enriched samples are or not contaminated with other cell types as well as assess the protein levels of IP_3R isoforms in the context of MJD.

2) Evaluate if IP_3R2 physically interacts with ATXN3

Determine whether mutant ataxin-3 physically interacts with IP_3R2, by performing an immunoprecipitation, using an antibody against ataxin-3 and perform immunoblot with an antibody to IP_3R isoform type 2 and by proximity ligand assay (PLA). In case of IP_3R2 interacts with mutant ataxin-3, we will further study the effects of this interaction in the pathological progression of MJD.

3) Evaluate Ca^{2+} signalling in MJD and double mutant mice

To perform the assessment of Ca^{2+} signalling in CMVMJDQ135 and in the double mutant mice by using the two-photon excitation microscopy technique. In this *in vivo* microscopic physiological analysis, we will inject a calcium indicator dye as well as astrocyte-specific virus (that will allow us to differentiate neurons from astrocytes) in a mouse cranial imaging window (205). The record of activity in specific subpopulations of neurons and astrocytes with time lapse calcium imaging should help us understand impairments in the Ca^{2+} signalling, and the records will also be correlated to our behaviour results.

7. REFERENCES

1. Nakano KK, Dawson DM, Spence A. Machado disease: A hereditary ataxia in Portuguese emigrants to Massachusetts. Neurology. 1972;22(1):49–49.

2. Woods BT, Schaumburg HH. Nigro-spino-dentatal degeneration with nuclear ophthalmoplegia. J Neurol Sci. 1972;17(2):149–66.

3. Rosenberg RN, Nyhan WL, Bay C, Shore P. Autosomal dominant striatonigral degeneration: A clinical, pathologic, and biochemical study of a new genetic disorder. Neurology. 1976;26(8):703–703.

4. Coutinho P, Calheiros JM, Andrade C. On a new degenerative disorder of the central nervous system, inherited in an autosomal dominate mode and affecting people of Azorean extraction. O Medico. 1997;82:446–448.

5. Coutinho MPM do A. Doença de Machado-Joseph : Tentativa de definição. 1992

6. Coutinho P, Andrade C. Autosomal dominant system degeneration in Portuguese families of the Azores Islands: A new genetic disorder involving cerebellar, pyramidal, extrapyramidal and spinal cord motor functions. Neurology. 1978;28(7):703–703.

7. Lima L, Coutinho P. Clinical criteria for diagnosis of Machado-Joseph disease: report of a non-Azorena Portuguese family. Neurology.1980;30(3):319–22.

8. Stevanin G, Le Guern E, Ravisé N, Chneiweiss H, Dürr A, Cancel G, et al. A Third Locus for Autosomal Dominant Cerebellar Ataxia Type 1 Maps to Chromosome 14q24.3-qter: Evidence for the Existence of a Fourth Locus. Am J Hum Genet.1994;54(1):11–20.

9. Haberhausen G, Damian MS, Leweke F, Müller U. Spinocerebellar ataxia, type 3 (SCA3) is genetically identical to Machado-Joseph disease (MJD). J Neurol Sci. 1995;132(1):71–5.

10. T M, A M, Sh S, Hy Z. Molecular and clinical correlations in spinocerebellar ataxia type 3 and Machado-Joseph disease. Ann Neurol.1995;38(1):68–72.

11. Bird TD. Hereditary Ataxia Overview. Em: Adam MP, Ardinger HH, Pagon RA, Wallace SE, Bean LJ, Stephens K, et al., editores. GeneReviews® [Internet]. Seattle (WA): University of Washington, Seattle; 1993

12. Schöls L, Bauer P, Schmidt T, Schulte T, Riess O. Autosomal dominant cerebellar ataxias: clinical features, genetics, and pathogenesis. Lancet Neurol. 2004;3(5):291–304.

13. Epidemiological Data [Internet]. Disponível em: http://www.orphadata.org/cgi-bin/epidemio.html

14. Silveira I, Coutinho P, Maciel P, Gaspar C, Hayes S, Dias A, et al. Analysis of SCA1, DRPLA, MJD, SCA2, and SCA6 CAG repeats in 48 portuguese ataxia families. Am J Med Genet. 1998;81(2):134–8.

15. Vale J, Bugalho P, Silveira I, Sequeiros J, Guimarães J, Coutinho P. Autosomal dominant cerebellar ataxia: frequency analysis and clinical characterization of 45 families from Portugal. Eur J Neurol. 2010;17(1):124–8.

16. Jardim LB, Silveira I, Pereira ML, Ferro A, Alonso I, do Céu Moreira M, et al. A survey of spinocerebellar ataxia in South Brazil - 66 new cases with Machado-Joseph disease, SCA7, SCA8, or unidentified disease-causing mutations. J Neurol. 2001;248(10):870–6.

17. Teive HAG, Munhoz RP, Raskin S, Werneck LC. Spinocerebellar ataxia type 6 in Brazil. Arq Neuropsiquiatr.2008;66(3B):691–4.

18. Teive HAG, Munhoz RP, Arruda WO, Lopes-Cendes I, Raskin S, Werneck LC, et al. Spinocerebellar ataxias: genotype-phenotype correlations in 104 Brazilian families. Clin Sao Paulo Braz. 2012;67(5):443–9.

19. Rodríguez-Labrada R, Martins AC, Magaña JJ, Vazquez-Mojena Y, Medrano-Montero J, Fernandez-Ruíz J, et al. Founder Effects of Spinocerebellar Ataxias in the American Continents and the Caribbean. The Cerebellum. 2020;19(3):446–58.

20. Soong B W, Lu Y C, Choo K B, Lee H Y. Frequency analysis of autosomal dominant cerebellar ataxias in Taiwanese patients and clinical and molecular characterization of spinocerebellar ataxia type 6. Arch Neurol. 2001;58(7):1105–9.

21. Jiang H, Tang B, Xu B, Zhao G, Shen L, Tang J, et al. Frequency analysis of autosomal dominant spinocerebellar ataxias in mainland Chinese patients and clinical and molecular characterization of spinocerebellar ataxia type 6. Chin Med J (Engl). 2005;118(10):837–43.

22. Gan S-R, Shi S-S, Wu J-J, Wang N, Zhao G-X, Weng S-T, et al. High frequency of Machado-Joseph disease identified in Southeastern Chinese kindreds with spinocerebellar ataxia. BMC Med Genet. 2010;11(1):47.

23. van de Warrenburg BPC, Sinke RJ, Verschuuren-Bemelmans CC, Scheffer H, Brunt ER, Ippel PF, et al. Spinocerebellar ataxias in the Netherlands: prevalence and age at onset variance analysis. Neurology. 2002;58(5):702–8.

24. L S, G A, T B, H P, Jt E, O R. Autosomal dominant cerebellar ataxia: phenotypic differences in genetically defined subtypes? Ann Neurol. 1997;42(6):924–32.

25. Maruyama H, Izumi Y, Morino H, Oda M, Toji H, Nakamura S, et al. Difference in disease-free survival curve and regional distribution according to subtype of spinocerebellar ataxia: a study of 1,286 Japanese patients. Am J Med Genet. 2002;114(5):578–83.

26. Shibata-Hamaguchi A, Ishida C, Iwasa K, Yamada M. Prevalence of spinocerebellar degenerations in the Hokuriku district in Japan. Neuroepidemiology. 2009;32(3):176–83.

27. Kraft S, Furtado S, Ranawaya R, Parboosingh J, Bleoo S, McElligott K, et al. Adult onset spinocerebellar ataxia in a Canadian movement disorders clinic. Can J Neurol Sci J Can Sci Neurol. 2005;32(4):450–8.

28. Moseley ML, Benzow KA, Schut LJ, Bird TD, Gomez CM, Barkhaus PE, et al. Incidence of dominant spinocerebellar and Friedreich triplet repeats among 361 ataxia families. Neurology. 1998;51(6):1666–71.

29. Alonso E, Martínez-Ruano L, De Biase I, Mader C, Ochoa A, Yescas P, et al. Distinct distribution of autosomal dominant spinocerebellar ataxia in the Mexican population. Mov Disord Off J Mov Disord Soc. 2007;22(7):1050–3.

30. Storey E, du Sart D, Shaw JH, Lorentzos P, Kelly L, McKinley Gardner RJ, et al. Frequency of spinocerebellar ataxia types 1, 2, 3, 6, and 7 in Australian patients with spinocerebellar ataxia. Am J Med Genet. 2000;95(4):351–7.

31. Krishna N, Mohan S, Yashavantha BS, Rammurthy A, Kiran Kumar HB, Mittal U, et al. SCA 1, SCA 2 & SCA 3/MJD mutations in ataxia syndromes in southern India. Indian J Med Res. 2007;126(5):465–70.

32. Faruq M, Scaria V, Singh I, Tyagi S, Srivastava AK, Mukerji M. SCA-LSVD: a repeat-oriented locus-specific variation database for genotype to phenotype correlations in spinocerebellar ataxias. Hum Mutat. 2009;30(7):1037–42.

33. Bryer A, Krause A, Bill P, Davids V, Bryant D, Butler J, et al. The hereditary adult-onset ataxias in South Africa. J Neurol Sci. 2003;216(1):47–54.

34. Brusco A, Gellera C, Cagnoli C, Saluto A, Castucci A, Michielotto C, et al. Molecular genetics of hereditary spinocerebellar ataxia: mutation analysis of spinocerebellar ataxia genes and CAG/CTG repeat expansion detection in 225 Italian families. Arch Neurol. 2004;61(5):727–33.

35. Gaspar C, Lopes-Cendes I, Hayes S, Goto J, Arvidsson K, Dias A, et al. Ancestral Origins of the Machado-Joseph Disease Mutation: A Worldwide Haplotype Study. Am J Hum Genet. e 2001;68(2):523–8.

36. Martins S, Calafell F, Gaspar C, Wong VCN, Silveira I, Nicholson GA, et al. Asian Origin for the Worldwide-Spread Mutational Event in Machado-Joseph Disease. Arch Neurol. 2007;64(10):1502.

37. Martins S, Sequeiros J. Origins and Spread of Machado-Joseph Disease Ancestral Mutations Events. Adv Exp Med Biol. 2018;1049:243–54.

38. Mendonça N, França MC, Gonçalves AF, Januário C. Clinical Features of Machado-Joseph Disease. Adv Exp Med Biol. 2018;1049:255–73.

39. Fowler HL. Machado-Joseph-Azorean Disease: A Ten-Year Study. Arch Neurol. 1984;41(9):921–5.

40. Rosenberg RN. Machado-Joseph disease: an autosomal dominant motor system degeneration. Mov Disord Off J Mov Disord Soc. 1992;7(3):193–203.

41. Sequeiros J, Coutinho P. Epidemiology and clinical aspects of Machado-Joseph disease. Adv Neurol. 1993;61:139–53.

42. Sudarsky L, Coutinho P. Machado-Joseph disease. Clin Neurosci N Y N. 1995;3(1):17–22.

43. Dürr A, Stevanin G, Cancel G, Duyckaerts C, Abbas N, Didierjean O, et al. Spinocerebellar ataxia 3 and Machado-Joseph disease: clinical, molecular, and neuropathological features. Ann Neurol. 1996;39(4):490–9.

44. Pedroso JL, Braga-Neto P, Felício AC, Dutra LA, Santos WAC, do Prado GF, et al. Sleep disorders in machado-joseph disease: frequency, discriminative thresholds, predictive values, and correlation with ataxia-related motor and non-motor features. Cerebellum Lond Engl. 2011;10(2):291–5.

45. Roeske S, Filla I, Heim S, Amunts K, Helmstaedter C, Wüllner U, et al. Progressive cognitive dysfunction in spinocerebellar ataxia type 3. Mov Disord. 2013;28(10):1435–8.

46. Tamura I, Takei A, Hamada S, Soma H, Nonaka M, Homma S, et al. Executive dysfunction in patients with spinocerebellar ataxia type 3. J Neurol. 2018;265(7):1563–72.

47. Elyoseph Z, Mintz M, Vakil E, Zaltzman R, Gordon C. Selective Procedural Memory Impairment but Preserved Declarative Memory in Spinocerebellar Ataxia Type 3. Cerebellum Lond Engl. 2020;19.

48. Kieling C, Prestes PR, Saraiva-Pereira ML, Jardim LB. Survival estimates for patients with Machado-Joseph disease (SCA3). Clin Genet. 2007;72(6):543–5.

49. Carvalho DR, La Rocque-Ferreira A, Rizzo IM, Imamura EU, Speck-Martins CE. Homozygosity enhances severity in spinocerebellar ataxia type 3. Pediatr Neurol. 2008;38(4):296–9.

50. Maciel P, Gaspar C, DeStefano AL, Silveira I, Coutinho P, Radvany J, et al. Correlation between CAG repeat length and clinical features in Machado-Joseph disease. Am J Hum Genet. 1995;57(1):54–61.

51. Scherzed W, Brunt ER, Heinsen H, de Vos RA, Seidel K, Bürk K, et al. Pathoanatomy of cerebellar degeneration in spinocerebellar ataxia type 2 (SCA2) and type 3 (SCA3). Cerebellum Lond Engl. 2012;11(3):749–60.

52. Paulson HL, Das SS, Crino PB, Perez MK, Patel SC, Gotsdiner D, et al. Machado-Joseph disease gene product is a cytoplasmic protein widely expressed in brain. Ann Neurol. 1997;41(4):453–62.

53. Riess O, Rüb U, Pastore A, Bauer P, Schöls L. SCA3: neurological features, pathogenesis and animal models. Cerebellum Lond Engl. 2008;7(2):125–37.

54. Bettencourt C, Lima M. Machado-Joseph Disease: from first descriptions to new perspectives. Orphanet J Rare Dis. 2011;6:35.

55. Moro A, Munhoz RP, Arruda WO, Raskin S, Moscovich M, Teive HAG. Spinocerebellar ataxia type 3: subphenotypes in a cohort of Brazilian patients. Arq Neuropsiquiatr. 2014;72(9):659–62.

56. Suite ND, Sequeiros J, McKhann GM. Machado-Joseph disease in a Sicilian-American family. J Neurogenet. 1986;3(3):177–82.

57. Tuite PJ, Rogaeva EA, St George-Hyslop PH, Lang AE. Dopa-responsive parkinsonism phenotype of Machado-Joseph disease: confirmation of 14q CAG expansion. Ann Neurol. 1995;38(4):684–7.

58. Gwinn-Hardy K, Singleton A, O'Suilleabhain P, Boss M, Nicholl D, Adam A, et al. Spinocerebellar ataxia type 3 phenotypically resembling parkinson disease in a black family. Arch Neurol. 2001;58(2):296–9.

59. Ross CA. When more is less: pathogenesis of glutamine repeat neurodegenerative diseases. Neuron. 1995;15(3):493–6.

60. Coutinho P, Guimarães A, Scaravilli F. The pathology of Machado-Joseph disease. Acta Neuropathol (Berl). 1982;58(1):48–54.

61. Meira AT, Arruda WO, Ono SE, Neto A de C, Raskin S, Camargo CHF, et al. Neuroradiological Findings in the Spinocerebellar Ataxias. Tremor Hyperkinetic Mov. 2019

62. Taniwaki T, Sakai T, Kobayashi T, Kuwabara Y, Otsuka M, Ichiya Y, et al. Positron emission tomography (PET) in Machado-Joseph disease. J Neurol Sci. 1997;145(1):63–7.

63. Klockgether T, Skalej M, Wedekind D, Luft AR, Welte D, Schulz JB, et al. Autosomal dominant cerebellar ataxia type I. MRI-based volumetry of posterior fossa structures and basal ganglia in spinocerebellar ataxia types 1, 2 and 3. Brain J Neurol. 1998;121 (Pt 9):1687–93.

64. Murata Y, Yamaguchi S, Kawakami H, Imon Y, Maruyama H, Sakai T, et al. Characteristic Magnetic Resonance Imaging Findings in Machado-Joseph Disease. Arch Neurol. 1998;55(1):33.

65. Etchebehere EC, Cendes F, Lopes-Cendes I, Pereira JA, Lima MC, Sansana CR, et al. Brain single-photon emission computed tomography and magnetic resonance imaging in Machado-Joseph disease. Arch Neurol. 2001;58(8):1257–63.

66. Rüb U, de Vos R a. I, Schultz C, Brunt ER, Paulson H, Braak H. Spinocerebellar ataxia type 3 (Machado-Joseph disease): severe destruction of the lateral reticular nucleus. Brain J Neurol. 2002;125(Pt 9):2115–24.

67. Rüb U, Brunt ER, Deller T. New insights into the pathoanatomy of spinocerebellar ataxia type 3 (Machado-Joseph disease). Curr Opin Neurol. 2008;21(2):111–6.

68. Horimoto Y, Matsumoto M, Akatsu H, Kojima A, Yoshida M, Nokura K, et al. Longitudinal study on MRI intensity changes of Machado-Joseph disease: correlation between MRI findings and neuropathological changes. J Neurol. 2011;258(9):1657–64.

69. de Oliveira MS, D'Abreu A, França MC, Lopes-Cendes I, Cendes F, Castellano G. MRI-texture analysis of corpus callosum, thalamus, putamen, and caudate in Machado-Joseph disease. J Neuroimaging Off J Am Soc Neuroimaging. 2012;22(1):46–52.

70. Wüllner U, Reimold M, Abele M, Bürk K, Minnerop M, Dohmen B-M, et al. Dopamine Transporter Positron Emission Tomography in Spinocerebellar Ataxias Type 1, 2, 3, and 6. Arch Neurol. 2005;62(8):1280.

71. Yeh T-H, Lu C-S, Chou Y-HW, Chong C-C, Wu T, Han N-H, et al. Autonomic dysfunction in Machado-Joseph disease. Arch Neurol. 2005;62(4):630–6.

72. Rüb U, Brunt ER, Petrasch-Parwez E, Schöls L, Theegarten D, Auburger G, et al. Degeneration of ingestion-related brainstem nuclei in spinocerebellar ataxia type 2, 3, 6 and 7. Neuropathol Appl Neurobiol. 2006;32(6):635–49.

73. Maciel P, Costa MC, Ferro A, Rousseau M, Santos CS, Gaspar C, et al. Improvement in the molecular diagnosis of Machado-Joseph disease. Arch Neurol. 2001;58(11):1821–7.

74. Drüsedau M, Dreesen JCFM, de Die-Smulders C, Hardy K, Bras M, Dumoulin JCM, et al. Preimplantation genetic diagnosis of spinocerebellar ataxia 3 by (CAG)n repeat detection. Mol Hum Reprod. 2004;10(1):71–5.

75. Takiyama Y, Nishizawa M, Tanaka H, Kawashima S, Sakamoto H, Karube Y, et al. The gene for Machado–Joseph disease maps to human chromosome 14q. Nat Genet. 1993;4(3):300–4.

76. Kawaguchi Y, Okamoto T, Taniwaki M, Aizawa M, Inoue M, Katayama S, et al. CAG expansions in a novel gene for Machado-Joseph disease at chromosome 14q32.1. Nat Genet. 1994;8(3):221–8.

77. Ichikawa Y, Goto J, Hattori M, Toyoda A, Ishii K, Jeong SY, et al. The genomic structure and expression of MJD, the Machado-Joseph disease gene. J Hum Genet. 2001;46(7):413–22.

78. Goto J, Watanabe M, Ichikawa Y, Yee SB, Ihara N, Endo K, et al. Machado-Joseph disease gene products carrying different carboxyl termini. Neurosci Res. 1997;28(4):373–7.

79. Bettencourt C, Santos C, Montiel R, Costa M do C, Cruz-Morales P, Santos LR, et al. Increased transcript diversity: novel splicing variants of Machado-Joseph disease gene (ATXN3). Neurogenetics. 2010;11(2):193–202.

80. Maruyama H, Nakamura S, Matsuyama Z, Sakai T, Doyu M, Sobue G, et al. Molecular features of the CAG repeats and clinical manifestation of Machado-Joseph disease. Hum Mol Genet. 1995;4(5):807–12.

81. Lindblad K, Lunkes A, Maciel P, Stevanin G, Zander C, Klockgether T, et al. Mutation detection in Machado-Joseph disease using repeat expansion detection. Mol Med Camb Mass. 1996;2(1):77–85.

82. Maciel P, LopesCendes I, Gaspar C, Silveira I, Rouleau GA, Kish S, et al. Somatic mosaicism of the CAG repeat length in brain specimens of spinocerebellar ataxia type 1 and Machado-Joseph disease. Em: Neurology. LITTLE BROWN CO 34 BEACON STREET, BOSTON, MA 02108-1493; 1996. p. 30004–30004.

83. DeStefano AL, Cupples LA, Maciel P, Gaspar C, Radvany J, Dawson DM, et al. A Familial Factor Independent of CAG Repeat Length Influences Age at Onset of Machado-Joseph Disease. Am J Hum Genet. 1996;59(1):119–27.

84. Lopes-Cendes I, Silveira I, Maciel P, Gaspar C, Radvany J, Chitayat D, et al. Limits of Clinical Assessment in the Accurate Diagnosis of Machado-Joseph Disease. Arch Neurol. 1996;53(11):1168–74.

85. Lopes-Cendes I, Maciel P, Kish S, Gaspar C, Robitaille Y, Clark HB, et al. Somatic mosaicism in the central nervous system in spinocerebellar ataxia type 1 and Machado-Joseph disease. Ann Neurol. A 1996;40(2):199–206.

86. Sequeiros J, Maciel P, Taborda F, Lêdo S, Rocha JC, Lopes A, et al. Prenatal diagnosis of Machado-Joseph disease by direct mutation analysis. Prenat Diagn. 1998;18(6):611–7.

87. Maciel P, Gaspar C, Guimarães L, Goto J, Lopes-Cendes I, Hayes S, et al. Study of three intragenic polymorphisms in the Machado-Joseph disease gene (MJD1) in relation to genetic instability of the (CAG)n tract. Eur J Hum Genet EJHG. 1999;7(2):147–56.

88. do Carmo Costa M, Sequeiros J, Maciel P. Identification of three novel polymorphisms in the MJD1 gene and study of their frequency in the Portuguese population. J Hum Genet. 2002;47(4):205–7.

89. Cancel G, Abbas N, Stevanin G, Dürr A, Chneiweiss H, Néri C, et al. Marked phenotypic heterogeneity associated with expansion of a CAG repeat sequence at the spinocerebellar ataxia 3/Machado-Joseph disease locus. Am J Hum Genet. 1995;57(4):809–16.

90. Sasaki H, Wakisaka A, Fukazawa T, Iwabuchi K, Hamada T, Takada A, et al. CAG repeat expansion of Machado-Joseph disease in the Japanese: analysis of the repeat instability for parental transmission, and correlation with disease phenotype. J Neurol Sci. 1995;133(1–2):128–33.

91. Takiyama Y, Igarashi S, Rogaeva EA, Endo K, Rogaev EI, Tanaka H, et al. Evidence for inter-generational instability in the CAG repeat in the MJD1 gene and for conserved haplotypes at flanking markers amongst Japanese and Caucasian subjects with Machado-Joseph disease. Hum Mol Genet. 1995;4(7):1137–46.

92. Lunt PW, Jardine PE, Koch MC, Maynard J, Osborn M, Williams M, et al. Correlation between fragment size at D4F104S1 and age at onset or at wheelchair use, with a possible generational effect, accounts for much phenotypic variation in 4q35-facioscapulohumeral muscular dystrophy (FSHD). Hum Mol Genet. 1995;4(5):951–8.

93. Masino L, Musi V, Menon RP, Fusi P, Kelly G, Frenkiel TA, et al. Domain architecture of the polyglutamine protein ataxin-3: a globular domain followed by a flexible tail. FEBS Lett. 2003;549(1):21–5.

94. Nicastro G, Masino L, Esposito V, Menon RP, De Simone A, Fraternali F, et al. Josephin domain of ataxin-3 contains two distinct ubiquitin-binding sites. Biopolymers. 2009;91(12):1203–14.

95. Schmidt T, Landwehrmeyer GB, Schmitt I, Trottier Y, Auburger G, Laccone F, et al. An isoform of ataxin-3 accumulates in the nucleus of neuronal cells in affected brain regions of SCA3 patients. Brain Pathol Zurich Switz. 1998;8(4):669–79.

96. Burnett B, Li F, Pittman RN. The polyglutamine neurodegenerative protein ataxin-3 binds polyubiquitylated proteins and has ubiquitin protease activity. Hum Mol Genet. 2003;12(23):3195–205.

97. Rodrigues A-J, Coppola G, Santos C, Costa M do C, Ailion M, Sequeiros J, et al. Functional genomics and biochemical characterization of the C. elegans orthologue of the Machado-Joseph disease protein ataxin-3. FASEB J Off Publ Fed Am Soc Exp Biol. 2007;21(4):1126–36.

98. Li F, Macfarlan T, Pittman RN, Chakravarti D. Ataxin-3 is a histone-binding protein with two independent transcriptional corepressor activities. J Biol Chem. 2002;277(47):45004–12.

99. Albrecht M, Golatta M, Wüllner U, Lengauer T. Structural and functional analysis of ataxin-2 and ataxin-3. Eur J Biochem. 2004;271(15):3155–70.

100. Seki T, Gong L, Williams AJ, Sakai N, Todi SV, Paulson HL. JosD1, a membrane-targeted deubiquitinating enzyme, is activated by ubiquitination and regulates membrane dynamics, cell motility, and endocytosis. J Biol Chem. de 2013;288(24):17145–55.

101. Ashkenazi A, Bento CF, Ricketts T, Vicinanza M, Siddiqi F, Pavel M, et al. Polyglutamine tracts regulate beclin 1-dependent autophagy. Nature. 2017;545(7652):108–11.

102. Barrio R, Sutherland JD, Rodriguez MS, editores. Proteostasis and Disease : From Basic Mechanisms to Clinics [Internet]. Springer International Publishing; 2020 (Advances in Experimental Medicine and Biology).

103. Hershko A. Lessons from the discovery of the ubiquitin system. Trends Biochem Sci. 1996;21(11):445–9.

104. Wilkinson KD. Ubiquitination and deubiquitination: targeting of proteins for degradation by the proteasome. Semin Cell Dev Biol. 2000;11(3):141–8.

105. Harris GM, Dodelzon K, Gong L, Gonzalez-Alegre P, Paulson HL. Splice Isoforms of the Polyglutamine Disease Protein Ataxin-3 Exhibit Similar Enzymatic yet Different Aggregation Properties. PLoS ONE. 2010

106. Fei E, Jia N, Zhang T, Ma X, Wang H, Liu C, et al. Phosphorylation of ataxin-3 by glycogen synthase kinase 3beta at serine 256 regulates the aggregation of ataxin-3. Biochem Biophys Res Commun. 2007;357(2):487–92.

107. Mueller T, Breuer P, Schmitt I, Walter J, Evert BO, Wüllner U. CK2-dependent phosphorylation determines cellular localization and stability of ataxin-3. Hum Mol Genet. 2009;18(17):3334–43.

108. Matos CA, Nóbrega C, Louros SR, Almeida B, Ferreiro E, Valero J, et al. Ataxin-3 phosphorylation decreases neuronal defects in spinocerebellar ataxia type 3 models. J Cell Biol. de 2016;212(4):465–80.

109. Todi SV, Winborn BJ, Scaglione KM, Blount JR, Travis SM, Paulson HL. Ubiquitination directly enhances activity of the deubiquitinating enzyme ataxin-3. EMBO J. 2009;28(4):372–82.

110. Tsou W-L, Burr AA, Ouyang M, Blount JR, Scaglione KM, Todi SV. Ubiquitination regulates the neuroprotective function of the deubiquitinase ataxin-3 in vivo. J Biol Chem. 2013;288(48):34460–9.

111. Zhou Y-F, Liao S-S, Luo Y-Y, Tang J-G, Wang J-L, Lei L-F, et al. SUMO-1 modification on K166 of polyQ-expanded ataxin-3 strengthens its stability and increases its cytotoxicity. PloS One. 2013;8(1):e54214.

112. Almeida B, Abreu IA, Matos CA, Fraga JS, Fernandes S, Macedo MG, et al. SUMOylation of the brain-predominant Ataxin-3 isoform modulates its interaction with p97. Biochim Biophys Acta. 2015;1852(9):1950–9.

113. Wang G, Sawai N, Kotliarova S, Kanazawa I, Nukina N. Ataxin-3, the MJD1 gene product, interacts with the two human homologs of yeast DNA repair protein RAD23, HHR23A and HHR23B. Hum Mol Genet. 2000;9(12):1795–803.

114. Zoghbi HY, Orr HT. Glutamine repeats and neurodegeneration. Annu Rev Neurosci. 2000;23:217–47.

115. Williams AJ, Paulson HL. Polyglutamine neurodegeneration: protein misfolding revisited. Trends Neurosci. 2008;31(10):521–8.

116. Chen X, Tang T-S, Tu H, Nelson O, Pook M, Hammer R, et al. Deranged calcium signaling and neurodegeneration in spinocerebellar ataxia type 3. J Neurosci Off J Soc Neurosci. 26 de 2008;28(48):12713–24.

117. Cummings CJ, Zoghbi HY. Fourteen and counting: unraveling trinucleotide repeat diseases. Hum Mol Genet. 2000;9(6):909–16.

118. Paulson HL, Perez MK, Trottier Y, Trojanowski JQ, Subramony SH, Das SS, et al. Intranuclear inclusions of expanded polyglutamine protein in spinocerebellar ataxia type 3. Neuron. 1997;19(2):333–44.

119. Ikeda H, Yamaguchi M, Sugai S, Aze Y, Narumiya S, Kakizuka A. Expanded polyglutamine in the Machado–Joseph disease protein induces cell death in vitro and in vivo. Nat Genet. 1996;13(2):196–202.

120. Evert BO, Wüllner U, Schulz JB, Weller M, Groscurth P, Trottier Y, et al. High Level Expression of Expanded Full-length Ataxin-3 In Vitro Causes Cell Death and Formation of Intranuclear Inclusions in Neuronal Cells. Hum Mol Genet. 1999;8(7):1169–76.

121. Dantuma NP, Herzog LK. Machado-Joseph Disease: A Stress Combating Deubiquitylating Enzyme Changing Sides. Adv Exp Med Biol. 2020;1233:237–60.

122. Fujigasaki H, Uchihara T, Koyano S, Iwabuchi K, Yagishita S, Makifuchi T, et al. Ataxin-3 Is Translocated into the Nucleus for the Formation of Intranuclear Inclusions in Normal and Machado–Joseph Disease Brains. Exp Neurol. 2000;165(2):248–56.

123. Cemal CK, Carroll CJ, Lawrence L, Lowrie MB, Ruddle P, Al-Mahdawi S, et al. YAC transgenic mice carrying pathological alleles of the MJD1 locus exhibit a mild and slowly progressive cerebellar deficit. Hum Mol Genet. 2002;11(9):1075–94.

124. Yamada M, Tan C-F, Inenaga C, Tsuji S, Takahashi H. Sharing of polyglutamine localization by the neuronal nucleus and cytoplasm in CAG-repeat diseases. Neuropathol Appl Neurobiol. 2004;30(6):665–75.

125. Carvalho AL, Silva A, Macedo-Ribeiro S. Polyglutamine-Independent Features in Ataxin-3 Aggregation and Pathogenesis of Machado-Joseph Disease. Adv Exp Med Biol. 2018;1049:275–88.

126. Miyai I, Ito M, Hattori N, Mihara M, Hatakenaka M, Yagura H, et al. Cerebellar Ataxia Rehabilitation Trial in Degenerative Cerebellar Diseases. Neurorehabil Neural Repair. 2012;26(5):515–22.

127. Svensson M, Lexell J, Deierborg T. Effects of Physical Exercise on Neuroinflammation, Neuroplasticity, Neurodegeneration, and Behavior: What We Can Learn From Animal Models in Clinical Settings. Neurorehabil Neural Repair. 2015;29(6):577–89.

128. Buhmann C, Bussopulos A, Oechsner M. Dopaminergic response in Parkinsonian phenotype of Machado-Joseph disease. Mov Disord Off J Mov Disord Soc. 2003;18(2):219–21.

129. Nandagopal R, Moorthy SGK. Dramatic levodopa responsiveness of dystonia in a sporadic case of spinocerebellar ataxia type 3. Postgrad Med J. 2004;80(944):363–5.

130. Costa M do C, Paulson HL. Toward understanding Machado-Joseph disease. Prog Neurobiol. 2012;97(2):239–57.

131. Chadman KK, Yang M, Crawley JN. Criteria for Validating Mouse Models of Psychiatric Diseases. Am J Med Genet Part B Neuropsychiatr Genet Off Publ Int Soc Psychiatr Genet. 2009;150B(1):1–11.

132. Colomer Gould VF. Mouse models of spinocerebellar ataxia type 3 (Machado-Joseph disease). Neurother J Am Soc Exp Neurother. 2012;9(2):285–96.

133. Silva-Fernandes A, Duarte-Silva S, Neves-Carvalho A, Amorim M, Soares-Cunha C, Oliveira P, et al. Chronic treatment with 17-DMAG improves balance and coordination in a new mouse model of Machado-Joseph disease. Neurother J Am Soc Exp Neurother. 2014;11(2):433–49.

134. Silva-Fernandes A, Costa M do C, Duarte-Silva S, Oliveira P, Botelho CM, Martins L, et al. Motor uncoordination and neuropathology in a transgenic mouse model of Machado-Joseph disease lacking intranuclear inclusions and ataxin-3 cleavage products. Neurobiol Dis. 2010;40(1):163–76.

135. Teixeira-Castro A, Jalles A, Esteves S, Kang S, da Silva Santos L, Silva-Fernandes A, et al. Serotonergic signalling suppresses ataxin 3 aggregation and neurotoxicity in animal models of Machado-Joseph disease. Brain J Neurol. 2015;138(Pt 11):3221–37.

136. Pekny M, Nilsson M. Astrocyte activation and reactive gliosis. Glia. 2005;50(4):427–34.

137. Li YX, Sibon OCM, Dijkers PF. Inhibition of NF-κB in astrocytes is sufficient to delay neurodegeneration induced by proteotoxicity in neurons. J Neuroinflammation. 2018;15(1):261.

138. Rüb U, Gierga K, Brunt ER, de Vos R a. I, Bauer M, Schöls L, et al. Spinocerebellar ataxias types 2 and 3: degeneration of the pre-cerebellar nuclei isolates the three phylogenetically defined regions of the cerebellum. J Neural Transm Vienna Austria 1996. 2005;112(11):1523–45.

139. Jessen KR. Glial cells. Int J Biochem Cell Biol. 2004;36(10):1861–7.

140. Kettenmann H, Verkhratsky A. Neuroglia: the 150 years after. Trends Neurosci. 2008;31(12):653–9.

141. McIver SR, Faideau M, Haydon PG. Astrocyte–neuron communications. Em: Neural-Immune Interactions in Brain Function and Alcohol Related Disorders. Springer; 2013. p. 31–64.

142. Miller FD, Gauthier AS. Timing Is Everything: Making Neurons versus Glia in the Developing Cortex. Neuron. 2007;54(3):357–69.

143. Wang DD, Bordey A. The Astrocyte Odyssey. Prog Neurobiol. 2008;86(4):342–67.

144. Molofsky AV, Krenick R, Ullian E, Tsai H, Deneen B, Richardson WD, et al. Astrocytes and disease: a neurodevelopmental perspective. Genes Dev. 2012;26(9):891–907.

145. Bayraktar OA, Fuentealba LC, Alvarez-Buylla A, Rowitch DH. Astrocyte Development and Heterogeneity. Cold Spring Harb Perspect Biol.2015

146. Edlund T, Jessell TM. Progression from extrinsic to intrinsic signaling in cell fate specification: a view from the nervous system. Cell. 1999;96(2):211–24.

147. EMSLEY JG, MACKLIS JD. Astroglial heterogeneity closely reflects the neuronal-defined anatomy of the adult murine CNS. Neuron Glia Biol. 2006;2(3):175–86.

148. Parpura V, Verkhratsky A. Homeostatic function of astrocytes: Ca2+ and Na+ signalling. Transl Neurosci. 2012;3(4):334–44.

149. Ben Haim L, Rowitch DH. Functional diversity of astrocytes in neural circuit regulation. Nat Rev Neurosci. 2017;18(1):31–41.

150. Mederos S, González-Arias C, Perea G. Astrocyte–Neuron Networks: A Multilane Highway of Signaling for Homeostatic Brain Function. Front Synaptic Neurosci. 2018

151. Araque A, Parpura V, Sanzgiri RP, Haydon PG. Tripartite synapses: glia, the unacknowledged partner. Trends Neurosci. 1999;22(5):208–15.

152. Perea G, Navarrete M, Araque A. Tripartite synapses: astrocytes process and control synaptic information. Trends Neurosci. 2009;32(8):421–31.

153. Pannasch U, Rouach N. Emerging role for astroglial networks in information processing: from synapse to behavior. Trends Neurosci. 2013;36(7):405–17.

154. Allen NJ. Astrocyte regulation of synaptic behavior. Annu Rev Cell Dev Biol. 2014;30:439–63.

155. Araque A, Carmignoto G, Haydon PG, Oliet SHR, Robitaille R, Volterra A. Gliotransmitters Travel in Time and Space. Neuron. 2014;81(4):728–39.

156. Guerra-Gomes S, Sousa N, Pinto L, Oliveira JF. Functional Roles of Astrocyte Calcium Elevations: From Synapses to Behavior. Front Cell Neurosci. 2017;11:427.

157. Agulhon C, Petravicz J, McMullen AB, Sweger EJ, Minton SK, Taves SR, et al. What Is the Role of Astrocyte Calcium in Neurophysiology? Neuron. 2008;59(6):932–46.

158. Agarwal A, Wu P-H, Hughes EG, Fukaya M, Tischfield MA, Langseth AJ, et al. Transient Opening of the Mitochondrial Permeability Transition Pore Induces Microdomain Calcium Transients in Astrocyte Processes. Neuron. 2017;93(3):587-605.e7.

159. Matyash M, Matyash V, Nolte C, Sorrentino V, Kettenmann H. Requirement of functional ryanodine receptor type 3 for astrocyte migration. FASEB J Off Publ Fed Am Soc Exp Biol. 2002;16(1):84–6.

160. Chai H, Diaz-Castro B, Shigetomi E, Monte E, Octeau JC, Yu X, et al. Neural Circuit-Specialized Astrocytes: Transcriptomic, Proteomic, Morphological, and Functional Evidence. Neuron. 2017;95(3):531-549.e9.

161. Okubo Y, Kanemaru K, Suzuki J, Kobayashi K, Hirose K, Iino M. Inositol 1,4,5-trisphosphate receptor type 2-independent Ca2+ release from the endoplasmic reticulum in astrocytes. Glia. 2019;67(1):113–24.

162. Kanemaru K, Sekiya H, Xu M, Satoh K, Kitajima N, Yoshida K, et al. In Vivo Visualization of Subtle, Transient, and Local Activity of Astrocytes Using an Ultrasensitive Ca2+ Indicator. Cell Rep. 2014;8(1):311–8.

163. Srinivasan R, Huang BS, Venugopal S, Johnston AD, Chai H, Zeng H, et al. Ca(2+) signaling in astrocytes from Ip3r2(-/-) mice in brain slices and during startle responses in vivo. Nat Neurosci. 2015;18(5):708–17.

164. Verkhratsky A, Nedergaard M. Physiology of Astroglia. Physiol Rev. 2018;98:151.

165. Harada K, Kamiya T, Tsuboi T. Gliotransmitter Release from Astrocytes: Functional, Developmental, and Pathological Implications in the Brain. Front Neurosci. 2016;9.

166. De Pittà M, Brunel N, Volterra A. Astrocytes: Orchestrating synaptic plasticity? Neuroscience. 2016;323:43–61.

167. Guerra-Gomes S, Viana J, Nascimento D, Correia J, Sardinha V, Caetano I, et al. The Role of Astrocytic Calcium Signaling in the Aged Prefrontal Cortex. Front Cell Neurosci. 2018;12:379.

168. Di Castro MA, Chuquet J, Liaudet N, Bhaukaurally K, Santello M, Bouvier D, et al. Local Ca2+ detection and modulation of synaptic release by astrocytes. Nat Neurosci. 2011;14(10):1276–84.

169. Shigetomi E, Tong X, Kwan KY, Corey DP, Khakh BS. TRPA1 channels regulate astrocyte resting calcium and inhibitory synapse efficacy through GAT-3. Nat Neurosci. 2011;15(1):70–80.

170. Volterra A, Liaudet N, Savtchouk I. Astrocyte Ca^{2+} signalling: an unexpected complexity. Nat Rev Neurosci. 2014;15(5):327–35.

171. Capiod T. Extracellular Calcium Has Multiple Targets to Control Cell Proliferation. Adv Exp Med Biol. 2016;898:133–56.

172. Clapham DE. Calcium signaling. Cell. 1995;80(2):259–68.

173. La Rovere RML, Roest G, Bultynck G, Parys JB. Intracellular Ca(2+) signaling and Ca(2+) microdomains in the control of cell survival, apoptosis and autophagy. Cell Calcium. 2016;60(2):74–87.

174. Li X, Zima AV, Sheikh F, Blatter LA, Chen J. Endothelin-1-induced arrhythmogenic Ca2+ signaling is abolished in atrial myocytes of inositol-1,4,5-trisphosphate(IP3)-receptor type 2-deficient mice. Circ Res. 2005;96(12):1274–81.

175. Li H, Xie Y, Zhang N, Yu Y, Zhang Q, Ding S. Disruption of IP_3R2-mediated Ca^{2+} signaling pathway in astrocytes ameliorates neuronal death and brain damage while reducing behavioral deficits after focal ischemic stroke. Cell Calcium. 015;58(6):565–76.

176. Guerra-Gomes S, Cunha-Garcia D, Nascimento DSM, Duarte-Silva S, Loureiro-Campos E, Sardinha VM, et al. IP3R2 null mice display a normal acquisition of somatic and neurological development milestones. Eur J Neurosci. 2020

177. Ben Haim L, Carrillo-de Sauvage M-A, Ceyzériat K, Escartin C. Elusive roles for reactive astrocytes in neurodegenerative diseases. Front Cell Neurosci. 2015

178. Li K, Li J, Zheng J, Qin S. Reactive Astrocytes in Neurodegenerative Diseases. Aging Dis. 2019;10(3):664–75.

179. Liddelow SA, Guttenplan KA, Clarke LE, Bennett FC, Bohlen CJ, Schirmer L, et al. Neurotoxic reactive astrocytes are induced by activated microglia. Nature. 2017;541(7638):481–7.

180. Colangelo AM, Alberghina L, Papa M. Astrogliosis as a therapeutic target for neurodegenerative diseases. Neurosci Lett. 2014;565:59–64.

181. Faideau M, Kim J, Cormier K, Gilmore R, Welch M, Auregan G, et al. In vivo expression of polyglutamine-expanded huntingtin by mouse striatal astrocytes impairs glutamate transport: a correlation with Huntington's disease subjects. Hum Mol Genet. 2010;19(15):3053–67.

182. Bezprozvanny I. Calcium signaling and neurodegenerative diseases. Trends Mol Med. 2009;15(3):89–100.

183. Arispe N, Rojas E, Pollard HB. Alzheimer disease amyloid beta protein forms calcium channels in bilayer membranes: blockade by tromethamine and aluminum. Proc Natl Acad Sci U S A. 1993;90(2):567–71.

184. Surmeier DJ. Calcium, ageing, and neuronal vulnerability in Parkinson's disease. Lancet Neurol. 2007;6(10):933–8.

185. Appel SH, Beers D, Siklos L, Engelhardt JI, Mosier DR. Calcium: the Darth Vader of ALS. Amyotroph Lateral Scler Mot Neuron Disord Off Publ World Fed Neurol Res Group Mot Neuron Dis. 2001;2 Suppl 1:S47-54.

186. Haacke A, Hartl FU, Breuer P. Calpain inhibition is sufficient to suppress aggregation of polyglutamine-expanded ataxin-3. J Biol Chem. 2007;282(26):18851–6.

187. Carter RJ, Lione LA, Humby T, Mangiarini L, Mahal A, Bates GP, et al. Characterization of progressive motor deficits in mice transgenic for the human Huntington's disease mutation. J Neurosci Off J Soc Neurosci. 1999;19(8):3248–57.

188. Rogers DC, Fisher EMC, Brown SDM, Peters J, Hunter AJ, Martin JE. Behavioral and functional analysis of mouse phenotype: SHIRPA, a proposed protocol for comprehensive phenotype assessment. Mamm Genome. 1997;8(10):711–3.

189. Rafael JA, Nitta Y, Peters J, Davies KE. Testing of SHIRPA, a mouse phenotypic assessment protocol, on Dmd mdx and Dmd mdx3cv dystrophin-deficient mice. Mamm Genome. 2000;11(9):725–8.

190. Schallert T, Upchurch M, Lobaugh N, Farrar SB, Spirduso WW, Gilliam P, et al. Tactile extinction: Distinguishing between sensorimotor and motor asymmetries in rats with unilateral nigrostriatal damage. Pharmacol Biochem Behav. 1982;16(3):455–62.

191. Bouet V, Boulouard M, Toutain J, Divoux D, Bernaudin M, Schumann-Bard P, et al. The adhesive removal test: a sensitive method to assess sensorimotor deficits in mice. Nat Protoc. 2009;4(10):1560–4.

192. Grüsser C, Grüsser-Cornehls U. Improvement in motor performance of Weaver mutant mice following lesions of the cerebellum. Behav Brain Res. 1998;97(1–2):189–94.

193. Lever C, Burton S, O'Keefe J. Rearing on Hind Legs, Environmental Novelty, and the Hippocampal Formation. Rev Neurosci. 2006;17:111–33.

194. Gerlai R, Millen KJ, Herrup K, Fabien K, Joyner AL, Roder J. Impaired motor learning performance in cerebellar En-2 mutant mice. Behav Neurosci. 1996;110(1):126–33.

195. Biesiadecki BJ, Brand PH, Metting PJ, Koch LG, Britton SL. Phenotypic variation in strength among eleven inbred strains of rats. Proc Soc Exp Biol Med Soc Exp Biol Med N Y N. 1998;219(2):126–31.

196. Staats KA, Humblet-Baron S, Bento-Abreu A, Scheveneels W, Nikolaou A, Deckers K, et al. Genetic ablation of IP3 receptor 2 increases cytokines and decreases survival of SOD1G93A mice. Hum Mol Genet. 2016;25(16):3491–9.

197. van Es MA, Van Vught PW, Blauw HM, Franke L, Saris CG, Andersen PM, et al. ITPR2 as a susceptibility gene in sporadic amyotrophic lateral sclerosis: a genome-wide association study. Lancet Neurol. 2007;6(10):869–77.

198. Brown SA, Loew LM. Inositol 1, 4, 5-trisphosphate receptor 1 is essential to spinocerebellar ataxia modeling. Front Neurosci. 2015;8(453):10–3389.

199. Futatsugi A, Ebisui E, Mikoshiba K. Type 2 and type 3 inositol 1,4,5-trisphosphate (IP3) receptors promote the differentiation of granule cell precursors in the postnatal cerebellum. J Neurochem. 2008;105(4):1153–64.

200. Shimobayashi E, Kapfhammer JP. Calcium Signaling, PKC Gamma, IP3R1 and CAR8 Link Spinocerebellar Ataxias and Purkinje Cell Dendritic Development. Curr Neuropharmacol. 2018;16(2):151–9.

201. Hamby ME, Coppola G, Ao Y, Geschwind DH, Khakh BS, Sofroniew MV. Inflammatory Mediators Alter the Astrocyte Transcriptome and Calcium Signaling Elicited by Multiple G-Protein-Coupled Receptors. J Neurosci. 2012;32(42):14489–510.

202. Anderson MA, Burda JE, Ren Y, Ao Y, O'Shea TM, Kawaguchi R, et al. Astrocyte scar formation aids central nervous system axon regeneration. Nature. 2016;532(7598):195–200.

203. Staats KA, Bogaert E, Hersmus N, Jaspers T, Luyten T, Bultynck G, et al. Neuronal overexpression of IP3 receptor 2 is detrimental in mutant SOD1 mice. Biochem Biophys Res Commun. 2012;429(3):210–3.

204. Rakers C, Petzold GC. Astrocytic calcium release mediates peri-infarct depolarizations in a rodent stroke model. J Clin Invest. 2017;127(2):511–6.

205. Denk W, Strickler J, Webb W. Two-photon laser scanning fluorescence microscopy. Science. 1990;

206. Zhang Y, Chen K, Sloan SA, Bennett ML, Scholze AR, O'Keeffe S, et al. An RNA-Sequencing Transcriptome and Splicing Database of Glia, Neurons, and Vascular Cells of the Cerebral Cortex. J Neurosci. 2014;34(36):11929–47.

8. SUPPLEMENTARY INFORMATION

Table 3 – Primers efficiency for the *Itpr1* for the IP_3R1 and *Itpr2* for the IP_3R2.

PRIMERS	CONCENTRATION (μM)	LOG DILUTION	CT VALUE	R^2	SLOPE	EFFICIENCY
Itpr1	16	1.204	-	0.996	-2.990	**116%**
	8	0.903	25.52			
	4	0.602	26.30			
	2	0.301	27.20			
	1	0.000	28.22			
Itpr2	16	1.204		0.996	-3.933	**80%**
	8	0.903	27.60			
	4	0.602	29.00			
	2	0.301	30.10			
	1	0.000	31.18			

Note: [1] The IP_3R1 is a receptor known to be enriched in neurons, while the IP_3R2 receptor is mostly present in astrocytes. In astrocytes, the IP_3R2 is an important structure associated to the modulation of Ca^{2+}signalling. [2]

Table 4 – Statistical information: Behaviour characterization.

BEHAVIOURAL TEST	FIGURE	PAGE	STATISTICAL REPORT
Motor Swimming Test (Total mean)	IP_3R2 KO 9A IP_3R2 KO; Q135 17A	IP_3R2 KO 36 IP_3R2 KO; Q135 45	**Repeat Measures ANOVA** [between-subjects factor: genotype (WT, Q135, IP_3R2 KO, IP_3R2 HET and IP_3R2 KO;Q135 | covariate: age (6,8,12,16,20,24,30 weeks)] **Mauchly'sW (0.154): $\chi 2(20) = 44.559$ $p=0.001$** **ε(Greenhouse-Geisser)=0.586** Within-Subjects effects (Greenhouse-Geisser): [Age] **$F(4,92)=7.934$ $p>0.001$** [Age x Genotype] **$F(14,92)=4.122$ $p>0.001$** Between-subjects effects [Genotype]: **$F(4,26)=10.108$ $p>0.001$** **Multiple comparisons (Dunnett T3)**:

			WT vs Q135 p=0.076 (N.S) WT vs IP_3R2 KO p=1.000 (N.S) WT vs IP_3R2 HET p=0.996 (N.S) WT vs IP_3R2 KO;Q135 p=0.020 Q135 vs IP_3R2 KO p=0.077 (N.S) Q135 vs IP_3R2 HET p=0.055 (N.S) Q135 vs IP_3R2 KO;Q135 p=0.998 (N.S) IP_3R2 KO vs IP_3R2 HET p=0.992 (N.S) IP_3R2 KO vs IP_3R2 KO; Q135 p=0.021 IP_3R2 HET vs IP_3R2 KO;Q135 p=0.011
			One-way ANOVA [between-subjects factor: genotype] week 6: **F(4,43)=4.535 , p=0.004, n^2= 0.317** week 8: **F(4,46)=4.908 , p=0.002, n^2= 0.319** week 12: **F(4,47)=9.202 p<0.001, n^2= 0.461** week 16: **F(4,47)=6.291 p<0.001, n^2= 0.369** week 20: **F(4,46)=12.680 p<0.001, n^2= 0.547** week 24: **F(4,45)=18.597 p<0.001, n^2= 0.645** week 30: **F(4,38)=13.157 p<0.001, n^2= 0.608** **Post-Hoc analyses (Dunnett T3)**: **[week 6]** WT vs Q135 p=0.950 (N.S) WT vs IP_3R2 KO p=0.395 (N.S) WT vs IP_3R2 HET p=0.235 (N.S) WT vs IP_3R2 KO;Q135 p=0.789 (N.S) Q135 vs IP_3R2 KO p=0.154 (N.S) Q135 vs IP_3R2 HET p=0.094 (N.S) Q135 vs IP_3R2 KO;Q135 p=1.000 (N.S) IP_3R2 KO vs IP_3R2 HET p=1.000 (N.S) IP_3R2 KO vs IP_3R2 KO; Q135 p=0.067 (N.S) IP_3R2 HET vs IP_3R2 KO;Q135 p=0.042 **[week 8]** WT vs Q135 p=0.399 (N.S) WT vs IP_3R2 KO p=0.906 (N.S) WT vs IP_3R2 HET p=1.000 (N.S) WT vs IP_3R2 KO ;Q135 p=0.093 (N.S) Q135 vs IP_3R2 KO p=0.129 (N.S) Q135 vs IP_3R2 HET p=0.472 (N.S) Q135 vs IP_3R2 KO;Q135 p=1.000 (N.S) IP_3R2 KO vs IP_3R2 HET p=0.670 (N.S) IP_3R2 KO vs IP_3R2 KO; Q135 p=0.006 IP_3R2 HET vs IP_3R2 KO;Q135 p=0.127 (N.S) **[week 12]** WT vs Q135 p=0.175 (N.S) WT vs IP_3R2 KO p=0.620 (N.S) WT vs IP_3R2 HET p=0.150 (N.S)

			WT vs IP_3R2 KO ;Q135 p=0.381 (N.S) Q135 vs IP_3R2 KO p=0.031 Q135 vs IP_3R2 HET p=0.008 Q135 vs IP_3R2 KO;Q135 p=0.859 (N.S) IP_3R2 KO vs IP_3R2 HET p=0.741 (N.S) IP_3R2 KO vs IP_3R2 KO; Q135 p=0.019 IP_3R2 HET vs IP_3R2 KO;Q135 p=0.016 [week 16] WT vs Q135 p=0.159 (N.S) WT vs IP_3R2 KO p=1.000 (N.S) WT vs IP_3R2 HET p=1.000 (N.S) WT vs IP_3R2 KO;Q135 p=0.035 Q135 vs IP_3R2 KO p=0.158 (N.S) Q135 vs IP_3R2 HET p=0.145 (N.S) Q135 vs IP_3R2 KO;Q135 p=1.000 (N.S) IP_3R2 KO vs IP_3R2 HET p=1.000 (N.S) IP_3R2 KO vs IP_3R2 KO; Q135 p=0.035 IP_3R2 HET vs IP_3R2 KO;Q135 p=0.044 [week 20] WT vs Q135 p=0.026 WT vs IP_3R2 KO p=1,000 (N.S) WT vs IP_3R2 HET p=1.000 (N.S) WT vs IP_3R2 KO;Q135 p=0.001 Q135 vs IP_3R2 KO p=0.025 Q135 vs IP_3R2 HET p=0.034 Q135 vs IP_3R2 KO;Q135 p=1.000 (N.S) IP_3R2 KO vs IP_3R2 HET p=1.000 (N.S) IP_3R2 KO vs IP_3R2 KO; Q135 p=0.001 IP_3R2 HET vs IP_3R2 KO;Q135 p=0.005 [week 24] WT vs Q135 p=0.038 WT vs IP_3R2 KO p=1.000 (N.S) WT vs IP_3R2 HET p=0.200 (N.S) WT vs IP_3R2 KO;Q135 p<0.001 Q135 vs IP_3R2 KO *p=0.026* Q135 vs IP_3R2 HET *p=0.007* Q135 vs IP_3R2 KO;Q135 p=1.000 (N.S) IP_3R2 KO vs IP_3R2 HET p=0.497 (N.S) IP_3R2 KO vs IP_3R2 KO; Q135 p<0.001 IP_3R2 HET vs IP_3R2 KO;Q135 p<0.001 [week 30] WT vs Q135 p=0.092 (N.S) WT vs IP_3R2 KO p=1.000 (N.S) WT vs IP_3R2 HET p=1.000 (N.S)

			WT vs IP_3R2 KO;Q135 ***p*=0.004** Q135 vs IP_3R2 KO ***p*=0.084 (N.S)** Q135 vs IP_3R2 HET ***p*=0.095 (N.S)** Q135 vs IP_3R2 KO;Q135 ***p*=1.000 (N.S)** IP_3R2 KO vs IP_3R2 HET ***p*=0.988 (N.S)** IP_3R2 KO vs IP_3R2 KO; Q135 ***p*=0.003** IP_3R2 HET vs IP_3R2 KO;Q135 ***p*=0.004**
Beam walk test square beam (12mm) – until 16 weeks of age	IP_3R2 KO 9B IP_3R2 KO; Q135 17.B	IP_3R2 KO 36 IP_3R2 KO; Q135 45	**Repeat Measures ANOVA** [between-subjects factor: genotype (WT, Q135, IP_3R2 KO, IP_3R2 HET and IP_3R2 KO;Q135 | covariate: age (6,8,12,16,20,24,30 weeks)] Mauchly'sW (0.668): $\chi 2(5)=12.398$ p=0.030 $\varepsilon_{(Greenhouse-Geisser)}=0.777$ Within-Subjects effects (Huynh-Feldt): [Age] **F(3,91)=10.675 *p<0,001*** [Age x Genotype] **F(11,91)=8.126 *p<0,001*** Between-subjects effects [Genotype] **F(4,32)=15.928 p<0.001** **Multiple comparisons (Dunnett T3)**: WT vs Q135 ***p*=0.932 (N.S)** WT vs IP_3R2 KO ***p*=0.281 (N.S)** WT vs IP_3R2 HET ***p*=0.945 (N.S)** WT vs IP_3R2 KO;Q135 ***p*=0.002** Q135 vs IP_3R2 KO ***p*=0.752 (N.S)** Q135 vs IP_3R2 HET ***p*=0.996 (N.S)** Q135 vs IP_3R2 KO;Q135 ***p*=0.258 (N.S)** IP_3R2 KO vs IP_3R2 HET ***p*=0.309 (N.S)** IP_3R2 KO vs IP_3R2 KO; Q135 ***p*=0.001** IP_3R2 HET vs IP_3R2 KO;Q135 ***p*=0.004**
			One way ANOVA [between-subjects factor: genotype] week 6: **F(4,46)=6.051 , *p*=0.001, n^2= 0.366** week 8: **F(4,45)=2.958 , *p*=0.031, n^2= 0.224** week 12: **F(4,43)=12.599 p<0.001, n^2= 0.564** week 16: **F(4,43)=20.205, p<0.001, n^2=0.675** **Post-Hoc analyses (Dunnett T3)**: **[week 6]** WT vs Q135 ***p*=0.999 (N.S)** WT vs IP_3R2 KO ***p*=0.223 (N.S)** WT vs IP_3R2 HET ***p*=0.999 (N.S)** WT vs IP_3R2 KO ;Q135 ***p*=0.142 (N.S)** Q135 vs IP_3R2 KO ***p*=0.867 (N.S)** Q135 vs IP_3R2 HET ***p*=1.000 (N.S)** Q135 vs IP_3R2 KO;Q135 ***p*=0.083 (N.S)** IP_3R2 KO vs IP_3R2 HET ***p*=0.941 (N.S)** IP_3R2 KO vs IP_3R2 KO; Q135 ***p*=0.008** IP_3R2 HET vs IP_3R2 KO;Q135 ***p*=0.107 (N.S)**

			[week 8] WT vs Q135 p=0.737 (N.S) WT vs IP_3R2 KO p=0.390 (N.S) WT vs IP_3R2 HET p=1.000 (N.S) WT vs IP_3R2 KO ;Q135 p=0.115 (N.S) Q135 vs IP_3R2 KO p=0.452 (N.S) Q135 vs IP_3R2 HET p=0.749 (N.S) Q135 vs IP_3R2 KO;Q135 p=1.000 (N.S) IP_3R2 KO vs IP_3R2 HET p=0.976 (N.S) IP_3R2 KO vs IP_3R2 KO; Q135 p=0.016 IP_3R2 HET vs IP_3R2 KO;Q135 p=0.265 (N.S) **[week 12]** WT vs Q135 p=0.170 (N.S) WT vs IP_3R2 KO p=1.000 (N.S) WT vs IP_3R2 HET p=0.803 (N.S) WT vs IP_3R2 KO ;Q135 p=0.002 Q135 vs IP_3R2 KO p=0.212 (N.S) Q135 vs IP_3R2 HET p=0.402 (N.S) Q135 vs IP_3R2 KO;Q135 p=0.912 (N.S) IP_3R2 KO vs IP_3R2 HET p=0.972 (N.S) IP_3R2 KO vs IP_3R2 KO; Q135 p=0.003 IP_3R2 HET vs IP_3R2 KO;Q135 p=0.009 **[week 16]** WT vs Q135 p=0.369 (N.S) WT vs IP_3R2 KO p=0.985 (N.S) WT vs IP_3R2 HET p=0.998 (N.S) WT vs IP_3R2 KO ;Q135 p<0.001 Q135 vs IP_3R2 KO p=0.306 (N.S) Q135 vs IP_3R2 HET p=0.489 (N.S) Q135 vs IP_3R2 KO;Q135 p=0.270 (N.S) IP_3R2 KO vs IP_3R2 HET p=0.892 (N.S) IP_3R2 KO vs IP_3R2 KO; Q135 p<0.001 IP_3R2 HET vs IP_3R2 KO;Q135 p=0.001
Beam walk test **square beam -** **12mm** **(Score)**	IP_3R2 KO 9C IP_3R2 KO; Q135 17C	IP_3R2 KO 36 IP_3R2 KO; Q135 45	**Friedman Test** χ_w^2 (2,134) =238.853 p<0.001 **Kruskal-Wallis test** [between-subjects factor: genotype] **Week 20: χ_w^2 (4,47)=15.847 p=0.003 n^2= 0.299** Pairwise comparisons: WT vs Q135 p=0.176 (N.S) WT vs IP_3R2 KO p=1.000 (N.S) WT vs IP_3R2 HET p=1.000 (N.S) WT vs IP_3R2 KO;Q135 p=0.001 Q135 vs IP_3R2 KO p=0.186 (N.S) Q135 vs IP_3R2 HET p=0.249 (N.S) Q135 vs IP_3R2 KO;Q135 p=0.074 (N.S)

			IP_3R2 KO vs IP_3R2 HET ***p*=1.000 (N.S)** IP_3R2 KO vs IP_3R2 KO; Q135 ***p*=0.001** IP_3R2 HET vs IP_3R2 KO;Q135 ***p*=0.005** **<u>Week 24:</u> χ_w^2 (4,47)=28.174 *p*<0.001 n^2=0.585** Pairwise comparisons: WT vs Q135 ***p*<0.001** WT vs IP_3R2 KO ***p*=1.000 (N.S)** WT vs IP_3R2 HET ***p*=1.000 (N.S)** WT vs IP_3R2 KO;Q135 ***p*<0.001** Q135 vs IP_3R2 KO ***p*=0.001** Q135 vs IP_3R2 HET ***p*=0.003** Q135 vs IP_3R2 KO;Q135 ***p*=0.972 (N.S)** IP_3R2 KO vs IP_3R2 HET ***p*=1.000 (N.S)** IP_3R2 KO vs IP_3R2 KO; Q135 ***p*<0.001** IP_3R2 HET vs IP_3R2 KO;Q135 ***p*=0.002** **<u>Week 30:</u> χ_w^2 (4,40)=27.513 *p*<0.001 n^2= 0.681** Pairwise comparisons: WT vs Q135 ***p=0.002*** WT vs IP_3R2 KO ***p*=1.000 (N.S)** WT vs IP_3R2 HET ***p*=1.000 (N.S)** WT vs IP_3R2 KO;Q135 ***p*<0.001** Q135 vs IP_3R2 KO ***p*=0.002** Q135 vs IP_3R2 HET ***p*=0.004** Q135 vs IP_3R2 KO;Q135 ***p*=0.743 (N.S)** IP_3R2 KO vs IP_3R2 HET ***p*=1.000 (N.S)** IP_3R2 KO vs IP_3R2 KO; Q135 ***p*<0.001** IP_3R2 HET vs IP_3R2 KO;Q135 ***p*=0.001**
Beam walk test **circle beam -** **11mm** **(Score)**	<u>IP_3R2 KO</u> 9D <u>IP_3R2 KO;</u> <u>Q135</u> 17D	<u>IP_3R2 KO</u> 36 <u>IP_3R2 KO;</u> <u>Q135</u> 45	**Friedman Test** χ_w^2 (2,330) =581.068 *p*<0.001 **Kruskal-Wallis test** [between-subjects factor: genotype] **<u>Week 6:</u> χ_w^2 (4,49)=4.369 *p*=0.358 n^2=0.030** **<u>Week 8:</u> χ_w^2 (4,49)=18.287 *p*=0.001 n^2=0.340** Pairwise comparisons: WT vs Q135 ***p*=0.003** WT vs IP_3R2 KO ***p*=1.000 (N.S)** WT vs IP_3R2 HET ***p*=1.000 (N.S)** WT vs IP_3R2 KO;Q135 ***p*=0.004** Q135 vs IP_3R2 KO ***p*=0.005** Q135 vs IP_3R2 HET ***p*=0.014** Q135 vs IP_3R2 KO;Q135 ***p*=0.816 (N.S)** IP_3R2 KO vs IP_3R2 HET ***p*=1.000 (N.S)** IP_3R2 KO vs IP_3R2 KO; Q135 ***p*=0.006** IP_3R2 HET vs IP_3R2 KO;Q135 ***p*=0.017**

			<u>Week 12:</u> χ_w^2 (4,49)=29.833 $p<0.001$ n^2=0.596 Pairwise comparisons: WT vs Q135 p=0.002 WT vs IP_3R2 KO p=1.000 (N.S) WT vs IP_3R2 HET p=0.460 (N.S) WT vs IP_3R2 KO;Q135 p<0.001 Q135 vs IP_3R2 KO p=0.002 Q135 vs IP_3R2 HET p=0.052 Q135 vs IP_3R2 KO;Q135 p=0.377 (N.S) IP_3R2 KO vs IP_3R2 HET p=0.475 (N.S) IP_3R2 KO vs IP_3R2 KO; Q135 p<0.001 IP_3R2 HET vs IP_3R2 KO;Q135 p=0.005 <u>Week 16:</u> χ_w^2 (4,49)=36.432 $p<0.001$ n^2=0.743 Pairwise comparisons: WT vs Q135 p<0.001 WT vs IP_3R2 KO p=1.000 (N.S) WT vs IP_3R2 HET p=1.000 (N.S) WT vs IP_3R2 KO ;Q135 p<0.001 Q135 vs IP_3R2 KO p=0.001 Q135 vs IP_3R2 HET p=0.003 Q135 vs IP_3R2 KO;Q135 p=0.560 (N.S) IP_3R2 KO vs IP_3R2 HET p=1.000 (N.S) IP_3R2 KO vs IP_3R2 KO; Q135 p<0.001 IP_3R2 HET vs IP_3R2 KO;Q135 p<0.001 <u>Week 20:</u> χ_w^2 (4,47)=35.008 p<0.001 n^2=0.744 Pairwise comparisons: WT vs Q135 p<0.001 WT vs IP_3R2 KO p=1.000 (N.S) WT vs IP_3R2 HET p=1.000 (N.S) WT vs IP_3R2 KO;Q135 p<0.001 Q135 vs IP_3R2 KO p<0.001 Q135 vs IP_3R2 HET p=0.002 Q135 vs IP_3R2 KO;Q135 p=0.645 (N.S) IP_3R2 KO vs IP_3R2 HET p=1.000 (N.S) IP_3R2 KO vs IP_3R2 KO; Q135 p<0.001 IP_3R2 HET vs IP_3R2 KO;Q135 p<0.001 <u>Week 24:</u> χ_w^2 (4,47)=38.818 p<0.001 n^2=0.833 Pairwise comparisons: WT vs Q135 p<0.001 WT vs IP_3R2 KO p=1.000 (N.S) WT vs IP_3R2 HET p=1.000 (N.S) WT vs IP_3R2 KO;Q135 p<0.001 Q135 vs IP_3R2 KO p<0.001 Q135 vs IP_3R2 HET p=0.002 Q135 vs IP_3R2 KO;Q135 p=0.387(N.S)

			IP_3R2 KO vs IP_3R2 HET p=1.000 (N.S) IP_3R2 KO vs IP_3R2 KO; Q135 p<0.001 IP_3R2 HET vs IP_3R2 KO;Q135 p<0.001 Week 30: χ_w2 (4,40)=25.497 p<0.001 n^2=0.625 Pairwise comparisons: WT vs Q135 p=0.003 WT vs IP_3R2 KO p=1.000 (N.S) WT vs IP_3R2 HET p=0.513 (N.S) WT vs IP_3R2 KO;Q135 p<0.001 Q135 vs IP_3R2 KO p=0.003 Q135 vs IP_3R2 HET p=0.042 Q135 vs IP_3R2 KO;Q135 p=0.473 (N.S) IP_3R2 KO vs IP_3R2 HET p=0.513 (N.S) IP_3R2 KO vs IP_3R2 KO; Q135 p<0.001 IP_3R2 HET vs IP_3R2 KO;Q135 p=0.005
Stride length (Gait Analysis)	IP_3R2 KO 10A IP_3R2 KO; Q135 18A	IP_3R2 KO 37 IP_3R2 KO; Q135 46	Repeat Measures ANOVA [between-subjects factor: genotype (WT, Q135, IP_3R2 KO, IP_3R2 HET and IP_3R2 KO;Q135 | covariate: age (6,8,12,16,20,24,30 weeks)] Mauchly'sW (0.777): χ2(5)=6.752 p=0.240 $\varepsilon_{(Greenhouse-Geisser)}$=0.867 Within-Subjects effects (Huynh-Feldt): [Age] F(3,84)=1.391 p=0.251 [Age x Genotype] F(12,84)=4.070 p<0.001 Between-subjects effects [Genotype] F(4,28)=8.610 p<0.001 Multiple comparisons (Tukey HSD): WT vs Q135 p=0.656 (N.S) WT vs IP_3R2 KO p=0.206 (N.S) WT vs IP_3R2 HET p=0.608 (N.S) WT vs IP_3R2 KO;Q135 p=0.004 Q135 vs IP_3R2 KO p=0.044 Q135 vs IP_3R2 HET p=1.000 (N.S) Q135 vs IP_3R2 KO;Q135 p=0.278 (N.S) IP_3R2 KO vs IP_3R2 HET p=0.028 IP_3R2 KO vs IP_3R2 KO; Q135 p<0.001 IP_3R2 HET vs IP_3R2 KO;Q135 p=0.215
			One-way ANOVA [between-subjects factor: genotype] week 6: F(4,47)=5.147 , p=0.002, n^2=0.324 week 8: F(4,48)=3.123 , p=0.024, n^2 = 0.221 week 12: F(4,44)=3.580 , p=0.014 n^2 = 0.264 week 16: F(4,33)=16.902 , p<0.001, n^2 = 0.700 Post-Hoc analyses (Dunnett T3):

			[week 6] WT vs Q135 p=0.314 (N.S) WT vs IP_3R2 KO p=0.034 WT vs IP_3R2 HET p=1.000 (N.S) WT vs IP_3R2 KO;Q135 p=1.000 (N.S) Q135 vs IP_3R2 KO p=0.508 (N.S) Q135 vs IP_3R2 HET p=0.661 (N.S) Q135 vs IP_3R2 KO;Q135 p=0.046 IP_3R2 KO vs IP_3R2 HET p=0.172(N.S) IP_3R2 KO vs IP_3R2 KO; Q135 p=0,001 IP_3R2 HET vs IP_3R2 KO;Q135 p=1.000 (N.S) [week 8] WT vs Q135 p=0.804 (N.S) WT vs IP_3R2 KO p=0.999 (N.S) WT vs IP_3R2 HET p=0.998 (N.S) WT vs IP_3R2 KO;Q135 p=0.218 (N.S) Q135 vs IP_3R2 KO p=0.264 (N.S) Q135 vs IP_3R2 HET p=0.997 (N.S) Q135 vs IP_3R2 KO;Q135 p=0.991 (N.S) IP_3R2 KO vs IP_3R2 HET p=0.809 (N.S) IP_3R2 KO vs IP_3R2 KO; Q135 p=0.013 IP_3R2 HET vs IP_3R2 KO;Q135 p=0.709 (N.S) [week 12] WT vs Q135 p=0.996 (N.S) WT vs IP_3R2 KO p=1.000 (N.S) WT vs IP_3R2 HET p=1.000 (N.S) WT vs IP_3R2 KO ;Q135 p=0.099 (N.S) Q135 vs IP_3R2 KO p=0.947 (N.S) Q135 vs IP_3R2 HET p=1.000 (N.S) Q135 vs IP_3R2 KO;Q135 p=0.439 (N.S) IP_3R2 KO vs IP_3R2 HET p=0.998 (N.S) IP_3R2 KO vs IP_3R2 KO; Q135 p=0.056 IP_3R2 HET vs IP_3R2 KO;Q135 p=0.378 [week 16] WT vs Q135 p=0.001 WT vs IP_3R2 KO p=0.84 (N.S) WT vs IP_3R2 HET p=0.587 (N.S) WT vs IP_3R2 KO;Q135 p<0.001 Q135 vs IP_3R2 KO p=0.001 (N.S) Q135 vs IP_3R2 HET p=0.263 (N.S) Q135 vs IP_3R2 KO;Q135 p=0.998 (N.S) IP_3R2 KO vs IP_3R2 HET p=0.241 (N.S) IP_3R2 KO vs IP_3R2 KO; Q135 p<0.001 IP_3R2 HET vs IP_3R2 KO;Q135 p=0.162

Body Weight (SHIRPA Protocol)	IP_3R2 KO 11A IP_3R2 KO; Q135 19A	IP_3R2 KO 38 IP_3R2 KO; Q135 47	**Repeat Measures ANOVA** [between-subjects factor: genotype (WT, Q135, IP_3R2 KO, IP_3R2 HET and IP_3R2 KO;Q135 | covariate: age (6,8,12,16,20,24,30 weeks)] Mauchly'sW (0.036): $\chi 2(20)=112.661$ $p<0.001$ $\varepsilon_{(Greenhouse-Geisser)}=0.406$ Within-Subjects effects (Greenhouse-Geisser): [Age] **F(2.88)=154.127 p<0.001** [Age x Genotype] **F(10.88)=14.334 p<0.001** Between-subjects effects [Genotype] **F(4.36)=19.485 p<0.001** **Multiple comparisons (Dunnett T3):** WT vs Q135 **p=0.173 (N.S)** WT vs IP_3R2 KO **p=0.996 (N.S)** WT vs IP_3R2 HET **p=0.978 (N.S)** WT vs IP_3R2 KO;Q135 **p<0,001** Q135 vs IP_3R2 KO **p=0.397 (N.S)** Q135 vs IP_3R2 HET **p=0.261 (N.S)** Q135 vs IP_3R2 KO;Q135 **p=0.353 (N.S)** IP_3R2 KO vs IP_3R2 HET **p=1.000 (N.S)** IP_3R2 KO vs IP_3R2 KO; Q135 **p<0.001** IP_3R2 HET vs IP_3R2 KO;Q135 **p<0.001**
			One-way ANOVA [between-subjects factor: genotype] week 6: **F(4,48)=1.197 , p=0.326, n^2 = 0.098** week 8: **F(4,48)=3.997 , p=0.007, n^2 = 0.267** week 12: **F(4,48)=11.075 , p<0.001 n^2 = 0.502** week 16: **F(4,48)=12.052 , p<0.001, n^2 = 0.523** week 20: **F(4,47)=28.619 , p<0.001, n^2 = 0.727** week 24: **F(4,47)=34.103 , p<0.001, n^2 = 0.760** week 30: **F(4,41)=30.343 , p<0.001, n^2 = 0.766** **Post-Hoc analyses (Dunnett T3)**: **[week 6]** WT vs Q135 **p=1.000 (N.S)** WT vs IP_3R2 KO **p=1.000 (N.S)** WT vs IP_3R2 HET **p=0.647 (N.S)** WT vs IP_3R2 KO;Q135 **p=0.978 (N.S)** Q135 vs IP_3R2 KO **p=1.000 (N.S)** Q135 vs IP_3R2 HET **p=0.264 (N.S)** Q135 vs IP_3R2 KO;Q135 **p=0.632 (N.S)** IP_3R2 KO vs IP_3R2 HET **p=0.646 (N.S)** IP_3R2 KO vs IP_3R2 KO; Q135 **p=0.970 (N.S)** IP_3R2 HET vs IP_3R2 KO;Q135 **p=0.978 (N.S)** **[week 8]**

			WT vs Q135 p=0.663 (N.S) WT vs IP_3R2 KO p=0.981 (N.S) WT vs IP_3R2 HET p=0.985 (N.S) WT vs IP_3R2 KO;Q135 p=0.005 Q135 vs IP_3R2 KO p=1.000 (N.S) Q135 vs IP_3R2 HET p=1.000 (N.S) Q135 vs IP_3R2 KO;Q135 p=0.372 (N.S) IP_3R2 KO vs IP_3R2 HET p=1.000 (N.S) IP_3R2 KO vs IP_3R2 KO; Q135 p=0.223 IP_3R2 HET vs IP_3R2 KO;Q135 p=0.245 (N.S) [week 12] WT vs Q135 p=0.022 WT vs IP_3R2 KO p=0.961 (N.S) WT vs IP_3R2 HET p=0.760 (N.S) WT vs IP_3R2 KO;Q135 p<0.001 Q135 vs IP_3R2 KO p=0.453 (N.S) Q135 vs IP_3R2 HET p=0.255 (N.S) Q135 vs IP_3R2 KO;Q135 p=0.443 (N.S) IP_3R2 KO vs IP_3R2 HET p=1.000 (N.S) IP_3R2 KO vs IP_3R2 KO; Q135 p=0.014 IP_3R2 HET vs IP_3R2 KO;Q135 p=0.002 [week 16] WT vs Q135 p=0.137 (N.S) WT vs IP_3R2 KO p=1.000 (N.S) WT vs IP_3R2 HET p=0.999 (N.S) WT vs IP_3R2 KO;Q135 p=0.001 Q135 vs IP_3R2 KO p=0.072 (N.S) Q135 vs IP_3R2 HET p=0.024 (N.S) Q135 vs IP_3R2 KO;Q135 p=0.601 (N.S) IP_3R2 KO vs IP_3R2 HET p=0.999 (N.S) IP_3R2 KO vs IP_3R2 KO; Q135 p<0.001 IP_3R2 HET vs IP_3R2 KO;Q135 p<0.001 [week 20] WT vs Q135 p=0.016 WT vs IP_3R2 KO p=0.983 (N.S) WT vs IP_3R2 HET p=0.994 (N.S) WT vs IP_3R2 KO;Q135 p<0.001 Q135 vs IP_3R2 KO p=0.040 Q135 vs IP_3R2 HET p=0.026 Q135 vs IP_3R2 KO;Q135 p=0.617 (N.S) IP_3R2 KO vs IP_3R2 HET p=1.000 (N.S) IP_3R2 KO vs IP_3R2 KO; Q135 p<0.001 IP_3R2 HET vs IP_3R2 KO;Q135 p<0.001 [week 24]

			WT vs Q135 p=0.016 WT vs IP_3R2 KO p=0.785 (N.S) WT vs IP_3R2 HET p=1.000 (N.S) WT vs IP_3R2 KO;Q135 p<0.001 Q135 vs IP_3R2 KO p=0.039 Q135 vs IP_3R2 HET p=0.015 Q135 vs IP_3R2 KO;Q135 p=0.594 (N.S) IP_3R2 KO vs IP_3R2 HET p=0.838 (N.S) IP_3R2 KO vs IP_3R2 KO; Q135 p<0.001 IP_3R2 HET vs IP_3R2 KO;Q135 p<0.001 [week 30] WT vs Q135 p=0.091 (N.S) WT vs IP_3R2 KO p=1.000 (N.S) WT vs IP_3R2 HET p=1.000 (N.S) WT vs IP_3R2 KO ;Q135 p<0.001 Q135 vs IP_3R2 KO p=0.105 (N.S) Q135 vs IP_3R2 HET p=0.089 (N.S) Q135 vs IP_3R2 KO;Q135 p=0.635 (N.S) IP_3R2 KO vs IP_3R2 HET p=1.000 (N.S) IP_3R2 KO vs IP_3R2 KO; Q135 p<0.001 IP_3R2 HET vs IP_3R2 KO;Q135 p<0.001
Number of vertical movements (Spontaneous activity) - SHIRPA Protocol)	IP_3R2 KO 11.B IP_3R2 KO; Q135 19.B	IP_3R2 KO 38 IP_3R2 KO; Q135 47	**Repeat Measures ANOVA** [between-subjects factor: genotype (WT, Q135, IP_3R2 KO, IP_3R2 HET and IP_3R2 KO;Q135 | covariate: age (6,8,12,16,20,24,30 weeks)] Mauchly'sW (0.033): $\chi 2(20)=74.364$ $p<0.001$ $\varepsilon_{(Greenhouse-Geisser)}=0.478$ Within-Subjects effects (Greenhouse-Geisser): [Age] F(3,69)=39.279 p<0.001 [Age x Genotype] F(12,69)=1.219 p=0.290 Between-subjects effects [Genotype] F(4,24)=7.406 p<0.001 **Multiple comparisons (Dunnett T3):** WT vs Q135 p=0.189 (N.S) WT vs IP_3R2 KO p=0.999(N.S) WT vs IP_3R2 HET p=1.000 (N.S) WT vs IP_3R2 KO;Q135 p=0.064 Q135 vs IP_3R2 KO p=0.019 Q135 vs IP_3R2 HET p=0.643(N.S) Q135 vs IP_3R2 KO;Q135 p=0.654 (N.S) IP_3R2 KO vs IP_3R2 HET p=0.978 (N.S) IP_3R2 KO vs IP_3R2 KO;Q135 p=0.004 (N.S) IP_3R2 HET vs IP_3R2 KO;Q135 p=0.370 (N.S)

			One-way ANOVA [between-subjects factor: genotype] week 6: **F(4,48)=1.970 , p=0.116, n_p^2 = 0.152** week 8: **F(4,46)=5.938 , p=0.001, n_p^2 = 0.361** week 12: **F(4,47)=7.564 , p<0.001n_p^2 = 0.413** week 16: **F(4,46)=3.095 , p=0.025, n_p^2 = 0.228** week 20: **F(4,46)=4.490 , p=0.004 n_p^2 = 0.300** week 24: **F(4,44)=5.610 , p=0.001, n_p^2 = 0.359** week 30: **F(4,36)=5.648 , p=0.001, n_p^2 = 0.414** **Post-Hoc analyses (Dunnett T3)**: **[week 6]** WT vs Q135 ***p*=0.882 (N.S)** WT vs IP_3R2 KO ***p*=1.000 (N.S)** WT vs IP_3R2 HET ***p*=0.998 (N.S)** WT vs IP_3R2 KO;Q135 ***p*=0.145 (N.S)** Q135 vs IP_3R2 KO ***p*=0.946 (N.S)** Q135 vs IP_3R2 HET ***p*=1.000(N.S)** Q135 vs IP_3R2 KO;Q135 ***p*=0.751 (N.S)** IP_3R2 KO vs IP_3R2 HET ***p*=0.999 (N.S)** IP_3R2 KO vs IP_3R2 KO; Q135 ***p*=0.198 (N.S)** IP_3R2 HET vs IP_3R2 KO;Q135 ***p*=0.969 (N.S)** **[week 8]** WT vs Q135 ***p*=0.420** WT vs IP_3R2 KO ***p*=0.993 (N.S)** WT vs IP_3R2 HET ***p*=1.000 (N.S))** WT vs IP_3R2 KO;Q135 ***p*=0.007** Q135 vs IP_3R2 KO ***p*=0.128** Q135 vs IP_3R2 HET ***p*=0.611** Q135 vs IP_3R2 KO;Q135 ***p*=0.674 (N.S)** IP_3R2 KO vs IP_3R2 HET ***p*=1.000 (N.S)** IP_3R2 KO vs IP_3R2 KO; Q135 ***p*=0.004 (N.S)** IP_3R2 HET vs IP_3R2 KO;Q135 ***p*=0.169 (N.S)** **[week 12]** WT vs Q135 ***p*=0.424** WT vs IP_3R2 KO ***p*=0.517 (N.S)** WT vs IP_3R2 HET ***p*=1.000 (N.S)** WT vs IP_3R2 KO;Q135 ***p*=0.002** Q135 vs IP_3R2 KO ***p*=0.059** Q135 vs IP_3R2 HET ***p*=0.846 (N.S)** Q135 vs IP_3R2 KO;Q135 ***p*=0.487 (N.S)** IP_3R2 KO vs IP_3R2 HET ***p*=0.907 (N.S)** IP_3R2 KO vs IP_3R2 KO; Q135 ***p*=0.008 (N.S)** IP_3R2 HET vs IP_3R2 KO;Q135 ***p*=0.332 (N.S)** **[week 16]** WT vs Q135 ***p*=0.008**

			WT vs IP_3R2 KO p=1.000(N.S) WT vs IP_3R2 HET p=1.000 (N.S) WT vs IP_3R2 KO;Q135 p=0.006 Q135 vs IP_3R2 KO p=0.418 (N.S) Q135 vs IP_3R2 HET p=0.597 (N.S) Q135 vs IP_3R2 KO;Q135 p=0.959(N.S) IP_3R2 KO vs IP_3R2 HET p=1.000 (N.S) IP_3R2 KO vs IP_3R2 KO; Q135 p=0.387 (N.S) IP_3R2 HET vs IP_3R2 KO;Q135 p=0.555(N.S) [week 20] WT vs Q135 p=0.140 (N.S) WT vs IP_3R2 KO p=1.000 (N.S) WT vs IP_3R2 HET p=1.000 (N.S) WT vs IP_3R2 KO;Q135 p=0.113 Q135 vs IP_3R2 KO p=0.155 (N.S) Q135 vs IP_3R2 HET p=0.143 (N.S) Q135 vs IP_3R2 KO;Q135 p=0.957 (N.S) IP_3R2 KO vs IP_3R2 HET p=1.000 (N.S) IP_3R2 KO vs IP_3R2 KO; Q135 p=0.131 (N.S) IP_3R2 HET vs IP_3R2 KO;Q135 p=0.125 (N.S) [week 24] WT vs Q135 p=0.207 (N.S) WT vs IP_3R2 KO p=0.845(N.S) WT vs IP_3R2 HET p=0.289 (N.S) WT vs IP_3R2 KO;Q135 p=0.133 (N.S) Q135 vs IP_3R2 KO p=0.101 (N.S) Q135 vs IP_3R2 HET p=1.000(N.S) Q135 vs IP_3R2 KO;Q135 p=0.957 (N.S) IP_3R2 KO vs IP_3R2 HET p=0.119 (N.S) IP_3R2 KO vs IP_3R2 KO;Q135 p=0.081 (N.S) IP_3R2 HET vs IP_3R2 KO;Q135 p=0.945 (N.S) [week 30] WT vs Q135 p=0.371 (N.S) WT vs IP_3R2 KO p=0.307 (N.S) WT vs IP_3R2 HET p=0.097 (N.S) WT vs IP_3R2 KO;Q135 p=0.060 (N.S) Q135 vs IP_3R2 KO p=1.000 (N.S) Q135 vs IP_3R2 HET p=0.999(N.S) Q135 vs IP_3R2 KO;Q135 p=0.950N.S) IP_3R2 KO vs IP_3R2 HET p=0.981 (N.S) IP_3R2 KO vs IP_3R2 KO;Q135 p=0.718 (N.S) IP_3R2 HET vs IP_3R2 KO;Q135 p=0.945 (N.S)
	IP_3R2 KO	IP_3R2 KO	Repeat Measures ANOVA

Number of squares Travelled (Spontaneous locomotor activity-SHIRPA Protocol)	11C IP₃R2 KO; Q135 19C	38 IP₃R2 KO; Q135 47	[between-subjects factor: genotype (WT, Q135, IP₃R2 KO, IP₃R2 HET and IP₃R2 KO;Q135 | covariate: age (6,8,12,16,20,24,30 weeks)] Mauchly'sW (0.232): $\chi 2(20)=39.173$ p=0.007 $\varepsilon_{(Greenhouse-Geisser)}=0.633$ Within-Subjects effects (Greenhouse-Geisser): [Age] **F(4,110)=56.524 p<0.001** [Age x Genotype] **F(15,110)=1.626 p=0.077** Between-subjects effects [Genotype] **F(4,29)=19.698 p<0.001** **Multiple comparisons (Dunnett T3):** WT vs Q135 **p=0.061 (N.S)** WT vs IP₃R2 KO **p=0.097 (N.S)** WT vs IP₃R2 HET **p=1.000 (N.S)** WT vs IP₃R2 KO;Q135 **p<0.001** Q135 vs IP₃R2 KO **p=0.002** Q135 vs IP₃R2 HET **p=0.305 (N.S)** Q135 vs IP₃R2 KO;Q135 **p=0.952 (N.S)** IP₃R2 KO vs IP₃R2 HET **p=0.498 (N.S)** IP₃R2 KO vs IP₃R2 KO; Q135 **p=0.001** IP₃R2 HET vs IP₃R2 KO;Q135 **p=0.142 (N.S)**
			One-way ANOVA [between-subjects factor: genotype] week 6: **F(4,46)=3.615 , p=0.013, n^2 =0,256** week 8: **F(4,45)=7.564 , p<0.001, n^2 = 0,425** week 12: **F(4,45)=16.579 , p<0.001, n^2 = 0,618** week 16: **F(4,48)=13.244 , p<0.001, n^2 = 0,546** week 20: **F(4,47)=7.241, p<0.001, n^2 = 0,402** week 24: **F(4,47)=8.108 , p<0.001, n^2 = 0,430** week 30: **F(4,40)=4.894 , p=0.003 , n^2 = 0,352** **Post-Hoc analyses (Dunnett T3)**: **[week 6]** WT vs Q135 **p=1.000 (N.S)** WT vs IP₃R2 KO **p=0.057 (N.S)** WT vs IP₃R2 HET **p=1.000 (N.S)** WT vs IP₃R2 KO;Q135 **p=0.885 (N.S)** Q135 vs IP₃R2 KO **p=0.403 (N.S)** Q135 vs IP₃R2 HET **p=1.000 (N.S)** Q135 vs IP₃R2 KO;Q135 **p=0.640 (N.S)** IP₃R2 KO vs IP₃R2 HET **p=0.065 (N.S)** IP₃R2 KO vs IP₃R2 KO; Q135 **p=0.011** IP₃R2 HET vs IP₃R2 KO;Q135 **p=0.609 (N.S)** **[week 8]** WT vs Q135 **p=0.479 (N.S)**

			WT vs IP_3R2 KO p=0.519 (N.S) WT vs IP_3R2 HET p=0.908 (N.S) WT vs IP_3R2 KO;Q135 p=0.026 Q135 vs IP_3R2 KO p=0.056 (N.S) Q135 vs IP_3R2 HET p=0.155 (N.S) Q135 vs IP_3R2 KO;Q135 p=0.930 (N.S) IP_3R2 KO vs IP_3R2 HET p=0.999 (N.S) IP_3R2 KO vs IP_3R2 KO; Q135 p=0.002 IP_3R2 HET vs IP_3R2 KO;Q135 p=0.010 [week 12] WT vs Q135 p=0.004 WT vs IP_3R2 KO p=0.999 (N.S) WT vs IP_3R2 HET p=0.905 (N.S) WT vs IP_3R2 KO;Q135 p<0.001 Q135 vs IP_3R2 KO p=0.001 Q135 vs IP_3R2 HET p=0.246 (N.S) Q135 vs IP_3R2 KO;Q135 p=0.970 (N.S) IP_3R2 KO vs IP_3R2 HET p=0.592 (N.S) IP_3R2 KO vs IP_3R2 KO; Q135 *p<0.001* (N.S) IP_3R2 HET vs IP_3R2 KO;Q135 p=0.077 (N.S) [week 16] WT vs Q135 p=0.001 WT vs IP_3R2 KO p=1.000 (N.S) WT vs IP_3R2 HET p=0.949(N.S) WT vs IP_3R2 KO;Q135 p=0.001 Q135 vs IP_3R2 KO p=0.002 Q135 vs IP_3R2 HET p=0.380 (N.S) Q135 vs IP_3R2 KO;Q135 p=0.998 (N.S) IP_3R2 KO vs IP_3R2 HET p=0.838 (N.S) IP_3R2 KO vs IP_3R2 KO; Q135 p=0.001 IP_3R2 HET vs IP_3R2 KO;Q135 p=0.303 (N.S) [week 20] WT vs Q135 p=0.068 (N.S) WT vs IP_3R2 KO p=1.000 (N.S) WT vs IP_3R2 HET p=0.912 (N.S) WT vs IP_3R2 KO;Q135 p=0.032 Q135 vs IP_3R2 KO p=0.015 Q135 vs IP_3R2 HET p=0.581 (N.S) Q135 vs IP_3R2 KO;Q135 p=0.653 (N.S) IP_3R2 KO vs IP_3R2 HET p=0.919 (N.S) IP_3R2 KO vs IP_3R2 KO; Q135 p=0.006 IP_3R2 HET vs IP_3R2 KO;Q135 p=0.351 (N.S) [week 24] WT vs Q135 p=0.041

			WT vs IP_3R2 KO ***p*=0.860 (N.S)** WT vs IP_3R2 HET ***p*=1.000 (N.S)** WT vs IP_3R2 KO;Q135 ***p*=0.010** Q135 vs IP_3R2 KO ***p*=0.037** Q135 vs IP_3R2 HET ***p*=0.092 (N.S)** Q135 vs IP_3R2 KO;Q135 ***p*=0.940 (N.S)** IP_3R2 KO vs IP_3R2 HET ***p*=0.804 (N.S)** IP_3R2 KO vs IP_3R2 KO; Q135 ***p*=0.020** IP_3R2 HET vs IP_3R2 KO;Q135 ***p*=0.045** **[week 30]** WT vs Q135 ***p*=0.159 (N.S)** WT vs IP_3R2 KO ***p*=1.000 (N.S)** WT vs IP_3R2 HET ***p*=1.000 (N.S)** WT vs IP_3R2 KO;Q135 ***p*=0.073 (N.S)** Q135 vs IP_3R2 KO ***p*=0.216 (N.S)** Q135 vs IP_3R2 HET ***p*=0.266 (N.S)** Q135 vs IP_3R2 KO;Q135 ***p*=0.897 (N.S)** IP_3R2 KO vs IP_3R2 HET ***p*=1.000 (N.S)** IP_3R2 KO vs IP_3R2 KO; Q135 ***p*=0.090 (N.S)** IP_3R2 HET vs IP_3R2 KO;Q135 ***p*=0.146 (N.S)**
Hanging wire grid **(SHIRPA Protocol)**	<u>IP_3R2 KO</u> 12A <u>IP_3R2 KO;</u> <u>Q135</u> 20A	<u>IP_3R2 KO</u> 39 <u>IP_3R2 KO;</u> <u>Q135</u> 48	**Friedman Test** χ_w^2 (2,334) =482,772 p<0,001 **Kruskal-Wallis test** [between-subjects factor: genotype] **<u>Week 6:</u> χ_w^2 (4,49)=26.958 *p*<0.001 n^2=0.532** Pairwise comparisons: WT vs Q135 ***p*=0.019** WT vs IP_3R2 KO ***p*=0.855 (N.S)** WT vs IP_3R2 HET ***p*=0.637 (N.S)** WT vs IP_3R2 KO;Q135 ***p<0.001*** Q135 vs IP_3R2 KO ***p=0.016*** Q135 vs IP_3R2 HET ***p*=0.016** Q135 vs IP_3R2 KO;Q135 ***p*=0.187(N.S)** IP_3R2 KO vs IP_3R2 HET ***p*=0.760 (N.S)** IP_3R2 KO vs IP_3R2 KO; Q135 ***p<0.001*** IP_3R2 HET vs IP_3R2 KO;Q135 ***p<0.001*** **<u>Week 8:</u> χ_w^2 (4.49)=21.021 *p<0.001* n^2=0.400** Pairwise comparisons: WT vs Q135 ***p*=0.004** WT vs IP_3R2 KO ***p*=0.719 (N.S)** WT vs IP_3R2 HET ***p*=0.758(N.S)** WT vs IP_3R2 KO;Q135 ***p*=0.001** Q135 vs IP_3R2 KO ***p=0.002*** Q135 vs IP_3R2 HET ***p*=0.033** Q135 vs IP_3R2 KO;Q135 ***p*=0.970 (N.S)** IP_3R2 KO vs IP_3R2 HET ***p*=0.550 (N.S)** IP_3R2 KO vs IP_3R2 KO; Q135 ***p*=0.001**

			IP_3R2 HET vs IP_3R2 KO;Q135 p=0.022 Week 12: χ_w^2 (4,49)=26.969 p<0.001 n^2=0.533 Pairwise comparisons: WT vs Q135 p=0.009 WT vs IP_3R2 KO p=0.678(N.S) WT vs IP_3R2 HET p=0.718 (N.S) WT vs IP_3R2 KO;Q135 *p<0.001* Q135 vs IP_3R2 KO *p=0.004* Q135 vs IP_3R2 HET p=0.011 Q135 vs IP_3R2 KO;Q135 p=0.391 (N.S) IP_3R2 KO vs IP_3R2 HET p=0.996 (N.S) IP_3R2 KO vs IP_3R2 KO; Q135 *p<0.001* IP_3R2 HET vs IP_3R2 KO;Q135 *p<0.001* Week 16: χ_w^2 (4,49)=23.184 p<0.001 n^2=0.449 Pairwise comparisons: WT vs Q135 p=0.031 WT vs IP_3R2 KO p=0.799(N.S) WT vs IP_3R2 HET p=0.813 (N.S) WT vs IP_3R2 KO;Q135 *p<0.001* Q135 vs IP_3R2 KO *p=0.021* Q135 vs IP_3R2 HET p=0.043 Q135 vs IP_3R2 KO;Q135 p=0.201(N.S) IP_3R2 KO vs IP_3R2 HET p=0.985 (N.S) IP_3R2 KO vs IP_3R2 KO; Q135 *p<0.001* IP_3R2 HET vs IP_3R2 KO;Q135 *p=0.001* Week 20: χ_w^2 (4,48)=25.962 p<0.001 n^2=0.522 Pairwise comparisons: WT vs Q135 p=0.006 WT vs IP_3R2 KO p=0.675(N.S) WT vs IP_3R2 HET p=0.920 (N.S) WT vs IP_3R2 KO;Q135 *p<0.001* Q135 vs IP_3R2 KO *p=0.023* Q135 vs IP_3R2 HET p=0.015 Q135 vs IP_3R2 KO;Q135 p=0.282(N.S) IP_3R2 KO vs IP_3R2 HET p=0.650 (N.S) IP_3R2 KO vs IP_3R2 KO; Q135 *p<0.001* IP_3R2 HET vs IP_3R2 KO;Q135 *p<0.001* Week 24: χ_w^2 (4,48)=24.298 p<0.001 n^2=0.484 Pairwise comparisons: WT vs Q135 p=0.008 WT vs IP_3R2 KO p=0.587(N.S) WT vs IP_3R2 HET p=0.459 (N.S) WT vs IP_3R2 KO;Q135 *p=0.001* Q135 vs IP_3R2 KO *p=0.002*

			Q135 vs IP_3R2 HET ***p*=0.003** Q135 vs IP_3R2 KO;Q135 ***p*=0.719(N.S)** IP_3R2 KO vs IP_3R2 HET ***p*=0.790 (N.S)** IP_3R2 KO vs IP_3R2 KO; Q135 ***p<0.001*** IP_3R2 HET vs IP_3R2 KO;Q135 ***p=0.001*** **Week 30: χ_w2 (4,42)=25.541 *p*<0.001 n^2=0.593** Pairwise comparisons: WT vs Q135 ***p*=0.014** WT vs IP_3R2 KO ***p*=0.699(N.S)** WT vs IP_3R2 HET ***p*=0.883 (N.S)** WT vs IP_3R2 KO;Q135 ***p<0.001*** Q135 vs IP_3R2 KO ***p=0.005*** Q135 vs IP_3R2 HET ***p*=0.018** Q135 vs IP_3R2 KO;Q135 ***p*=0.444 (N.S)** IP_3R2 KO vs IP_3R2 HET ***p*=0.843 (N.S)** IP_3R2 KO vs IP_3R2 KO; Q135 ***p<0.001*** IP_3R2 HET vs IP_3R2 KO;Q135 ***p=0.001***
Wire manoeuvre (SHIRPA protocol)	IP_3R2 KO 12B IP_3R2 KO; Q135 20B	IP_3R2 KO 39 IP_3R2 KO; Q135 48	**Repeat Measures ANOVA** [between-subjects factor: genotype (WT, Q135, IP_3R2 KO, IP_3R2 HET and IP_3R2 KO;Q135 | covariate: age (6,8,12,16,20,24,30 weeks)] Mauchly'sW (0.088): $\chi2(20)=50.531$ p<0.001 $\varepsilon_{(Greenhouse-Geisser)}=0.580$ Within-Subjects effects (Greenhouse-Geisser): [Age] **F(4,80)=18.331 *p*<0.001** [Age x Genotype] **F(14,80)=1.984 *p*=0.030** Between-subjects effects [Genotype] **F(4,23)=9.120 *p<0.001*** **Multiple comparisons (Dunnett T3):** WT vs Q135 ***p*=0.012** WT vs IP_3R2 KO ***p*=1.000 (N.S)** WT vs IP_3R2 HET ***p*=0.999 (N.S)** WT vs P_3R2 KO;Q135 **p=0.011** Q135 vs IP_3R2 KO ***p*=0.022 (N.S)** Q135 vs IP_3R2 HET ***p*=0.351 (N.S)** Q135 vs IP_3R2 KO;Q135 ***p*=1.000 (N.S)** IP_3R2 KO vs IP_3R2 HET ***p*=0.998 (N.S)** IP_3R2 KO vs IP_3R2 KO; Q135 ***p*=0.020** IP_3R2 HET vs IP_3R2 KO;Q135 **p=0.350(N.S)**
			One-way ANOVA [between-subjects factor: genotype] week 6: **F(4,44)=4.538, *p*=0.004 , n^2= 0.312** week 8: **F(4,48)=2.611 , *p*=0.048, n^2= 0.192** week 12: **F(4,44)=6.787 p<0.001 n^2= 0.404** week 16: **F(4,45)=6.903 p<0.001, n^2=0.402**

			week 20: **F(4,44)=3.968, p=0.008, n^2=0.284** week 24: **F(4,44)=5.122, p=0.002, n^2=0.339** week 30: **F(4,37)=3.118, p=0.028, n^2=0.279** **Post-Hoc analyses (Dunnett T3)**: **[week 6]** WT vs Q135 ***p*=0.010 (N.S)** WT vs IP_3R2 KO ***p*=0.918 (N.S)** WT vs IP_3R2 HET ***p*=0.989 (N.S)** WT vs IP_3R2 KO;Q135 ***p*=0.065 (N.S)** Q135 vs IP_3R2 KO ***p*=0.284 N.S)** Q135 vs IP_3R2 HET ***p=0.080*(N.S)** Q135 vs IP_3R2 KO;Q135 ***p*=0.998 (N.S)** IP_3R2 KO vs IP_3R2 HET ***p*=0.997 (N.S)** IP_3R2 KO vs IP_3R2 KO; Q135 ***p*=0.357 (N.S)** IP_3R2 HET vs IP_3R2 KO;Q135 ***p*=0.199 (N.S)** **[week 8]** WT vs Q135 ***p*=0.080 (N.S)** WT vs IP_3R2 KO ***p*=0.999 (N.S)** WT vs IP_3R2 HET ***p*=1.000 (N.S)** WT vs IP_3R2 KO;Q135 ***p*=0.166(N.S)** Q135 vs IP_3R2 KO ***p*=0.241 (N.S)** Q135 vs IP_3R2 HET ***p*=0.803 (N.S)** Q135 vs IP_3R2 KO;Q135 ***p*=1.000 (N.S)** IP_3R2 KO vs IP_3R2 HET ***p*=1.000 (N.S)** IP_3R2 KO vs IP_3R2 KO;Q135 ***p*=0.320 (N.S)** IP_3R2 HET vs IP_3R2 KO;Q135 ***p*=0.857 (N.S)** **[week 12]** WT vs Q135 ***p*=0.049 (N.S)** WT vs IP_3R2 KO ***p*=1.000 (N.S)** WT vs IP_3R2 HET ***p*=1.000 (N.S)** WT vs IP_3R2 KO;Q135 ***p*=0.006 (N.S)** Q135 vs IP_3R2 KO ***p*=0.066 (N.S)** Q135 vs IP_3R2 HET ***p*=0.495 (N.S)** Q135 vs IP_3R2 KO;Q135 ***p*=0.399 (N.S)** IP_3R2 KO vs IP_3R2 HET ***p*=0.997 (N.S)** IP_3R2 KO vs IP_3R2 KO; Q135 ***p*=0.008 (N.S)** IP_3R2 HET vs IP_3R2 KO;Q135 ***p*=0.310 (N.S)** **[week 16]** WT vs Q135 ***p*=0.025** WT vs IP_3R2 KO ***p*=1.000 (N.S)** WT vs IP_3R2 HET ***p*=0.985 (N.S)** WT vs IP_3R2 KO;Q135 ***p*=0.017 (N.S)** Q135 vs IP_3R2 KO ***p*=0.043(N.S)** Q135 vs IP_3R2 HET ***p*=0.149 (N.S)**

			Q135 vs IP_3R2 KO;Q135 ***p*=0.998 (N.S)** IP_3R2 KO vs IP_3R2 HET ***p*=0.967 (N.S)** IP_3R2 KO vs IP_3R2 KO; Q135 ***p*=0.031** IP_3R2 HET vs IP_3R2 KO;Q135 ***p*=0.134 (N.S)** **[week 20]** WT vs Q135 ***p*=0.992 (N.S)** WT vs IP_3R2 KO ***p*=0.772 (N.S)** WT vs IP_3R2 HET ***p=0.884* (N.S)** WT vs IP_3R2 KO;Q135 ***p*=0.142 (N.S)** Q135 vs IP_3R2 KO ***p*=0.431 (N.S)** Q135 vs IP_3R2 HET ***p*=0.658 (N.S)** Q135 vs IP_3R2 KO;Q135 ***p*=0.583(N.S)** IP_3R2 KO vs IP_3R2 HET ***p*=1.000 (N.S)** IP_3R2 KO vs IP_3R2 KO; Q135 ***p*=0.093 (N.S)** IP_3R2 HET vs IP_3R2 KO;Q135 ***p*=0.304 (N.S)** **[week 24]** WT vs Q135 ***p*=0.988 (N.S)** WT vs IP_3R2 KO ***p*=0.766 (N.S)** WT vs IP_3R2 HET ***p*=0.254 (N.S)** WT vs IP_3R2 KO;Q135 ***p*=0.980 (N.S)** Q135 vs IP_3R2 KO ***p*=0.404 (N.S)** Q135 vs IP_3R2 HET ***p*=0.162 (N.S)** Q135 vs IP_3R2 KO;Q135 ***p*=1.000 (N.S)** IP_3R2 KO vs IP_3R2 HET ***p*=0.902 (N.S)** IP_3R2 KO vs IP_3R2 KO; Q135 ***p*=0.385 (N.S)** IP_3R2 HET vs IP_3R2 KO;Q135 ***p*=0.159 (N.S)** **[week 30]** WT vs Q135 ***p*=0.331 (N.S)** WT vs IP_3R2 KO ***p*=0.500 (N.S)** WT vs IP_3R2 HET ***p*=0.894 (N.S)** WT vs IP_3R2 KO;Q135 ***p=0.948* (N.S)** Q135 vs IP_3R2 KO ***p*=0.242 (N.S)** Q135 vs IP_3R2 HET ***p*=0.730 (N.S)** Q135 vs IP_3R2 KO;Q135 ***p*=0.631 (N.S)** IP_3R2 KO vs IP_3R2 HET ***p*=1.000 (N.S)** IP_3R2 KO vs IP_3R2 KO; Q135 ***p*=0.353 (N.S)** IP_3R2 HET vs IP_3R2 KO;Q135 ***p*=0.819 (N.S)**
Adhesive removal test (Until 16 weeks of age)	IP_3R2 KO 13A	IP_3R2 KO 40	**Repeat Measures ANOVA** [between-subjects factor: genotype (WT, Q135, IP_3R2 KO, IP_3R2 HET and IP_3R2 KO;Q135 | covariate: age (6,8,12,16,20,24,30 weeks)]

	IP₃R2 KO; Q135 21A	IP₃R2 KO; Q135 49	Mauchly'sW (0.196) χ2(5)=58.228 p<0.001 $\varepsilon_{(Greenhouse-Geisser)}$=0.519 Within-Subjects effects (Greenhouse-Geisser): [Age] **F(2,58)=4.535 *p*=0.022** [Age x Genotype] **F(6,58)=4.748 p<0.001** Between-subjects effects [Genotype] **F(4,37)=6.096 p=0.001** **Multiple comparisons (Dunnett T3):** WT vs Q135 ***p*=0.018** WT vs IP₃R2 KO ***p*=1.000 (N.S)** WT vs IP₃R2 HET ***p*=0.851(N.S)** WT vs IP₃R2 KO;Q135 **p=0.114 (N.S)** Q135 vs IP₃R2 KO ***p*=0.069 (N.S)** Q135 vs IP₃R2 HET ***p*=0.436 (N.S)** Q135 vs IP₃R2 KO;Q135 ***p*=0.629(N.S)** IP₃R2 KO vs IP₃R2 HET ***p*=0.894 (N.S)** IP₃R2 KO vs IP₃R2 KO; Q135 **p=0.108(N.S)** IP₃R2 HET vs IP₃R2 KO;Q135 ***p*=0.240 (N.S)**
			One-way ANOVA [between-subjects factor: genotype] week 6: **F(4,46)=1.595 *p*=0.193 n^2 = 0.132** week 8: **F(4,46)=0.773*p*=0.549, n^2 = 0.069** week 12: **F(4,45)=3.942 *p*=0.008, n^2 = 0.278** week 16: **F(4,47)=5.246 *p*=0.002, n^2 =0.328** **Post-Hoc analyses (Dunnett T3)**: **[week 6]** WT vs Q135 ***p*=1.000 (N.S)** WT vs IP₃R2 KO ***p*=1.000 (N.S)** WT vs IP₃R2 HET ***p*=1.000 (N.S)** WT vs IP₃R2 KO;Q135 ***p*=0.224(N.S)** Q135 vs IP₃R2 KO ***p=1.*000 (N.S)** Q135 vs IP₃R2 HET ***p*=1.000 (N.S)** Q135 vs IP₃R2 KO;Q135 ***p*=0.604(N.S)** IP₃R2 KO vs IP₃R2 HET ***p*=0.990 (N.S)** IP₃R2 KO vs IP₃R2 KO; Q135 ***p*=0.320 (N.S)** IP₃R2 HET vs IP₃R2 KO;Q135 ***p*=0.089 (N.S)** **[week 8]** WT vs Q135 ***p*=0.853(N.S)** WT vs IP₃R2 KO ***p*=0.999(N.S)** WT vs IP₃R2 HET ***p*=0.822(N.S)** WT vs IP₃R2 KO;Q135 ***p*=1.000 (N.S)** Q135 vs IP₃R2 KO ***p*=0.956 (N.S)** Q135 vs IP₃R2 HET ***p*=1.000 (N.S)** Q135 vs IP₃R2 KO;Q135 ***p*=0.982 (N.S)** IP₃R2 KO vs IP₃R2 HET ***p*=0.979(N.S)**

			IP_3R2 KO vs IP_3R2 KO; Q135 p=1.000 (N.S) IP_3R2 HET vs IP_3R2 KO;Q135 p=0.998 (N.S) [week 12] WT vs Q135 p=0.845(N.S) WT vs IP_3R2 KO p=1.000 (N.S) WT vs IP_3R2 HET p=0.908(N.S) WT vs IP_3R2 KO;Q135 p=0.064 (N.S) Q135 vs IP_3R2 KO p=0.640 (N.S) Q135 vs IP_3R2 HET p=1.000 (N.S) Q135 vs IP_3R2 KO;Q135 p=0.715(N.S) IP_3R2 KO vs IP_3R2 HET p=0.772 (N.S) IP_3R2 KO vs IP_3R2 KO; Q135 p=0.035 (N.S) IP_3R2 HET vs IP_3R2 KO;Q135 p=0.764 (N.S) [week 16] WT vs Q135 p=0.174(N.S) WT vs IP_3R2 KO p=1.000 (N.S) WT vs IP_3R2 HET p=1.000 (N.S) WT vs IP_3R2 KO;Q135 p=0.109 (N.S) Q135 vs IP_3R2 KO p=0.334 (N.S) Q135 vs IP_3R2 HET p=0.209 (N.S) Q135 vs IP_3R2 KO;Q135 p=0.445(N.S) IP_3R2 KO vs IP_3R2 HET p=1.000 (N.S) IP_3R2 KO vs IP_3R2 KO; Q135 p=0.124 (N.S) IP_3R2 HET vs IP_3R2 KO;Q135 p=0.112 (N.S)

Adhesive removal test (score)	IP_3R2 KO 13B IP_3R2 KO; Q135 21B	IP_3R2 KO 40 IP_3R2 KO; Q135 49	**Friedman Test** χ_w^2 (2,139)=262,396 p<0,001 **Kruskal-Wallis test** [between-subjects factor: genotype] **Week 20: χ_w^2 (4,49)=9.988 p=0.041 n^2=0.155** Pairwise comparisons: WT vs Q135 p=0.410 (N.S) WT vs IP_3R2 KO p=1.000 (N.S) WT vs IP_3R2 HET p=1.000 (N.S) WT vs IP_3R2 KO;Q135 p=0.008 Q135 vs IP_3R2 KO *p=0.429* Q135 vs IP_3R2 HET p=0.491 Q135 vs IP_3R2 KO;Q135 p=0.099 (N.S) IP_3R2 KO vs IP_3R2 HET p=1.000 (N.S) IP_3R2 KO vs IP_3R2 KO; Q135 p=0.011 IP_3R2 HET vs IP_3R2 KO;Q135 p=0.029 **Week 24: χ_w^2 (4,48)= 13.673 p=0.008 n^2=0.243** Pairwise comparisons: WT vs Q135 p=0.045 WT vs IP_3R2 KO p=1.000 (N.S) WT vs IP_3R2 HET p=1.000 (N.S) WT vs IP_3R2 KO;Q135 p=0.004 Q135 vs IP_3R2 KO *p=0.054* Q135 vs IP_3R2 HET p=0.093 Q135 vs IP_3R2 KO;Q135 p=0.474 (N.S) IP_3R2 KO vs IP_3R2 HET p=1.000 (N.S) IP_3R2 KO vs IP_3R2 KO; Q135 p=0.006 IP_3R2 HET vs IP_3R2 KO;Q135 p=0.017 **Week 30: χ_w^2 (4,42)=17.099 p=0.002 n^2=0.371** Pairwise comparisons: WT vs Q135 p=0.009 WT vs IP_3R2 KO p=1.000 (N.S) WT vs IP_3R2 HET p=1.000 (N.S) WT vs IP_3R2 KO;Q135 p=0.005 Q135 vs IP_3R2 KO *p=0.009* Q135 vs IP_3R2 HET p=0.017 Q135 vs IP_3R2 KO;Q135 p=0.901(N.S) IP_3R2 KO vs IP_3R2 HET p=1.000 (N.S) IP_3R2 KO vs IP_3R2 KO; Q135 p=0.005 IP_3R2 HET vs IP_3R2 KO;Q135 p=0.013

Table 5 – Statistical information: IP_3R receptors gene expression in affected brain areas of the CMVMJD135 mouse model.

BRAIN REGION	FIGURE	PAGE	STATISTICAL REPORT: INDEPENDENT T-TEST
Brainstem	14.A	41	*Itpr1* *Equal Variances:* F=0.355 *p=0,560* *t* (16)=0.066 p=0,948 d_{Cohen}=0.003
	14.B		*Itpr2* *Equal Variances:* F=1.114 *p=0,307* *t* (16)= -0.359 p=0,725 d_{Cohen}=0.017
Cerebellum	15A	42	*Itpr1* *Equal Variances:* F=2.253 *p=0.177* *t* (7)= -0.543 *p=0.604* d_{Cohen}=0.038
	15B		*Itpr2* *Equal Variances:* F=0,663 *p=0,447* *t* (6)= -0,563 *p=0,595* d_{Cohen}=0,039
Astrocytes enriched samples (samples: brainstem and cerebellum)	16A	43	*Itpr1* *Equal Variances:* F=0,719 *p=0,429* *t* (6)= - 0,089 p=0,932 d_{Cohen}=0,006
	16B		*Itpr2* *Equal Variances:* F=0,005 *p=0,944* *t* (5)= - 0,265 p=0,801 d_{Cohen}=0,020
	16C		*Slca2a3* *Equal Variances:* F=1,066 *p=0,349* *t* (5)= - 1,431 p=0,948 d_{Cohen}=0,104
	16D		*Reln* *Equal Variances:* F=1,539 *p=0,261* *t* (6)=- 0,641 p=0,545 d_{Cohen}=0,045
	16E		*Gfap* *Equal Variances:* F=1,464 *p=0,280* *t* (5)=- 0,815=0,453 d_{Cohen}=0,007

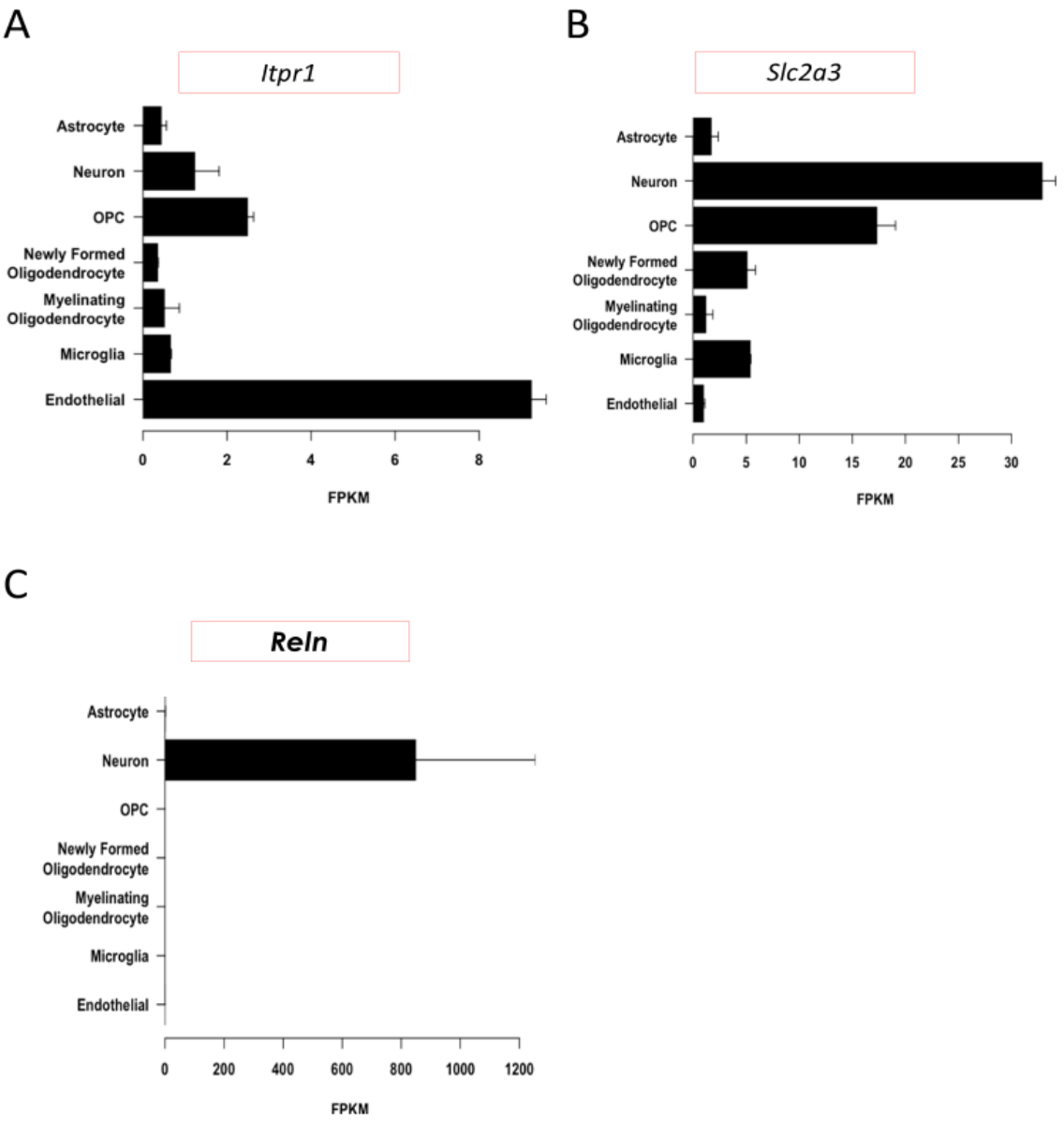

Figure 27 – Relative expression of *Itrp1, Slc2a3* and *Reln* in different cells types. The relative expression of the *Itrp1, Slc2a3* gene is higher in neurons but can be also found in other cells types. On the other hand, the relative expression of *Reln* appears to be specific for neurons. ***Adapted from*** (206) (available at http://web.stanford.edu/group/barres_lab/brain_rnaseq.html).

Table 6 – Statistical information: Relative expression of specific genes in the brainstem of double mutant animals.

GENE	FIGURE	PAGE	STATISTICAL REPORT
Itpr1	22A	50	One Way ANOVA [genotype: WT, Q135, IP_3R2 KO and IP_3R2 KO; Q135] F(3,25)=0.947 p=0.435 n^2=0.114 Multiple comparisons (Tukey HSD): WT vs Q135 *p*=0.993 (N.S.) WT vs IP_3R2 KO *p*=0.577(N.S.) WT vs IP_3R2 KO;Q135 *p*=0.897 (N.S.) Q135 vs IP_3R2 KO *p=0.435* (N.S.) Q135 vs IP_3R2 KO;Q135 *p*=0.780 (N.S.) IP_3R2 KO vs IP_3R2 KO;Q135 *p*=0.935
Itpr2	22B		One Way ANOVA [genotype: WT, Q135, IP_3R2 KO and IP_3R2 KO; Q135]]F(3,23)=6.848 p=0.002 n^2=0.507 Multiple comparisons (Dunnett T3): WT vs Q135 *p=1.000* (N.S.) WT vs IP_3R2 KO *p*=0.027 WT vs IP_3R2 KO;Q135 *p*=0.027 Q135 vs IP_3R2 KO *p<0.001* Q135 vs IP_3R2 KO;Q135 *p*<0.001 IP_3R2 KO vs IP_3R2 KO;Q135 *p=1.000* (N.S.)
Gfap	23A	51	One Way ANOVA [genotype: WT, Q135, IP_3R2 KO and IP_3R2 KO; Q135] F(3, 18)=0.616 p= 0.615 n^2=0.110 Multiple comparisons (Tukey HSD): WT vs Q135 *p*=0.758 (N.S.) WT vs IP_3R2 KO *p*=0.878 (N.S.) WT vs IP_3R2 KO;Q135 *p*=0.999 (N.S.) Q135 vs IP_3R2 KO *p=0.997* (N.S.) Q135 vs IP_3R2 KO;Q135 *p*=0.675 (N.S.) IP_3R2 KO vs IP_3R2 KO;Q135 *p=0.815* (N.S.)
Ccl2	23B		One Way ANOVA [genotype: WT, Q135, IP_3R2 KO and IP_3R2 KO; Q135] F(3, 17)=2.381 p= 0.129 n^2=0.324 Multiple comparisons (Dunnett T3): WT vs Q135 *p*=0.552 (N.S.) WT vs IP_3R2 KO *p*=0.355 (N.S.) WT vs IP_3R2 KO;Q135 *p*=0.552(N.S.) Q135 vs IP_3R2 KO *p=0.820* (N.S.) Q135 vs IP_3R2 KO;Q135 *p*=1.000 (N.S.) IP_3R2 KO vs IP_3R2 KO; Q135 *p=0.987* (N.S.)
Tnf-a	23C		One Way ANOVA

			[genotype: WT, Q135, IP_3R2 KO and IP_3R2 KO; Q135] **F(3, 15)=0.774 p= 0.531 n^2=0.162** **Multiple comparisons (Tukey HSD):** WT vs Q135 ***p*=0.982 (N.S.)** WT vs IP_3R2 KO ***p*=0.656 (N.S.)** WT vs IP_3R2 KO;Q135 ***p*=0.945 (N.S.)** Q135 vs IP_3R2 KO ***p=0.533* (N.S.)** Q135 vs IP_3R2 KO;Q135 ***p*=0.836 (N.S.)** IP_3R2 KO vs IP_3R2 KO;Q135 ***p=0.934* (N.S.)**
Serping1	24A	52	**One Way ANOVA** [genotype: WT, Q135, IP_3R2 KO and IP_3R2 KO; Q135] **F(3, 17)=2.361 p= 0.115 n^2=0.336** **Multiple comparisons (Dunnett T3):** WT vs Q135 ***p*=0.494 (N.S.)** WT vs IP_3R2 KO ***p*=0.412 (N.S.)** WT vs IP_3R2 KO;Q135 ***p*=0.294 (N.S.)** Q135 vs IP_3R2 KO ***p=1.000* (N.S.)** Q135 vs IP_3R2 KO;Q135 ***p*=0.995** IP_3R2 KO vs IP_3R2 KO;Q135 ***p=1.000* (N.S.)**
Fbln5	24B		**One Way ANOVA** [genotype: WT, Q135, IP_3R2 KO and IP_3R2 KO; Q135] **F(3, 18)=0.986 p=0.426 n^2=0.165** **Multiple comparisons (Tukey HSD):** WT vs Q135 ***p*=0.519 (N.S.)** WT vs IP_3R2 KO ***p*=0.738 (N.S.)** WT vs IP_3R2 KO;Q135 ***p*=0.428 (N.S.)** Q135 vs IP_3R2 KO ***p=0.991* (N.S.)** Q135 vs IP_3R2 KO;Q135 ***p*=0.998 (N.S.)** IP_3R2 KO vs IP_3R2 KO;Q135 ***p=0.969* (N.S.)**
Amigo2	24C		**One Way ANOVA** [genotype: WT, Q135, IP_3R2 KO and IP_3R2 KO; Q135] **F(3, 16)=3.217 p=0.058 n^2=0.426** **Multiple comparisons (Tukey HSD):** WT vs Q135 ***p*=0.069(N.S.)** WT vs IP_3R2 KO ***p*=0.296 (N.S.)** WT vs IP_3R2 KO;Q135 ***p*=0.079(N.S.)** Q135 vs IP_3R2 KO ***p=0.853* (N.S.)** Q135 vs IP_3R2 KO;Q135 ***p*=1.000 (N.S.)** IP_3R2 KO VS IP_3R2 KO;Q135 ***p=0.840* (N.S.)**
Ggta1	24D		**One Way ANOVA** [genotype: WT, Q135, IP_3R2 KO and IP_3R2 KO; Q135] **F(3, 17)=0.971 p=0.434 n^2=0.172** **Multiple comparisons (Dunnett T3):** WT vs Q135 ***p*=0.728 (N.S.)**

			WT vs IP_3R2 KO ***p*=0.744 (N.S.)** WT vs IP_3R2 KO;Q135 ***p*=0.687 (N.S.)** Q135 vs IP_3R2 KO ***p=1.000* (N.S.)** Q135 vs IP_3R2 KO;Q135 ***p*=0.890 (N.S.)** IP_3R2 KO vs IP_3R2 KO; Q135 ***p=0.945* (N.S.)**
S100aB	24E	52	**One Way ANOVA** [genotype: WT, Q135, IP_3R2 KO and IP_3R2 KO; Q135] **F(3, 15)=3.268 p=0.059 n^2=0.450** **Multiple comparisons (Tukey HSD):** WT vs Q135 ***p=1.000* (N.S.)** WT vs IP_3R2 KO ***p*=0.236 (N.S.)** WT vs IP_3R2 KO;Q135 ***p*=0.125 (N.S.)** Q135 vs IP_3R2 KO ***p=0.253* (N.S.)** Q135 vs IP_3R2 KO;Q135 ***p*=0.142 (N.S.)** IP_3R2 KO vs IP_3R2 KO;Q135 ***p=0.997* (N.S.)**
Sphk1	24F		**One Way ANOVA** [genotype: WT, Q135, IP_3R2 KO and IP_3R2 KO; Q135] **F(3, 16)=1.780 p=0.200 n^2=0.291** **Multiple comparisons (Dunnett T3):** WT vs Q135 ***p=0.716* (N.S.)** WT vs IP_3R2 KO ***p*=0.555 (N.S.)** WT vs IP_3R2 KO;Q135 ***p*=0.987 (N.S.)** Q135 vs IP_3R2 KO ***p=1.000* (N.S.)** Q135 vs IP_3R2 KO;Q135 ***p*=0.505 (N.S.)** IP_3R2 KO vs IP_3R2 KO; Q135 ***p=0.411* (N.S.)**
Ptgs2	24G		**One Way ANOVA** [genotype: WT, Q135, IP_3R2 KO and IP_3R2 KO; Q135] **F(3, 16)=1.788 p=0.199 n^2=0.292** **Multiple comparisons (Dunnett T3):** WT vs Q135 ***p=1.000* (N.S.)** WT vs IP_3R2 KO ***p=0.751* (N.S.)** WT vs IP_3R2 KO;Q135 ***p*=0.874 (N.S.)** Q135 vs IP_3R2 KO ***p=0.357* (N.S.)** Q135 vs IP_3R2 KO;Q135 ***p*=0.791(N.S.)** IP_3R2 KO vs IP_3R2 KO;Q135 ***p=0.493* (N.S.)**

Table 7 – Statistical information: Histopathological observation of brain sections of double mutant mice.

STAINING/ TECHNIQUE	BRAIN REGION	FIGURE	PAGE	STATISTICAL REPORT: INDEPENDENT T-TEST
H&E	Pontine nuclei	25A	53	One Way ANOVA [genotype: WT, Q135, IP_3R2 KO and IP_3R2 KO; Q135] F(3, 15)=1.543 p=0.254 n^2=0.278 Multiple comparisons (Dunnett T3): WT vs Q135 *p=0.688* (N.S.) WT vs IP_3R2 KO *p*=0.*572* (N.S.) WT vs IP_3R2 KO;Q135 *p*=0.068 (N.S.) Q135 vs IP_3R2 KO *p=0.944* (N.S.) Q135 vs IP_3R2 KO;Q135 *p*=0.245 (N.S.) IP_3R2 KO vs IP_3R2 KO;Q135 *p=1.000* (N.S.)
	Deep cerebellar nuclei	25B		One Way ANOVA [genotype: WT, Q135, IP_3R2 KO and IP_3R2 KO; Q135] F(3, 13)=3.333 p=0.053 n^2=0.435 Multiple comparisons (Tukey HSD): WT vs Q135 *p*=0.063 (N.S.) WT vs IP_3R2 KO *p=0.089* (N.S.) WT vs IP_3R2 KO;Q135 *p=0.371* (N.S.) Q135 vs IP_3R2 KO *p=0.985* (N.S.) Q135 vs IP_3R2 KO;Q135 *p*=0.829 (N.S.) IP_3R2 KO vs IP_3R2 KO;Q135 *p=0.938* (N.S.)